TRANSPORTATION RESEARCH RECORD 756

Concrete Pavements and Pavement Overlays

TRANSPORTATION RESEARCH BOARD

COMMISSION ON SOCIOTECHNICAL SYSTEMS
NATIONAL RESEARCH COUNCIL

NATIONAL ACADEMY OF SCIENCES
WASHINGTON, D.C. 1980

Transportation Research Record 756
Price $4.00
Edited for TRB by Brenda J. Vumbaco

modes
1 highway transportation
4 air transportation

subject area
24 pavement design and performance

Library of Congress Cataloging in Publication Data
National Research Council. Transportation Research Board.
Concrete pavements and pavement overlays.

(Transportation research record; 756 ISSN 0361-1981)
Reports prepared for the 59th annual meeting of the Transportation Research Board.
Includes bibliographical references.
1. Pavements, Concrete—Addresses, essays, lectures. 2. Pavements, Asphalt concrete—Addresses, essays, lectures. I. Title. II. Series.
TE7.H5 no. 756 [TE278] 380.5s 80-607869
ISBN 0-309-03070-6 [625.8'4]

Sponsorship of the Papers in This Transportation Research Record

GROUP 2—DESIGN AND CONSTRUCTION OF TRANSPORTATION FACILITIES
R. V. LeClerc, Washington State Department of Transportation, chairman

Pavement Design Section
W. Ronald Hudson, University of Texas at Austin, chairman

Committee on Rigid Pavement Design
Richard A. McComb, Federal Highway Administration, chairman
Kenneth J. Boedecker, Jr., William E. Brewer, William J. Carson, Bert E. Colley, Donald K. Emery, Jr., Wade L. Gramling, James L. Greene, Yang H. Huang, Ronald L. Hutchinson, Michael P. Jones, T.J. Larsen, B. Frank McCullough, Robert G. Packard, Dwight E. Patton, Karl H. Renner, Surendra K. Saxena, Don L. Spellman, T.C. Paul Teng, Paul J. Witkiewicz, William A. Yrjanson

Committee on Flexible Pavement Design
R.G. Hicks, Oregon State University, chairman
Leon M. Noel, Federal Highway Administration, secretary
Ernest J. Barenberg, Robert A. Crawford, R.N. Doty, W.B. Drake, Fred N. Finn, Wade L. Gramling, William Bryan Greene, R. V. LeClerc, J. W. Lyon, Jr., Frank P. Nichols, Jr., Adrian Pelzner, Dale E. Peterson, William A. Phang, Carl L. Schulten, James A. Sherwood, James F. Shook, Eugene L. Skok, Jr., William T. Stapler, Harvey J. Treybig, Harry H. Ulery, Jr., Loren M. Womack, Richard J. Worch

Committee on Pavement Rehabilitation Design
Matthew W. Witczak, University of Maryland, chairman
Gordon W. Beecroft, Oregon Department of Transportation, secretary
Ernest J. Barenberg, Walter R. Barker, W.G. Davison, Paul J. Diethelm, Fred N. Finn, William Bryan Greene, J.H. Havens, W.J. Head, Ali S. Kemahli, Edwin C. Lokken, Kamran Majidzadeh, Richard A. McComb, Carl L. Monismith, Gene R. Morris, August F. Muller, John L. Rice, Donald R. Schwartz, James F. Shook, Lawrence L. Smith, Richard L. Stewart, Harvey J. Treybig, Hugh L. Tyner, Loren M. Womack

Lawrence F. Spaine, Transportation Research Board staff

Sponsorship is indicated by a footnote at the end of each report. The organizational units, officers, and members are as of December 31, 1979.

Contents

MATERIAL PROPERTY REQUIREMENTS FOR ZERO MAINTENANCE OF CONTINUOUSLY REINFORCED CONCRETE PAVEMENTS
Gary E. Elkins, Freddy L. Roberts, and Thomas W. Kennedy 1

LIMITING CRITERIA FOR THE DESIGN OF CONTINUOUSLY REINFORCED CONCRETE PAVEMENTS
B. Frank McCullough, J. C. M. Ma, and C. S. Noble 7

NOMOGRAPHS FOR THE DESIGN OF STEEL REINFORCEMENT IN CONTINUOUSLY REINFORCED CONCRETE PAVEMENT
C. S. Noble, B. F. McCullough, and J. C. M. Ma 15

IMPLEMENTATION OF NEW OVERLAY DESIGN PROCEDURE IN TEXAS
Stephen Seeds, B. Frank McCullough, W. R. Hudson, and Manuel Gutierrez de Velasco 23

PREVENTION OF REFLECTIVE CRACKING IN ARIZONA
George B. Way 29

DYNAMIC SURFACE DEFLECTION MEASUREMENTS ON RIGID PAVEMENTS COMPARED WITH THE MODEL OF AN INFINITE PLATE ON AN ELASTIC FOUNDATION
Albert J. Bush III 33

FATIGUE CRACKING OF ASPHALT PAVEMENTS
D. V. Ramsamooj 43

Authors of the Papers in This Record

Bush, Albert J. III, U.S. Army Corps of Engineers, Waterways Experiment Station, Pavement Systems Division, P.O. Box 631, Vicksburg, MI 39180

Elkins, Gary E., Staff Engineer, Austin Research Engineers, Inc., 2600 Dellana Lane, Austin, TX 78746

Gutierrez de Velasco, Manuel, Research Assistant, Center for Transportation Research, University of Texas at Austin, Austin, TX 78712

Hudson, W. R., Professor of Civil Engineering, Center for Transportation Research, University of Texas at Austin, Austin, TX 78712

Kennedy, Thomas W., Professor of Civil Engineering, Center for Transportation Research, University of Texas at Austin, Austin, TX 78712

Ma, J. C. M., Austin Research Engineers, Inc., 2600 Dellana Lane, Austin, TX 78746

McCullough, B. Frank, Professor of Civil Engineering, Center for Transportation Research, University of Texas at Austin, Austin, TX 78712

Noble, C. S., Assistant Professor of Civil Engineering, Center for Transportation Research, University of Texas at Austin, Austin, TX 78712

Ramsamooj, D. V., Associate Professor of Civil Engineering, California State University, Fullerton, CA 92634

Roberts, Freddy L., Chief Engineer, Austin Research Engineers, Inc., 2600 Dellana Lane, Austin, TX 78746

Seeds, Stephen, Research Assistant, Center for Transportation Research, University of Texas at Austin, Austin, TX 78712

Way, George B., Senior Research Engineer, Arizona Department of Transportation, 206 South 17th Avenue, Phoenix, AZ 85007

Material Property Requirements for Zero Maintenance of Continuously Reinforced Concrete Pavements

GARY E. ELKINS, FREDDY L. ROBERTS, AND THOMAS W. KENNEDY

This study involved the (a) selection of models suitable for predicting important distresses that previously have been observed on continuously reinforced concrete pavement (CRCP) and (b) determination of a set of material properties that will provide satisfactory performance for 20 years without maintenance and satisfactory performance for the next 10-20 years with normal maintenance. To accomplish this goal, the most important distresses occurring in CRCPs and the material properties that affect those distresses were identified. Mathematical models to predict those distresses by using the identified material properties were selected. A range of values for each material property was selected and resulting distresses were predicted. The distresses studied included fatigue cracking, punchouts, crack spalling, steel rupture, and low-temperature and shrinkage cracking. The mathematical models selected for the analysis were ELSYM5 for modeling fatigue cracking and CRCP-2 for modeling low-temperature and shrinkage cracking. Punchouts, crack spalling, and steel rupture were incorporated into the analysis of low-temperature and shrinkage cracking. Input values were selected for each model, and ranges of the material properties affecting distress were identified and used in the analyses. The results for each study are discussed, and practical criteria are cited to evaluate the level of material properties required to provide zero-maintenance performance. A set of material properties is identified, and the trade-offs on material properties are discussed.

For several years, the Federal Highway Administration (FHWA) has pursued multiple research studies aimed at producing premium pavement structures for heavily traveled highways. The objective of these efforts has been to develop pavement structures that will be maintenance-free for 20 years and will require only routine maintenance for 10-20 years thereafter.

The research reported here is drawn from a portion of the FHWA-sponsored research project Material Property Requirements for Zero-Maintenance Pavements. The overall goal of this project is the identification of material properties that will provide optimal performance in flexible, rigid, and composite zero-maintenance or premium pavements.

The research methodology used to study the influence of material properties on distress in premium highway pavements involved the following steps:

1. Identify significant distresses,
2. Review and select models to predict distress,
3. Determine the effects of varying material properties while holding other inputs constant, and
4. Identify ranges of material properties to minimize distress.

The results of the first two steps noted above were previously published in an interim report (1). This paper contains the findings of the study of continuously reinforced concrete pavement (CRCP) related to steps 3 and 4 above.

SIGNIFICANT DISTRESSES

CRCP distresses, whose frequency of occurrence and severity significantly influence serviceability, were derived from field studies reported by McCullough and others (2) and Darter and Barenberg (3). These distresses are crack spalling, fatigue cracking, low-temperature and shrinkage cracking, punchouts, and steel rupture.

SELECTED DISTRESS MODELS

Analytical models were available to study the effect of material properties on fatigue cracking, low-temperature cracking, and shrinkage cracking. The other important distresses noted above were incorporated into the low-temperature and shrinkage analyses.

Fatigue Cracking

Elastic-layer theory was used to study fatigue cracking because the individual layers can be characterized and their separate effects on pavement response can be studied. Stresses and strains predicted by elastic-layer theory are distributed with depth in a more realistic fashion than for plate models and are more economical to use. The primary limitations of the elastic-layer theory are its inability to define any horizontal boundaries and its inability to simulate directly the existence of stiffness variations such as cracks or voids. Despite these limitations, elastic-layer theory, as a pavement structural model, is very useful for a comprehensive study of the various layer materials.

Since a variety of elastic-layer models exist, the various available computer codes were compared (4) and the program most suited to project needs was selected. Based on that study, ELSYM5 was judged to be the best overall elastic-layer computer code for this study.

Low-Temperature and Shrinkage Cracking

The dimensional changes in a continuously reinforced concrete pavement, caused by drying shrinkage of the concrete and temperature variation after curing, were investigated by McCullough and others (2), and a design method that used the CRCP-1 program was developed and subsequently improved by Ma (5) to consider stresses imposed by wheel loads. This model was selected for the analysis of CRCP.

MODEL INPUTS

The use of these analytical models required the development of a consistent set of input values for each variable that occurs in the models.

Common Inputs

Several input factors are common to both models and are independent of the pavement material properties. These factors are the environment in which the pavement occurs, the traffic level to which the pavement is subjected, and the thickness of the pavement layers. Other factors, or inputs, depend on the individual models.

Environmental effects were incorporated by using environmental characteristics of four Interstate highway sections located in distinctly different environmental regions. The sections chosen for use in this study and the environmental regions represented were the following:

1. Wet freeze (WF)--Cold climate with generally high humidity and abundant precipitation, I-80 in Illinois (AASHO Road Test);
2. Dry freeze (DF)--Cold climate with low humidity and little rainfall, I-80N in northern Utah (near Snowville);
3. Wet, no freeze (WNF)--Relatively warm climate with high humidity and abundant rainfall, I-20 in Florida (near Madison); and
4. Dry, no freeze (DNF)--Warm climate with low humidity and little rainfall, I-20 in Texas (between Midland and Odessa).

The traffic level was derived from past data on heavily trafficked rigid pavements. Traffic information reported in Darter and Barenberg (3) indicated that some rigid pavements are experiencing over 2 million 80-kN (18-kip)

Table 1. Levels of material property inputs varied in fatigue cracking analysis.

Material Property	Level		
	Low	Intermediate	High
E for PCC surface (psi 000 000s)	24	36	98
f_r for PCC corresponding to E (psi)	3860	5860	6890
E for subbase (psi 000s)	103	3450	6890
Poisson's ratio corresponding to E for subbase	0.40	0.30	0.20
Fatigue potential[a]: $N_{18k} = C_1(f_r/\sigma_t)^{C_2}$	C_1 = 18 000 C_2 = 3.9	—	C_1 = 100 000 C_2 = 3.9

Note: 1 psi = 6.89 kPa.

[a] N_{18k} = number of 18-kip (80-kN) ESAL applications to produce class 3 and class 4 cracking; f_r = PCC modulus of rupture; σ_t = tensile stress in bottom of PCC layer.

equivalent single-axle loads (ESALs) annually, with 1-1.25 million relatively common. Therefore, 2 million 80-kN (18-kip) ESALs per year was selected for the traffic level that a zero-maintenance rigid pavement should carry.

The AASHO design procedure was used as a preliminary design for rigid pavements. A small study that used two types of subbase, three subbase thicknesses, and their corresponding moduli was performed by using a load transfer value of 2.2. This study was followed by an analysis that used the serviceability index equation developed by Darter and Barenberg (6) for zero-maintenance rigid pavements. Since Darter's procedure is also based on data collected at the AASHO Road Test, but over a longer period of observation, it was used to select the following cross-section design: portland cement concrete (PCC) surface thickness = 279 mm (11 in) and subbase thickness = 203 mm (8 in).

Specific Inputs to Distress Models

The results of this study were greatly affected by the ranges of input values selected for individual material properties due to possible interactions of the material properties. The ranges selected are representative of the variability of conventional materials under field conditions.

The important material properties affecting fatigue cracking were identified as (a) modulus of elasticity of the PCC surface layer, (b) modulus of elasticity of the subbase, and (c) fatigue potential of the PCC layer (1). Three levels were selected for the modulus of elasticity of both the PCC surface layer and the subbase layer (Table 1). The flexural strength of the concrete corresponded to the modulus of elasticity.

The fatigue potential of the PCC layer is estimated from the fatigue equation that relates the allowable number of load applications to the ratio of induced stress to flexural strength. The fatigue relations were based on field performance of in-service pavements. The curve used in this study was developed from interior stresses predicted by elastic-layer theory and the number of repetitions required to produce class 3 and class 4 cracking at the AASHO Road Test. This curve was modified for edge stresses and the high-low range introduced through variation in the coefficients.

The value inputs held constant throughout this analysis are listed below. (The input values are presented in the form used during research; therefore, no conversion to SI units appears in this section.)

Input Variable	Value
Number of loads	2
Load magnitude (kips)	9
Distance between loads (ft)	6
Tire pressure (psi)	75
Modulus of elasticity of subgrade layer (10^3 psi)	20
Subgrade Poisson's ratio	0.45
PCC surface thickness (in)	11
PCC surface Poisson's ratio	0.15
Subbase thickness (in)	8
Stress adjustment factor	1.23

The interior stress adjustment factor, which accounts for transverse traffic distribution and fatigue damage, represents the increase in stress from the interior condition to a position approximately 406 mm (16 in) from the edge of the pavement that was found to accumulate greater fatigue damage as a result of increased load applications.

The effects of thermal coefficient, shrinkage, and tensile strength of the PCC surface layer were of primary interest in this study. Values for each material property combination are shown below:

Material Property	Level	
	Low	High
Ultimate PCC tensile strength (indirect) (psi)	400	800
PCC thermal coefficient (10^{-6}/°F)	4.5	9.0
Ultimate concrete shrinkage (10^{-6})	200	800

The constant input values for low-temperature and shrinkage cracking analysis are summarized here.

1. Steel properties have these values--Reinforcement type = deformed bars; bar diameter = 0.625 in (#5); yield stress = 60 ksi; elastic modulus = 29.0 x 10^6 psi; and thermal coefficient = 6.0 x 10^{-6} in/in/°F.
2. Concrete properties have these values--Slab thickness = 11 in; unit weight = 150 lb/ft³ (W); ratio of tensile and flexural strength$^{1.5}$ = 0.86 (STRNMUL); and the PCC modulus of elasticity = 33.0 $(W)^{1.5}$ x (tensile strength)/(STRNMUL x 7.5).
3. Slab-base friction characteristics used in low-temperature and shrinkage cracking analysis are as follows:

Concrete Movement (in)	Friction Stress (lb/in²)
0.0	0.0
0.01	0.21
0.10	0.63
0.15	0.80
0.20	0.94
0.30	0.97

4. Design low-temperature factors are (a) WF, 25°F; (b) DF, 29°F; (c) WNF, 56°F; and (d) DNF, 46°F.
5. Temperature data are as follows: curing temperature = 80°F, first 28-day temperature drop = 20°F, and the time until minimum temperature = 28 days.
6. Wheel-load considerations are (a) wheel load = 9000 lb, (b) effective tire radius = 6.18 in, (c) modulus of subgrade reaction = 600 lb/in³, and (d) time of load application = 28th day.
7. Iteration and tolerance control involve the maximum number of iterations, which is 60, and a relative closure tolerance of 5 percent.

The indicated relation between the concrete tensile strength and modulus of elasticity is internal in the program. The curing temperature is used to calculate the temperature drop for each environmental zone.

DISCUSSION OF DISTRESS STUDIES

Fatigue Cracking

The results of the fatigue cracking study are summarized in Table 2. The influence of the modulus of elasticity of the

Table 2. Summary of fatigue cracking analysis.

PCC Modulus of Elasticity (10^6 psi)	Subbase Modulus of Elasticity (10^3 psi)	Predicted 18-kip ESAL Applications to Produce Class 3 and Class 4 Cracking (000 000s)	
		Low Fatigue Potential[a]	High Fatigue Potential[b]
3.5	15	8.25[c]	45.8
	500	68.4	380
	1000	342	1900
5.25	15	31.9[c]	177
	500	149	827
	1000	493	2740
7.0	15	49	272
	500	166	924
	1000	438	2440

Note: 1 psi = 6.89 kPa.

[a] Low fatigue, $N_f = 18\,000\,(f_r/\sigma_t)^{3.9}$.
[b] High fatigue, $N_f = 100\,000\,(f_r/\sigma_t)^{3.9}$.
[c] Does not satisfy zero-maintenance requirements of 40 million 18-kip (80-kN) ESAL applications.

Figure 1. Influence of concrete modulus of elasticity on CRCP fatigue cracking.

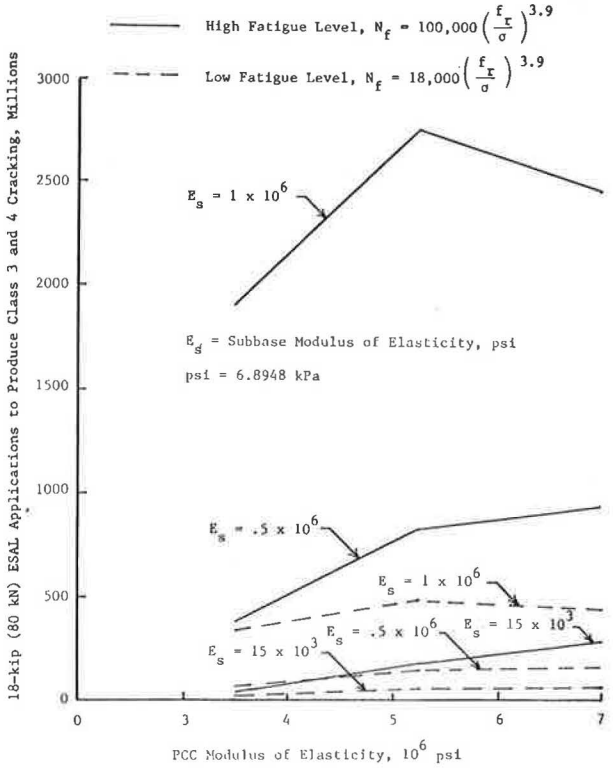

surface and subbase is illustrated in Figures 1 and 2.

The failure criterion used to determine the zero-maintenance potential was the ability of the pavement to carry 40 million 80-kN (18-kip) ESAL applications without developing class 3 or class 4 cracking. Treybig and others (7) found that the structural response of a pavement changed significantly when class 3 and class 4 cracking occurred; at that point, routine maintenance was required.

Increasing the subbase modulus, modulus of the concrete, and fatigue characteristics of the concrete increased the number of loads required to produce fatigue cracking. For the ranges investigated, increases of the subbase modulus produced larger improvements in fatigue performance than did increases in the modulus of elasticity of the concrete. For example, for the low fatigue level and subbase modulus, the traffic carried increased by about six times as the

Figure 2. Influence of subbase modulus of elasticity on CRCP fatigue cracking.

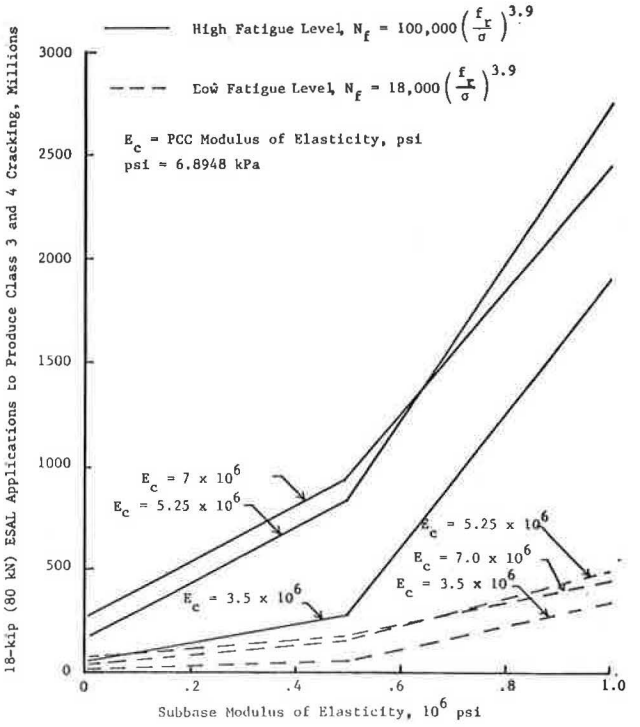

concrete modulus varied from 24 to 48 x 10^6 kPa (3.5 to 7.0 x 10^6 psi); however, for the low concrete modulus, the traffic carried increased by a factor of almost 40 over the range of subbase moduli. Changes in the traffic carried at other concrete moduli were not as large but did vary by a factor of 8 or more. Because the values of subbase moduli used in this analysis are quite common, efforts to improve the subbase moduli should be given prime consideration.

For the values used in this study, the effect of varying the fatigue relation on traffic was larger than the effect of varying the modulus of elasticity of the concrete. As shown in Figure 2, the fatigue life peaked at a concrete modulus of elasticity at 36.2 x 10^6 kPa (5.25 x 10^6 psi). This is probably not a significant observation because modulus and the fatigue characteristics are interrelated.

Conventional concrete offers excellent resistance to fatigue cracking, and it is quite capable of providing zero-maintenance service. All combinations of material properties except two carried traffic for 20 years without the class 3 and class 4 cracking. In fact, the traffic carried was substantially above that required before cracking. One missing element in the analysis was an evaluation of the effect of layer thickness that may be more significant than material properties. Zero-maintenance performance may not be produced at smaller thicknesses, even if the properties are significantly improved. Nevertheless, conventional materials exhibit material properties sufficient to meet the zero-maintenance fatigue criterion.

Punchouts, Crack Spalling, and Steel Rupture

The effects of material properties on the occurrence of punchouts, crack spalling, and steel rupture were studied by establishing limits on various pavement response parameters predicted by the CRCP-2 program, such as crack spacing and crack width, and by investigating the effects of material properties on these parameters. The limiting responses were established by theoretical consideration of the various distress mechanisms and correlation with observed performance.

Punchouts

Transverse cracks in CRCP develop as a result of restrained volume change. As the transverse crack spacing becomes smaller and load transfer across the transverse crack deteriorates, the pavement slab begins to respond to load as a transverse beam instead of a longitudinal beam. This subsequently causes short longitudinal cracks to occur within the transverse beam sections. These, in turn, produce small blocks of pavement that eventually lead to punchouts. Thus, punchouts can be prevented by limiting the crack spacing to ensure that the transverse stresses are less than the longitudinal stresses.

An analysis of crack spacing and the concrete stresses in the transverse and longitudinal direction was performed by using the SLAB-49 computer program (8,9). To determine a reasonable limit on crack spacing to minimize the occurrence of punchouts, a minimum load transfer across the transverse cracks of 50 percent was assumed. This corresponds to an interpolated value of crack spacing of 1.34 m (4.4 ft). This limit is slightly less than the 1.52-m (5-ft) optimum crack spacing determined by Majidzadeh (10) and the 1.52-m minimum suggested by McCullough and others (2) based on field observations of in-service pavements. Therefore, theoretically, crack spacings greater than 1.34 m (4.4 ft) should minimize the occurrence of punchouts on CRCP. However, this fact assumes that the concrete is in full contact with the subbase.

Crack Spalling

The primary causes of spalling on CRCP are believed to be (a) entrapment of road debris in cracks that causes stress concentration when the cracks close as temperature increases and (b) combined shear and tensile stress at joints or cracks due to a combination of horizontal temperature loading and vertical traffic loading. However, based on a laboratory study, McCullough and others (2) concluded that CRCP spalling caused by road-debris entrapment was relatively insignificant but that combined horizontal and vertical forces were the major causes of spalling. Because crack width and degree of spalling are both functions of horizontal stress, crack width and spalling are related. In a diagnostic study based on condition-survey data from Texas (2), crack widths and the occurrence of spalling were measured in the field. Results of these studies indicate that spalling was more prevalent at larger crack widths. A mean crack width of 0.54 mm (0.021 in) was reported for the spalled sections and 0.45 mm (0.0176 in) for the nonspalled sections. Cracks with widths of less than 0.51 mm (0.02 in) exhibited no spalling.

To control spalling, Ma and others (11) established a maximum allowable crack width of 0.61 mm (0.024 in). Since the crack widths were measured during the summer at relatively high temperatures, it was necessary to calculate the corresponding width at a lower temperature. The expected crack widths corresponding to the above maximum allowable crack width at the low temperatures for each environmental zone used as a criterion to limit spalling are DF, 1.02 mm (0.040 in); WF, 1.04 mm (0.041 in); DNF, 0.86 mm (0.034 in); and WNF, 0.76 mm (0.030 in).

Steel Rupture

Steel rupture may be prevented by limiting the calculated steel stress from the low-temperature and shrinkage analysis. Because the CRCP-2 program is based on a linearly elastic steel model, limiting the steel stress to the yield strength of the steel served as a conservative limit against steel rupture.

Low-Temperature and Shrinkage Cracking

Combinations of material property levels investigated in low-temperature and shrinkage cracking analysis and the constant input values, both described earlier in this paper, formed the basis of this analysis.

Initial Study

This analysis was performed in a sequential order beginning with the high and low values of tensile strength and 0.6 percent steel. The properties varied were the concrete thermal coefficient, ultimate concrete shrinkage, and tensile strength. The calculated crack spacing and crack widths for the WF zone are shown in Figure 3. Relations for the other environmental zones were similar.

The maximum desirable crack spacing for a CRCP, determined from field observations, has been set at 2.44 mm (8 ft) (2,10). Crack spacings greater than 2.44 mm (8 ft) produce detrimentally wide cracks. The relation between steel stress and concrete strength for each environmental zone is shown in Figure 4. Shaded areas of Figure 4 represent stress that meets zero-maintenance requirements. For high-strength concrete, the yield strength in the steel was exceeded.

Concrete strength had the greatest effect on the predicted CRCP response parameters. At the low-strength level, shrinkage exhibited greater effect than the thermal coefficient. At the high-strength level, thermal coefficient produced a greater change in the predicted response than did shrinkage. In general, crack spacing increased as the concrete shrinkage and thermal coefficient decreased and as the concrete strength increased.

Crack width increased as the concrete shrinkage and thermal coefficients decreased and as the concrete strength increased. This result may seem contrary to the reasoning that increasing concrete shrinkage and thermal coefficient cause the concrete to contract more, thus creating a wider crack. This phenomenon occurs because of the relation between crack width and crack spacing.

To demonstrate the effect of these variables on crack width alone, without the effect of crack spacing, the crack widths were divided by the corresponding crack spacings and plotted against the ultimate concrete strength. The resulting relation for the DF zone (Figure 5), which is typical of the other environmental zones, indicates that the crack width per foot of slab increased as the concrete shrinkage and thermal coefficients increased. Figure 5 also shows the insensitivity of predicted crack width to concrete strength.

One other effect on crack spacing was detected in the analysis of steel stresses. As shown in Figure 4, the predicted steel stress at the crack was directly proportional to concrete strength. For a constant crack spacing, steel stress was expected to (a) decrease as the concrete shrinkage and thermal coefficients decreased and (b) increase as the concrete strength increased. This result occurred as concrete shrinkage decreased for the high concrete thermal coefficient but not for the low value. These results occur because of the interaction of crack width and crack spacing as exhibited in Figure 3. In reviewing the results, the interactive effects of crack spacing, crack width, and steel stress cannot be optimized separately to achieve a zero-maintenance pavement. This analysis indicated that crack spacing was a very influential response parameter for a CRCP. The effects of material properties were not separable from their effects on crack width and steel stress.

In general, the material properties at the high level produced values of response parameters outside the recommended range developed from field studies to ensure zero-maintenance service. The combination of high concrete strength, low shrinkage, and low thermal coefficient produced crack spacings greater than 6.1 m (20 ft). The combinations of high concrete strength, high thermal coefficient, and both low and high levels of concrete shrinkage resulted in equal crack spacings in all zones. However, the crack widths and steel stresses for these combinations with high shrinkage greatly exceeded the recommended limits in all zones. The crack widths and steel stresses for the combination with low concrete

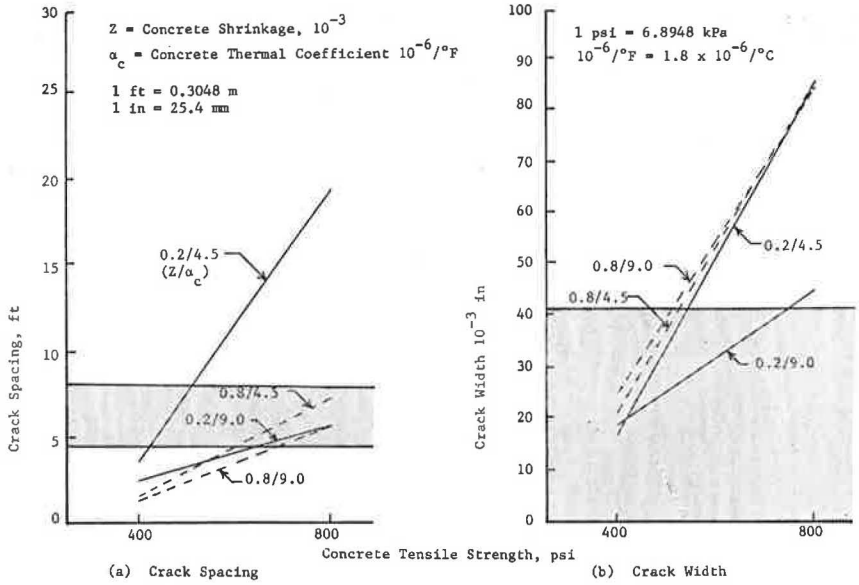

Figure 3. Effects of concrete strength and shrinkage characteristics on crack spacing and crack width in the wet-freeze zone.

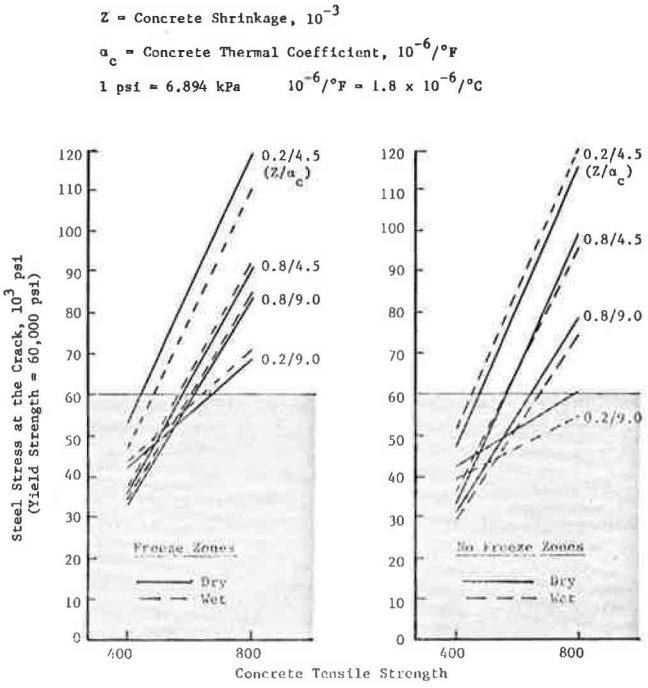

Figure 4. Effects on concrete strength, shrinkage, and thermal coefficients on steel stress at the crack for CRCP.

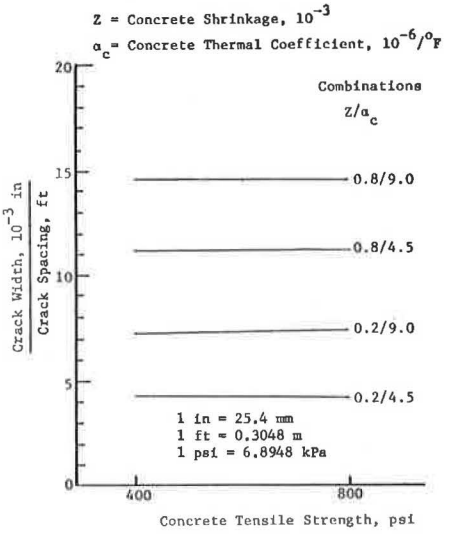

Figure 5. Effects of material property variables on crack width by crack spacing for the dry-freeze zone.

shrinkage fell within the recommended limits in all but the WF zone.

For the combination with all material properties at the low level, the response criteria were satisfied in all but the WF zone. For this zone, the crack spacing was closer than the recommended limit to prevent punchouts.

Second-Stage Study

A second set of material property combinations included steel reinforcement at 0.75 and 0.9 percent, ultimate concrete tensile strengths between 3.1 and 4.1 MPa (450 and 600 psi), and a steel thermal coefficient between 9.0 and 10.8 x 10^{-6}/°C (5.0 and 6.0 x 10^{-6}/°F).

The crack spacing, crack width, and steel stress decreased as the percentage of steel increased. Inspection of the results for higher percentages of steel showed that the calculated crack spacings were smaller than the punchout-limiting criterion of 1.54 m (4.4 ft). The concrete strength was high enough to resist the higher stresses produced by the increased restraint of the additional steel.

The results from this two-stage analysis that came closest to meeting the established zero-maintenance distress criteria are plotted in Figures 6 and 7. These results were all for a constant 0.6 percent steel. No material property combination investigated produced acceptable results for all four zones. Combination 1, which included low strength, low thermal coefficient, and low shrinkage satisfied the required criteria in all but the WF zone. In that zone, the crack spacing dropped below the required level. Combination 2 (Figure 6) met the crack-spacing and crack-width criteria for only the two freeze zones. The steel stresses for combination 2 exceeded yield strength in all zones. Combination 3 met all three criteria only in the no-freeze zones, while both crack width and steel stress exceeded the required limits in the freeze zones.

Figure 6. Summary of crack spacing and crack width with regions of acceptability for zero-maintenance pavements.

Material Properties	POINT NUMBERS		
	1	2	3
Tensile Strength, psi	400	550	800
Thermal Coefficient/°F	4.5×10^{-6}	5.0×10^{-6}	9.0×10^{-6}
Concrete Shrinkage	.0002	.0004	.0002

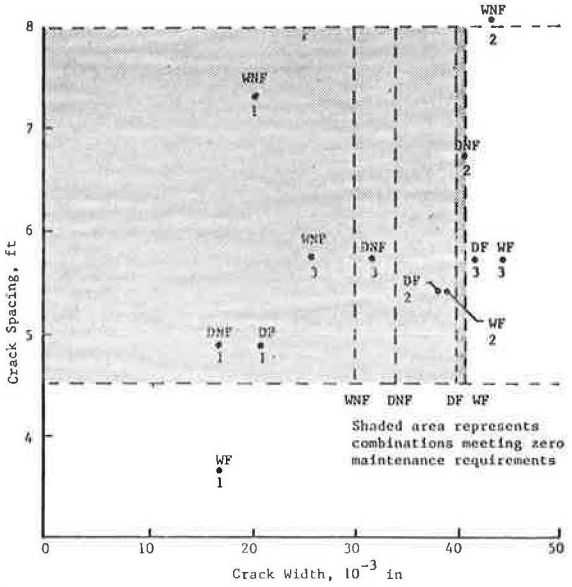

WF: Wet-Freeze Zone
DF: Dry-Freeze Zone
WNF: Wet/No-Freeze Zone
DNF: Dry/No-Freeze Zone

1 in = 25.4 mm
1 ft = 0.3048 m
1 psi = 6.8948 kPa
10^{-6}/°F = 1.8×10^{-6}/°C

Figure 7. Summary of crack spacing and steel stresses with regions of acceptability for zero-maintenance pavements.

Material Properties	POINT NUMBERS		
	1	2	3
Tensile Strength, psi	400	550	800
Thermal Coefficient/°F	4.5×10^{-6}	5.0×10^{-6}	9.0×10^{-6}
Concrete Shrinkage	.0002	.0004	.0002

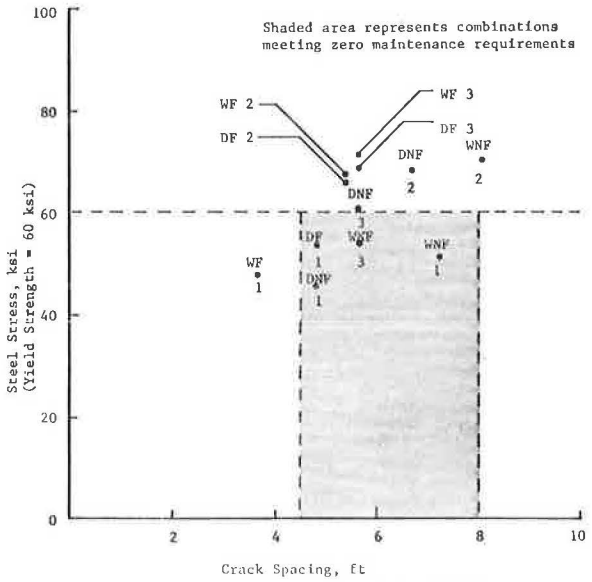

WF: Wet-Freeze Zone
DF: Dry-Freeze Zone
WNF: Wet/No-Freeze Zone
DNF: Dry/No-Freeze Zone

1 ft = 0.3048 m
1 ksi = 6894.8 kPa
10^{-6}/°F = 1.8×10^{-6}/°C

Several observations were made from these results. Combinations of material properties with a shrinkage greater than about 0.0004 yielded results outside the acceptable range. At low concrete shrinkage, the response parameters for the freeze regions approached the acceptable range when concrete strength was between 2.76 and 3.45 MPa (400 and 500 psi). The high-strength concrete was better suited for application in the no-freeze zones than in the freeze zones.

A subsequent analysis involved considering the effect on the response variables produced by changes in a material property. The response parameters used in this analysis were crack spacing and crack width. The effects on these two response parameters produced by the changes in the various material properties and percentage of steel were compared. The change in concrete strength produced the greatest change in both crack spacing and crack width. The second most influential material property was the thermal coefficient of concrete. Changes in both crack spacing and crack width were inversely related to changes in this coefficient. The concrete shrinkage was inversely related to crack spacing and directly related to crack width. Changes in steel percentage produced greater changes in both crack width and crack spacing than did changes in either the thermal coefficient or shrinkage. Crack spacing and crack width were inversely related to steel percentage.

The order of influence of material properties investigated, starting with the most influential, was concrete strength, thermal coefficient, and shrinkage. A CRCP with 0.6 percent steel combined with a concrete of sufficient thickness and a tensile strength of 3.45-3.79 MPa (500-550 psi), a thermal coefficient of 8.1-9.0 x 10^{-6}/°C (4.5-5.0 x 10^{-6}/°F), and a concrete shrinkage equal to or less than 0.0004 will provide performance compatible with zero-maintenance requirements.

In this study, concrete tensile strengths greater than 3.79 MPa (550 psi) produced steel stresses in excess of yield.

CONCLUSION

The CRCP structure investigated in this study exhibited excellent resistance to fatigue cracking. Only the combinations with (a) low subbase modulus of elasticity and low fatigue and (b) both low and intermediate concrete modulus of elasticity did not meet the zero-maintenance requirements. Other combinations carried traffic for 20 years without the occurrence of class 3 and class 4 cracking. This analysis showed that the subbase modulus of elasticity had a more significant effect on increased fatigue life than did improvements in PCC.

The low-temperature and shrinkage cracking analysis indicated that concrete tensile strength was the most influential material property in this distress. The thermal coefficient and shrinkage of the concrete were less influential than the amount of steel reinforcement, which is a design factor rather than a material property.

The set of material properties derived from the various distress-model studies that were identified as minimizing distress are noted below:

1. PCC modulus of elasticity = 34 million kPa (5.0 million psi) < E_c < 41 million kPa (6 million psi);
2. PCC indirect tensile strength = 3445 kPa (500 psi) < f_t < 3790 kPa (550 psi);
3. PCC thermal coefficient = 8.1 x 10^{-6}/°C < α_c < 9.0 x 10^{-6}/°C (4.5 x 10^{-6}/°F) < α_c < 5.0 x 10^{-6}/°F);
4. Ultimate concrete shrinkage = Z < 0.004; and
5. Subbase modulus of elasticity = E_s > 6.9 million kPa (1.0 million psi).

The relationship among these properties forms a set of properties consistent with conventional PCC. The level of

the tensile strength that corresponds to the modulus of elasticity of PCC determined from the fatigue analysis falls within the bounds determined from the low-temperature and shrinkage analysis. The lower bound on the tensile strength selected from the low-temperature and shrinkage analysis is greater than the minimum tensile strength indicated by the examination of spalling information. Thus, the set of material properties listed above may be considered an optimal combination of material properties for a premium CRCP designed with the pavement components that are described in the section of this paper that deals with specific inputs to distress models.

ACKNOWLEDGMENT

The work presented in this paper was accomplished by a team that included Thomas W. Kennedy, Freddy L. Roberts, Gary E. Elkins, J. Brent Rauhut, Fred N. Finn, Ralph Haas, James Ma, and Lee Jane Ream. Appreciation is extended to Carl L. Monismith for his ideas on models and for his review and discussion of distresses and material properties. Support for the project was provided by the Office of Research and Development, Federal Highway Administration. We are grateful for the technical coordination provided by Ken Clear, contract manager, and William Kenis, project manager, and for the time and effort they expended in technical discussions and meetings with project staff.

REFERENCES

1. J.B. Rauhut, F.L. Roberts, and T.W. Kennedy. Models and Significant Material Properties for Predicting Distresses in Zero-Maintenance Pavements. Austin Research Engineers, Austin, TX, Rept. FHWA-RD-78-84, Sept. 1978.
2. B.F. McCullough, A. Abou-Ayyash, W.R. Hudson, and J.P. Randall. Design of Continuously Reinforced Concrete Pavements for Highways. NCHRP, Project 1-5, 1975.
3. M.I. Darter and E.J. Barenberg. Zero-Maintenance Pavement Requirements and Capabilities of Conventional Pavement Systems. Federal Highway Administration, Interim Rept. FHWA-RD-76-105, April 1976.
4. O. Schnitter. Comparison of Stresses, Strains, and Deflections Calculated with Various Layer Programs. Univ. of Texas at Austin, Spring 1977.
5. J.C.M. Ma. CRCP-2: An Improved Computer Program for the Analysis of Continuously Reinforced Concrete Pavement. Univ. of Texas at Austin, M.Sc. thesis, Aug. 1977.
6. M.I. Darter and E.J. Barenberg. Design of Zero-Maintenance Plain-Jointed Concrete Pavement: Volume 2, Design Manual. Federal Highway Administration, Rept. FHWA-RD-77-112, June 1977.
7. H.J. Treybig, B.F. McCullough, P. Smith, and H. Von Quintus. Overlay Design and Reflection Cracking Analysis for Rigid Pavements: Volume 1, Development of New Design Criteria. Austin Research Engineers, Rept. FHWA-RD-77-66, Jan. 1978.
8. J.J. Panak and H. Matlock. A Discrete-Element Analysis for Orthogonal Slab and Grid Bridge Floor Systems. Center for Highway Research, Univ. of Texas at Austin, Res. Rept. 56-25, Aug. 1971.
9. W.R. Hudson and H. Matlock. Discontinuous Orthotropic Plates and Pavement Slabs. Center for Highway Research, Univ. of Texas at Austin, Res. Rept. 56-6, 1966.
10. K. Majidzadeh. Observations of Field Performance of Continuously Reinforced Concrete Pavements in Ohio. Ohio Department of Transportation, Columbus, Rept. OHIO-DOT-12-17, Sept. 1978.
11. J.C.M. Ma, C.S. Noble, and B.F. McCullough. Design Criteria for Continuously Reinforced Concrete Pavements. Center for Highway Research, Univ. of Texas at Austin, Res. Rept. 177-17, May 1979.

Publication of this paper sponsored by Committee on Rigid Pavement Design.

Limiting Criteria for the Design of Continuously Reinforced Concrete Pavements

B. FRANK McCULLOUGH, J. C. M. MA, AND C. S. NOBLE

The primary factors to consider in the thickness and reinforcement design for continuously reinforced concrete pavements (CRCPs) are the structural response variables—crack spacing, crack width, and maximum steel stress. They perform an important role in the outcome of the pavement's performance and can be related to the major distresses common to CRCPs. This paper describes the design-limiting criteria for these structural responses. Previous investigations of the design criteria are reviewed, and the most recently developed analytical models are studied. The basic procedures used to establish design criteria include an examination of the major distresses, such as punchout, spalling, and steel rupture, and a study of correlations between these distresses and the corresponding structural responses at appropriate levels. The procedure for use of the limiting criteria in CRCP design is outlined.

The design concept for continuously reinforced concrete pavement (CRCP) is to force cracks to form at relatively close intervals, thus controlling the tightness of the crack to provide good load transfer and prevent excessive water percolation. The frequency of cracks and the final crack width depend on a complex interaction of environmental variables, material properties, and magnitudes of applied loads. Initial cracks in the CRCP are primarily caused by critical stresses induced by the initial temperature drop and drying shrinkage of the concrete. Additional cracks may develop during application of an external load when the combined stresses of the internal and external forces exceed the concrete tensile strength. Close to 90 percent of the transverse cracks occur within one month after construction. The crack pattern will eventually reach a stabilized condition when the pavement has experienced the minimum temperature during the cold season and when most of the drying shrinkage in the concrete has occurred.

The CRCP-2 computer model (1) was designed to fully simulate the mechanistic behavior of the CRCP with respect to time and load. The model predicts the structural responses of the CRCP to environmental load and static external load from the time that initial cracks form to the time when the volumetric changes of the CRCP have stabilized. The final crack spacing, crack width, and steel stress appear to strongly influence the performance of the

CRCP because major distresses common to CRCP are highly correlated with the types of responses noted here.

In a report by Noble, McCullough, and Ma (2), relations between the significant input variables and the structural responses predicted by the CRCP-2 model are quantified by using regression techniques and are expressed as a set of nomographs. This set of design charts allows a graphic prediction of the final responses--crack spacing, crack width, and steel stress--and greatly reduces computation time and effort.

The first objective of this study is to investigate correlations between mechanisms of major distress and structural responses as predicted in works by Noble, McCullough, and Ma (2,3). Design criteria for each of the responses are then established to control and restrain distress that would otherwise adversely affect the performance of the continuous pavement.

MECHANISTIC BEHAVIOR OF CRCP

Much information concerning major distress in CRCPs can be found in studies conducted by Darter and Barenberg (4) and McCullough and others (5). The following table lists the predominant distress types found in CRCP and summarizes the frequency of occurrence and severity of the distress types in 12 projects (3,4):

Distress Type	Total Projects	Distressed	Maintained
Surface depression	12	7	0
Crack spalling	12	6	2
Punchout	12	4	4
Interconnecting cracks	12	4	2
Longitudinal cracking	12	2	0
Steel rupture	12	2	2

The information presented above was obtained from pavements that had survived for 20 years. Maintenance was applied only to the specific distress noted in the above table. Results from statewide condition surveys, along with the collected experience of prominent researchers, were used in establishing the significant distress types and rank order.

The following table shows the resulting priority ranking of distress types for CRCP in decreasing order of the significance of their effect on pavement performance:

Rank	Major Distress Type
1	Punchout
2	Crack spacing
3	Fatigue cracking
4	Low-temperature cracking
5	Shrinkage cracking
6	Steel rupture

Fatigue cracking, low-temperature cracking, and shrinkage cracking are secondary distress types that define the spacing of transverse cracks in the continuous pavement. Secondary distresses are responsible for the development of the primary distress that leads to reduction of serviceability in the pavement. Punchout, for instance, is a primary distress type that occurs between closely spaced transverse cracks that are subsequently connected by longitudinal cracks. Steel rupture is ranked last and does not usually occur in the southern United States.

Criteria for CRCP Structural Responses

The primary factors to consider in the design of CRCPs are the structural responses--crack spacing, crack width, maximum steel stress, and maximum concrete stress. They play an important role in the outcome of the pavement's performance and can be related to the major distresses discussed previously. These factors are also interrelated with each other. A design that forces cracks to form in either a narrow or wide space will affect the accumulated drag forces due to frictional restraint from the subbase and subsequently will alter the level of response of crack width, maximum steel stress, and maximum concrete stress.

Model Description

The computer program CRCP-2 (1) models the one-dimensional changes in concrete stress, steel stress, crack width, and crack spacing that occur in a CRCP and that are caused by drying shrinkage of the concrete, temperature variation, and wheel loads.

The difference in the thermal coefficients of the steel and the concrete, together with the drying shrinkage of the concrete, enables us to determine the internal stress in the reinforced slab. By using the friction-movement characteristic of the slab and the soil, as determined in laboratory experiments, the degree of restraint due to the soil frictional resistance can be estimated (1). By assuming equilibrium in the system, the stress of one material can be computed in terms of the stress of the adjacent materials. Finally, an incremental approach can be adopted to predict the formation of transverse cracks as a function of time by comparing the historical changes of the concrete stress with the strength of the concrete. A complete list of the assumptions made during the development of the model appears in Ma, McCullough, and Noble (3).

Structural Responses of CRCP

The transverse cracking in a continuous pavement is the result of the restraint of the pavement slab induced by internal environmental forces and external wheel-load forces. Most transverse cracks occur at an early age of the pavement when most of the moisture evaporation takes place. Additional cracks may later develop if the stress, which has been increased by the wheel-load application, exceeds the fatigue strength of the concrete.

Spacing of transverse cracks that occur in CRCPs is perhaps the most important variable directly affecting the behavior of the pavement. Relatively large distances between cracks result in a higher accumulated drag force due to frictional resistance from the subgrade, thus producing high steel stress at the crack and large crack width. Closer crack spacing reduces the frictional restraint and, thus, the steel stress and crack width. It is clear that the crack spacing is directly related to other responses such as steel stress and crack width. Control of one will immediately affect the behavior of the others. In general, assuming adequate foundation support, closely spaced cracks in CRCP are desirable because the steel stress and the crack width will be small. However, it is commonly known that the major distress observed on in-service CRCP is punchout, which can be associated with the combination of closely spaced transverse and longitudinal cracking. An optimum design, therefore, calls for a balance in all of the structural responses in the continuous pavement.

Failures in CRCP are usually manifested as isolated areas of premature distress in different forms (according to environment) such as steel rupture, excessive spalling at the crack, edge pumping, and punchout. Among the distresses, some can be associated with poor subbase and drainage (these are outside of the scope of this report), although others can be linked directly to the above pavement responses. As stated earlier, punchout is associated with transverse crack spacing in the continuous pavement. Narrow crack spacing, when combined with crack deterioration, will force the beam action of the continuous pavement to act transversely instead of longitudinally. Transverse beam action will, in turn, cause longitudinal cracks to appear and eventual deterioration into punchout failure. Punchout, therefore, can be alleviated by controlling the crack spacing of the continuous pavement while maintaining adequate foundation support. Similarly,

other failures, including spalling and steel rupture, can be controlled by tracing the origin of the distress mechanism and by assigning design criteria to the corresponding pavement responses.

Previous Design Criteria

Contemporary procedures for the design of CRCP are summarized in the AASHTO Interim Guide for the Design of Pavement Structures (6) and in the Texas State Department of Highways and Public Transportation Operations and Procedures Manual (7). These procedures are based on early developments in the modeling of CRCP behavior, and, as such, they restrict steel stress to values below yield. However, they do not consider other variables that have a significant effect on performance, such as crack width and spacing. More recent work (1,5) established newer design criteria for use with the computer program design approach. It is the purpose of this report to outline criteria for use in conjunction with the nomograph (regression equation) design techniques outlined in Noble, McCullough, and Ma (2).

DESIGN CRITERIA FOR CRACK SPACING

A CRCP can be simulated as a series of continuous beams resting on an elastic foundation. Transverse cracks develop as a result of frictional restraint of the slab against changes caused by shrinkage and temperature drop. Additional cracks due to bending in the longitudinal direction may develop when traffic loads are applied. As transverse crack spacing becomes relatively narrow and when load transfer at the crack deteriorates, the pavement structure no longer responds as a longitudinal beam. Rather, it responds as a transverse beam with stress in the transverse direction higher than that in the longitudinal direction. With further increase of fatigue loadings, longitudinal cracks crossing the transverse cracks will develop and eventually will deteriorate into punchout failure. One critical crack spacing, therefore, is the spacing at which the stress in the transverse direction becomes dominant.

Effect of Crack Spacing on Transverse and Longitudinal Stresses

The relation between crack spacing and stresses in the X-X and Y-Y directions is illustrated in Figure 1. Solid lines in the figure represent the relation for the condition of zero load transfer at the crack. For a crack spacing greater than B, the pavement slab acts as a longitudinal beam, and the stress in the X-X direction is more critical because it becomes larger than that in the Y-Y direction. The reverse is true for a crack spacing less than B, because the slab acts as a transverse beam. The spacing between cracks in the continuous slab can be thought of as the span length of a rectangular plate on an elastic foundation. Increase in crack spacing or span length will result in higher σ_x and lower σ_y. The increase in bending stress will gradually diminish as movement farther away from the midspan occurs--where the load was applied. The stress in the X-X direction remains constant after reaching the maximum level. The crack spacing B at the intersection of the σ_x and the σ_y curve is, therefore, the minimum allowable crack spacing for zero load transfer at the crack if σ_x is to control.

Figure 1. Illustration of critical stress location as affected by crack spacing for a given set of conditions.

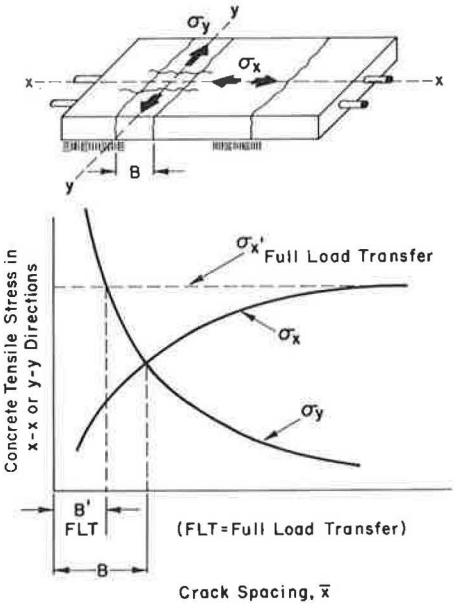

For full load transfer conditions, the pavement can be viewed as a continuous slab with no cracks. The σ'_x at the crack spacing under the full load transfer conditions, therefore, should be equal to the σ_x for an infinitely long slab. The horizontal dashed line in Figure 1 represents the stress in the X-X direction σ'_x for an infinitely long slab or one with full load transfer conditions at the cracks. It is obtained by drawing a line tangent to the point of maximum stress, which occurs when the slab length no longer influences the stress. The length B' is derived from the intersection of the σ'_x line and σ_y curve, and it represents the minimum allowable crack width for full load transfer. Thus, B' is the minimum crack spacing for full load transfer if σ_x is to control, and B is the minimum for zero load transfer as discussed above. In-service CRCP has a condition between these two extremes because it is closer to full transfer after construction and decreases with repeated load application.

Effect of Stiffness Reduction at the Crack

Load transfer at the crack is possible through moment transfer, granular interlock, and dowel action of the steel reinforcement, assuming adequate foundation support. In field conditions, neither full nor zero load transfer at the crack are likely to be found. Theoretically, if the granular interlock and dowel action of the reinforcing bars are 100 percent efficient, half the applied load will be transferred across the crack to the adjacent slab. This is true only if the same amount of deflection occurs on both slabs and each assumes half of the applied load. However, considering a certain amount of debonding of the steel and looseness that develops in the aggregates under repeated loads, a further reduction in load transfer of between 5 and 10 percent can be assumed (8). Thus, the design load transfer due to aggregate interlock and dowel action of the steel should be 45 percent of the design load.

Under vertical load, deflection of the slab at the crack will cause the crack width to decrease. Moment transfer occurs only when the slab segments at both sides of the crack are in contact. The amount of reduction in handling stiffness at the crack depends on a combination of design variables. Abou-Ayyash and Hudson (9) studied the effect of transverse cracks on the bending rigidity of continuous pavement. Figure 2 (9) shows the result of the investigation in which the percentage reduction in bending stiffness at the crack is related to the concrete compressive strength and to the percentage of longitudinal reinforcement for a given set of environmental conditions.

Crack Effect on Allowable Crack Spacing

Assuming that a linear relation exists between the structural response of the slab as affected by the load transfer at the crack and the spacing between cracks, allowable crack spacing for cracks with various degrees of load transfer capacities can be predicted. For example, if

Figure 2. Variation of the percentage reduction in bending stiffness at crack loaction with longitudinal percentage reinforcement.

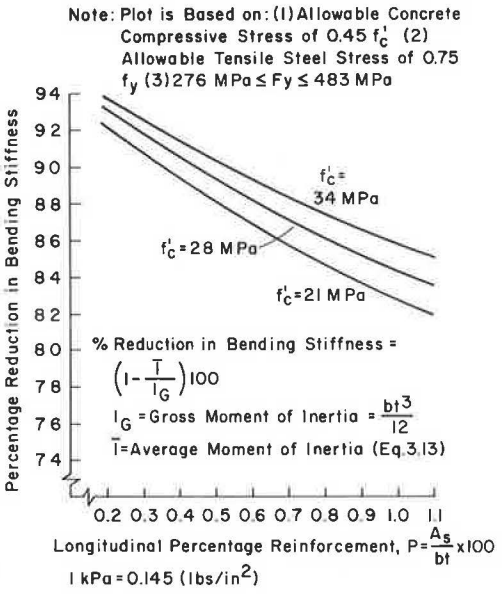

Figure 3. Variation of transverse and longitudinal concrete stresses with crack spacing for various axle loads.

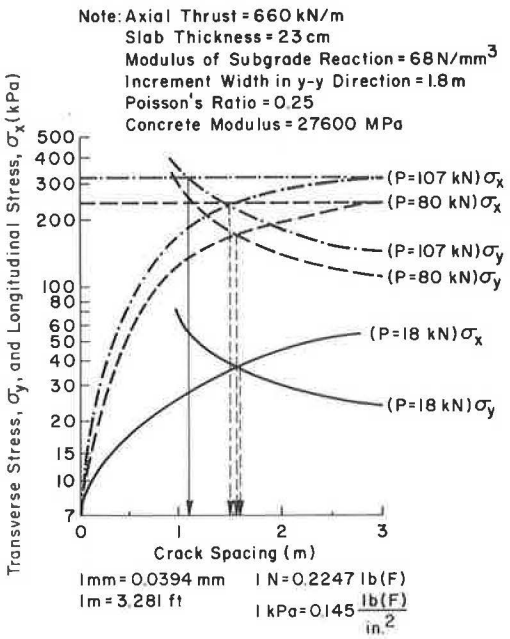

cracks in the slab can provide half of the structural integrity of the uncracked section, the critical crack spacing will be at the midpoint between B and B' in Figure 1.

Prediction of Allowable Crack-Spacing Range

Concrete Tensile Stress Condition

The SLAB-49 program (10,11) provides an excellent analysis tool for studying the effect of crack spacing on continuity and provides a basis for choosing a minimum crack spacing. The logic and procedures used herein are documented in the appendix to the work by Ma, McCullough, and Noble (3). In order to obtain a limiting (minimum) value for crack spacing, a factorial of representative values of the design

Figure 4. Variation in transverse and longitudinal concrete stresses with crack spacing for various slab thicknesses.

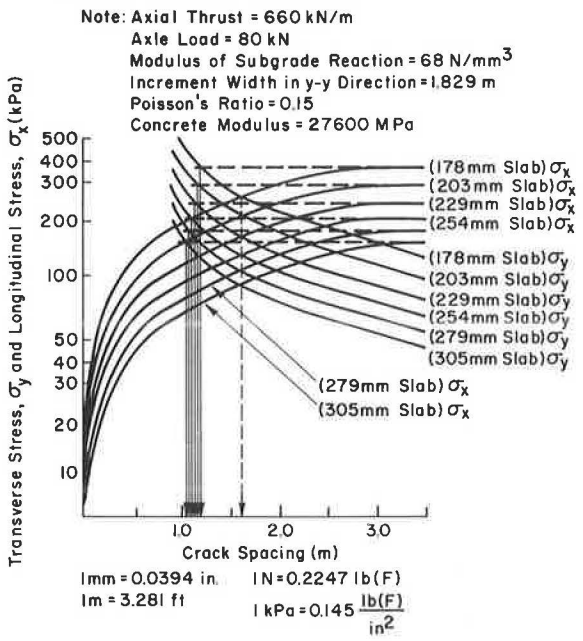

variables (3) was evaluated by using the SLAB-49 program. The magnitudes of the variables cover a broad range of slab thicknesses, axle loads, and crack spacings. Both longitudinal and transverse stresses with respect to crack spacing were computed (3) and plotted for various axle loads and slab thicknesses (Figures 3 and 4). The minimum allowable crack spacing B' is determined at the intersection of the σ'_x line and the σ_y curve. Allowance for reduced bending stiffness is made as indicated above (Figure 2).

Criterion of Bond Development Length

As discussed in Ma (1), the required length for full development of the bond between the reinforcing steel and the concrete in CRCP must be kept below a value equal to one-half the crack spacing. This bond development length, however, can be calculated in terms of the change in steel stress between the crack location and midspan (3), as movement occurs longitudinally down the concrete slab--that is,

$$\bar{x} \geq 2b \quad (1a)$$

and

$$b = (\Phi^2/38\sqrt{f'_c})(\sigma_{sc} - \sigma_{sm}) \quad (1b)$$

where

b = required bond development length,
Φ = bar diameter,
f'_c = concrete compressive strength,
σ_{sc} = steel stress at the crack, and
σ_{sm} = steel stress at midspan (3).

The maximum required value of b likely to be encountered in practice, then, is that for a low-strength concrete, a large bar diameter, zero steel stress at midspan, and a steel stress at the crack of just less than yield. If $\Phi \leq 19.1$ mm (0.75 in), $f'_c \geq 17\,240$ kPa (2500 psi), $\sigma_{sc} \leq 413\,700$ kPa (60 000 psi), and $\sigma_{sm} > 0$, then $b \leq 602$ mm (23.7 in) and $\bar{x} \geq 1.22$ m (4 ft).

Thus, because the maximum required length for full bond development is less than 0.61 m (2 ft), the minimum

Table 1. Effect of limited crack spacing on fraction of spalled cracks.

Maximum Allowable Crack Spacing (m)	Spalled Cracks (%)	Probability That < p Percent of Cracks Will Spall (%)
3.048	50	92
	40	86
	30	78
	20	58
2.743	50	93
	40	89
	30	79
	20	58
2.438	50	94
	40	90
	30	78
	20	61
2.134	50	94
	40	90
	30	80
	20	62
1.829	50	98
	40	96
	30	84
	20	66

Note: 1 m = 3.281 ft.

allowable crack spacing in this case is 1.22 m (4 ft). In general, this value may be used as a lower bound on crack spacing for all CRCP designs unless excessively large reinforcing bars—that is, 19.1 m (0.75 in)—are used in combination with very low-strength concrete [$f'_c \leq 17$ MPa (2500 psi)], which, of course, is very unlikely. However, in practice, the designer should calculate the lower bound on $\bar{x}$ peculiar to the design situation by using the procedure detailed above. In most cases, this value will be on the order of 0.9 m (3 ft).

Spalling (Condition Survey) Criterion

A scattergram of percent spalled cracks against crack spacing was plotted (3) by using data from the 1978 Texas CRCP condition survey (12). Based on this large sample of 212 observations taken from sections of CRCP all over the state, recommendations as to an upper bound on crack spacing can be safely made (Table 1). No allowance has been made here for regional or local variation because it is thought that separate estimates of the reliabilities for each district would not differ significantly from those listed in Table 1. From Table 1, it is clear that, if a designer wished to restrict the fraction of spalled cracks to less than 40 percent, this could be done with 90 percent confidence of restricting crack spacing to no more than 2.4 m (8 ft). However, if a designer wished to restrict this fraction further (for example, to less than 30 percent), the reliability of the design drops to 84 percent, even if the crack spacing were limited to no more than 1.8 m (6 ft).

Allowable Range

An allowable range of crack spacing can be obtained by any CRCP designer by choosing a maximum allowable value from the spalling criterion, along with a minimum allowable value from the criteria for concrete tensile stress and bond development length.

DESIGN CRITERIA FOR CRACK WIDTH

Design criteria for crack width are established from the standpoints of controlling both water flow and spalling. In considering the water flow problem, the design criteria are developed by limiting the permanent crack width for the continuous pavement. Because permanent crack width is related to the deformation of reinforcing steel at the crack, it will be discussed in both this section and the section on design criteria for steel stress.

Crack Width Criteria Based on Spalling Measurements

Spalling in CRCP

Spalling (i.e., minor or deflection spalling) is one of the distresses in CRCP. The primary causes for spalling are believed to be

1. Entrapment of road debris in cracks, which causes stress concentration when the cracks close as temperature increases;
2. Combined shear and tensile stress at joints or cracks due to horizontal temperature loading and vertical traffic loading; and
3. Poor material at surface due to overworking concrete during finishing.

Laboratory studies conducted by McCullough and others (5) indicated that spalling for CRCP caused by road-debris entrapment is relatively insignificant but that the combined horizontal and vertical forces produced by repeated loading seem to be the major contributors to spalling. Darter and Barenberg's study (4) on the ranking of major distresses in rigid pavements appears to corroborate McCullough's conclusions that combined horizontal and vertical forces are among the major contributors for jointed concrete pavement (JCP) and jointed reinforced concrete pavement (JRCP) as well as CRCP. Spalling occurred in 9 of 18 and 6 of 12 pavements surveyed. Because the reinforcement in both JRCP and CRCP exerts horizontal forces while resisting thermal or shrinkage volume change, higher concrete stresses generally occur in these pavements than in JCP. This action may contribute to stress concentrations that cause the spalling in these two types of pavements to be much more pronounced.

Correlation Between Crack Width and Spalling

Horizontal stresses developed in CRCP can be correlated with design parameters, such as percent reinforcement, slab thickness, concrete modulus of elasticity, concrete strength, base friction, and thermal and shrinkage coefficients. A good indicator for the amount of horizontal stress in CRCP is the crack width. In general, crack widths are directly proportional to the magnitude of horizontal stresses.

The primary spalling mechanism identified by McCullough and others (5) was the combination of horizontal and environmental stresses and stresses resulting from vertical traffic loads. Because both crack width and degree of spalling correlate highly with the horizontal stress, they should theoretically also correlate with each other. In the diagnostic study based on condition surveys of CRCP in Texas (5), crack widths were measured in the field for a temperature range of 27°-32°C (80°-90°F). The results were plotted with respect to the general condition of spalling, and it was shown that spalling increases with increased measured crack width. The mean crack width was reported to be 0.538 mm (0.0212 in) for the spalled sections and 0.447 mm (0.0176 in) for the nonspalled sections. Spalling of cracks with less than 0.51-mm (0.02-in) widths was not observed. Similar results were obtained from a set of measurements taken in Illinois (5).

Maximum Allowable Crack Width

Only 5 percent of the pavements surveyed (4,5) experienced spalling at crack widths of less than 0.61 mm (0.024 in). The 0.61-mm level is, therefore, used as the basis in the determination of the design criteria for crack width based on spalling discussed in this paper. This was confirmed when a similar value was obtained following analysis of the Illinois data (5). Note that the crack widths measured in the field surveys are temperature dependent, although the spalling occurred over a long period of time during which the pavement temperature varied widely. Accordingly, the crack width varied over a wide range of values during this

Figure 5. Variation of allowable crack width with temperature.

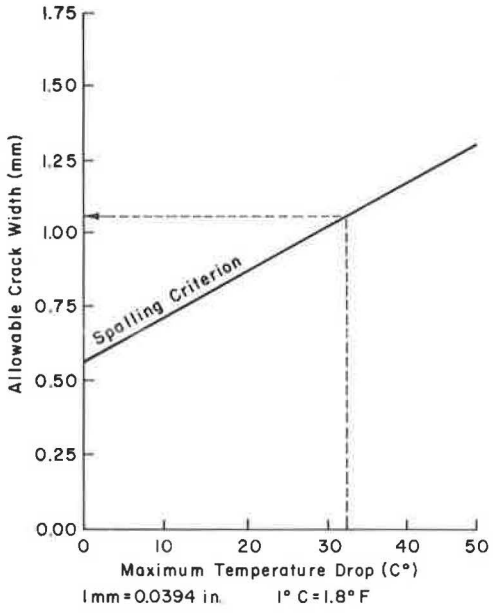

period. The curve labeled spalling criterion in Figure 5 characterizes this variation for the range of temperatures applicable to the surveyed pavements. Hence, Figure 5 must be used in the design process described below to determine the allowable crack width for minimum temperature. First, we need to calculate the value of temperature drop in the pavement when the crack width of 0.61 mm was measured; then, by using back calculation, the critical crack width for spalling under maximum temperature drop can be found. A section of CRCP under environmental conditions similar to those of the pavements surveyed, with a crack width equal to 0.61 mm, has been used to back-calculate the critical crack widths for various temperature drops. Ma (1) and Dhamrait, Jacobsen, and Schwartz (13) describe the theoretical approach used for the calculation of the allowable crack widths for various temperature drops for the surveyed sections, with the maximum drop approximated by a mean of 33°C (60°F). Thus, the limiting (maximum) value of crack width in the CRCP recommended is 1.07 mm (0.042 in), as indicated in Figure 5. This value would then be compared with a value based on other limiting criteria and the more conservative value used in the design.

Crack Width Criteria Based on Steel Corrosion and Subgrade Erosion (Permeability) Restrictions

Corrosion in CRCP

As recognized, the purpose of steel reinforcement is to limit the crack width to a level that will (a) provide adequate load transfer, (b) control spalling, and (c) avoid excessive water percolation and, subsequently, prevent subgrade erosion and steel corrosion. The design criterion for the crack width discussed previously has already put limits on the width of the pavements' cracks in line with objectives (a) and (b).

In considering the problem of water percolation, refer to the study conducted by McCullough and others (5), which also presents the results of the research described in this paper. The relation between various crack widths and time required for water to reach different depths in the crack was plotted. Assuming a water depth of 19.1 mm (0.75 in) and a 3.7-m (12-ft) wide pavement section, the time required for water to flow across a CRCP section (for various cross slopes) can be calculated by using Manning's formula for open channel flow. Then,

$$V = (1.49/N)(R^{2/3} S^{1/2}) \quad (2)$$

where

V = mean velocity,
n = approximately 0.016 for rough concrete,
R = hydraulic radius, and
S = slope of channel bed.

The time required for water to percolate to various depths and the cross-pavement flow times were superimposed on the above plots; it was shown that a crack width of less than 0.25 mm (0.01 in) can prevent water from reaching the subgrade. In that same study (5), it was found that, for a crack width of less than 0.25 mm, virtually no rusting of the steel developed. Similarly, a study conducted by the Illinois Department of Transportation (13) also supports this observation. It was found that a crack width equal to or greater than 0.20 mm (0.008 in) has a greater potential for the occurrence of significant rusting of the reinforcing steel. Ideally, based on these studies, the steel reinforcement would be designed to control the crack width to a level of less than 0.25 mm under the most critical situation (i.e., when the temperature is lowest and the pavement is flooded). However, to design for such a criterion is highly impractical, because to keep crack width at such a level will require an exorbitant amount of steel and will cause excessive cracking. Also, such a restriction is unnecessarily conservative, because this most critical situation occurs for only a small fraction of each year of pavement life. Consequently, by using the procedure discussed in the following paragraph, the designer should be able to choose the maximum crack width that is within a sensible range of values and yet keep the steel corrosion caused by any water that may reach the steel down to an acceptable level.

Maximum Allowable Crack Width

McCullough and others (5) relate the quantity of flow of water into the crack (permeability in gallons per minute per inch of crack as determined by measured headloss in ponded water) to crack width and to degree of steel corrosion and subgrade erosion. The permeability of cracks below the 0.25-mm level is really quite small (resulting in minor corrosion only), but the permeability of cracks and associated corrosion between the 0.25-mm and the 0.64-mm (0.025-in) levels are only slightly larger. However, above the 0.64-mm level, the cracks are extremely permeable, with substantial quantities of water flowing into the pavement and subsequent heavy corrosion and subgrade erosion occurring. Accordingly, for design purposes, if the pavement were to be continuously flooded and kept constantly at a temperature just above freezing, crack width would have to be kept below the 0.64-mm level.

Yet, because neither of these two extreme conditions is likely to occur constantly throughout the entire life of the pavement, the value of 0.64 mm should be adjusted accordingly. By examining the distribution of maximum daily temperature drops from curing temperature in any one year, the value of temperature drop from curing that will not be exceeded a chosen fraction of the time (usually 95 percent) may be calculated. The technique for calculation of change in crack width with change in temperature, which was discussed for the spalling restriction, should be applied. This would involve preparing a chart similar to Figure 5. It is important to note that the designer should obtain climatological data, a temperature distribution, and a crack width-temperature plot appropriate to the environment of the particular pavement being designed.

Maximum Crack Width for Design

The lower of the two maximum allowable crack widths, as recommended by the spalling and permeability restrictions, should be chosen as the design maximum crack width.

DESIGN CRITERIA FOR STEEL STRESS

Two criteria are used to define the allowable steel stress in CRCP. First, the steel stress must be lower than its ultimate tensile strength divided by a safety factor. This criterion is to safeguard against rupturing of the steel under high tension. Second, if the steel stress is to be greater than yield, permanent crack width associated with the permanent deformation of steel at the crack must be less than the allowable amount to avoid excessive water percolation.

Criteria for Steel Rupture

To guard against rupturing of the steel, the allowable stress in steel is set to be less than ultimate strength times a safety factor of 0.75. Table 2 (6) shows the ultimate strength for various types of deformed bars and their allowable stress against rupture.

Criteria for Permanent Deformation

Conventional design criteria for steel stress generally require that the stress be less than the yield strength times a safety factor. Such criteria prevent the steel from undergoing plastic deformation. Based on our experience, however, we know that many kilometers of CRCPs have been performing adequately although their steel stresses are predicted to be higher than yield. This prompts us to consider the adequacy of such steel stress limits as criteria by evaluating the response of steel reinforcement in the CRCP, when stressed beyond the elastic range. Less-conservative criteria can then be obtained by evaluating the maximum stress in the steel in terms of its permanent deformation, which is equal to crack width at the point of maximum stress. The maximum allowable steel stress is thus calculated by keeping the crack width below some suitable value.

Table 2. Maximum allowable steel stress to prevent rupture in CRCP.

Steel and Grade Type	Minimum Yield Strength, f_y (MPa)	Ultimate Strength, f_u (MPa)	Allowable Stress, f_s (MPa)
Billet			
Grade 40	276	414	362
Grade 60	345	621	465
Grade 75	690	690	517
Rail			
Grade 50	345	552	414
Grade 60	414	621	465

Note: 1 MPa = 145 psi.

Figure 6. Free-body diagram and stress distribution in CRCP model.

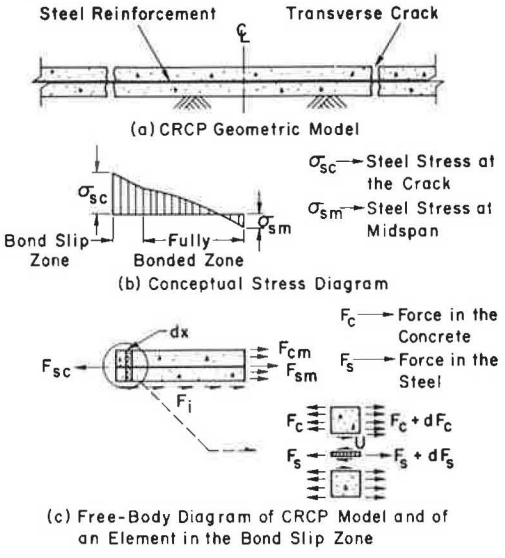

Evaluation of Permanent Deformation of Steel

Plastic deformation of steel in CRCP can be determined by multiplying the plastic strain at the crack by a defined gauge length. The gauge length at which the steel undergoes plastic deformation can be approximated as the length of the region in the bond slip zone where steel stress is above yield. To estimate the gauge length, it is necessary to review the basic CRCP model.

Figure 6 shows a steel stress distribution diagram for a CRCP section under the effect of volumetric change. At the crack, because concrete provides no resistance, the steel tension is at maximum. Moving away from the crack, a decreasing amount of tension force will be carried by the concrete, thus reducing the tensile stress in the steel. The rate of change in stress or the slope of the stress diagram at the bond slip zone depends on the bond strength between the steel and the concrete. The rate of change in steel stress can be determined by summing the forces acting on the steel bar. From Figure 6c at the bond slip zone, $F_S + dF_S = F_S + Udx$; by combining terms and solving for U, $U = dF_S/dx$, where U = average bond force per unit length of bar. The average bond force may also be expressed as

$$U = UE_o \tag{3}$$

where

u = shear strength = $9.5\sqrt{f'_c}/\Phi$,
f'_c = concrete compressive strength,
E_O = bar perimeter, and
Φ = bar diameter.

By equating the expression that solves for U and Equation 3 for average bond force and converting to stress, the following are obtained:

$$\Delta_s d\sigma_s/dx = uE_o \tag{4a}$$

$$(\pi\Phi^2/4) \cdot (d\sigma_s/dx) = u\pi\Phi \tag{4b}$$

$$d\sigma_s/dx = 4u/\Phi \tag{4c}$$

Knowing the slope of the steel stress diagram at the bond slip zone, the gauge length ℓ can be estimated as

$$\ell = 2 \cdot [(\sigma_{sc} - \sigma_{yield} \times SF)/d\sigma_{s/dx}] \tag{5a}$$

$$\ell = 2[(\Phi/4u)(\sigma_{sc} - \sigma_{yield} \times SF)] \tag{5b}$$

$$\ell = (\Phi^2/19\sqrt{f'_c}) \times (\sigma_{sc} - \sigma_{yield} \times 0.75) \tag{5c}$$

By approximating the plastic strain E_p to be σ_{yield}/E_S, the amount of permanent deformation Δx in the steel becomes

$$\Delta x = 2\ell(\sigma_{yield}/E_s) = (\Phi^2/19\sqrt{f'_c})(\sigma_{sc} - \sigma_{yield} \times 0.75)(\sigma_{yield}/E_s) \tag{6}$$

Prediction of Allowable Steel Stress

For permanent deformation of less than 0.25 mm (0.01 in), the maximum allowable steel stress at the crack can be obtained by setting Δx in Equation 7 equal to 0.25 mm so that

$$0.25 = (\Phi^2/19\sqrt{f'_c})(\sigma_{max} - \sigma_{yield} \times 0.75) \cdot (\sigma_{yield}/E_s) \tag{7a}$$

thus,

$$\sigma_{max} = (19E_s\sqrt{f'_c}/\Phi^2\sigma_y) + (\sigma_y \times 0.75) \quad (7b)$$

where σ_{max} = allowable steel stress and σ_y = steel yield stress.

Table 3 summarizes the maximum allowable steel stress for various bar diameters and steel yield strengths for low-strength [$f'_c < 24$ MPa (3500 psi)] and regular-strength [24 MPa (3500 psi) $\leq f'_c$] concretes.

Maximum Steel Stress for Design

The limiting value on steel stress to be used in design should be chosen as the lower of the maximum allowable steel stresses recommended in Tables 2 and 3. That is, the maximum recommendation from the steel rupture and permanent deformation criteria should be used.

USE OF LIMITING CRITERIA

The results from this study are presented in this paper and in Ma, McCullough, and Noble (3), which are to be used in conjunction with Nomographs for the Design of CRCP Steel Reinforcement (2). In that report, the relationship between the significant input variables and the structural responses predicted by the CRCP-2 model is quantified by using regression techniques and is expressed as a set of nomographs. This set of design charts permits graphic prediction of the final responses of the pavement to the total load. Crack spacing, crack width, and steel stress are predicted. It should be noted that the CRCP-2 model only simulates the loading conditions of environmental force and bending stress under application of a single wheel load. It should also be noted that fatigue cracking caused by the combination of repetitive wheel loads and reduction of tensile strength due to fatiguing of the concrete material was not considered in Noble, McCullough, and Ma (2). However, it is proposed to treat fatigue in the design process by following the procedure for CRCP thickness and reinforcement design outlined in that report and summarized here. The major steps in this design process are as follows:

1. Determine the design slab thickness on the basis of fatigue analysis alone (3, section on Guidelines for Selection of Design Input Variables);
2. By using this slab thickness and chosen values of the other trial input variables, predict the final crack spacing, crack width, and steel stress by means of the nomographs in Noble, McCullough, and Ma (2);
3. Check the predicted responses by means of the design criteria established in this paper and in Chapters 3, 4, and 5 of Ma, McCullough, and Noble (3);
4. If the predicted responses exceed the allowable criteria, lower or raise the level of design variables according to the general behavior of the CRCP as discussed in this paper and in Chapter 2 of Ma, McCullough, and Noble (3); and
5. If changes in input variables involve a change in slab thickness or concrete flexural strength, repeat step 1.

Table 3. Maximum allowable steel stress for control of permanent deformation.

Steel Yield Strength, f_y (MPa)	Steel Bar Diameter, ϕ (mm)	Maximum Allowable Steel Stress (MPa) and Concrete Compressive Strength, f'_c (MPa)	
		Low[a] ($f'_c < 24$ MPa)	Regular[b] ($f'_c \geq 24$ MPa)
276	13	415	447
	16	340	378
	19	299	326
	22	275	294
345	13	425	474
	16	365	396
	19	332	354
	22	313	329
414	13	449	489
	16	399	425
	19	371	390
	22	356	369
517	13	498	531
	16	459	479
	19	402	452
	22	390	434

Note: 1 MPa = 145 psi; 1 mm = 0.0394 in.

[a] Low = ≥4.5 percent air content or ≤4 cement sacks/yd^3 concrete.
[b] Regular = ≤4.5 percent air content and >4 cement sacks/yd^3 concrete.

CONCLUSIONS AND RECOMMENDATIONS

By establishing values for input variables by means of the procedures discussed above, the design of steel reinforcement for a CRCP can be performed by following the procedure that is outlined in Chapter 5 of Noble, McCullough, and Ma (2). Limiting criteria are also to be used in this process as described above and in Chapters 3, 4, and 5 of Ma, McCullough, and Noble (3).

The limiting criteria on crack spacing, crack width, and steel stress discussed in this report represent part of the only national, comprehensive, and easy-to-use procedure for the design of CRCP available at this time. It is strongly recommended, therefore, that the entire procedure summarized in this paper and detailed elsewhere (2,3) be incorporated into appropriate CRCP design manuals as soon as possible.

ACKNOWLEDGMENT

The material presented in this paper is part of the research on Development and Implementation of the Design, Construction, and Rehabilitation of Rigid Pavements conducted by the Center for Transportation Research, the University of Texas at Austin, the Texas State Department of Highways and Public Transportation (SDHPT), and the Federal Highway Administration (FHWA). The contents of this report reflect our views. We are responsible for the facts and the accuracy of the data presented herein. The contents do not necessarily reflect the official views or policies of the Texas SDHPT or FHWA. This report does not constitute a standard, specification, or regulation.

REFERENCES

1. J.C.M. Ma. CRCP-2: An Improved Computer Program for the Analysis of Continuously Reinforced Concrete Pavements. Center for Highway Research, Univ. of Texas at Austin, Research Rept. 177-9, Aug. 1977.
2. C.S. Noble, B. F. McCullough, and J.C.M. Ma. Nomographs for the Design of CRCP Steel Reinforcement. Center for Highway Research, Univ. of Texas at Austin, Research Rept. 177-16, Aug. 1979.
3. J.C.M. Ma, B.F. McCullough, and C.S. Noble. Limiting Criteria for the Design of CRCP. Center for Highway Research, Univ. of Texas at Austin, Research Rept. 177-17, Aug. 1979.
4. M.I. Darter and E.J. Barenberg. Zero-Maintenance Pavement Requirements and Capabilities of Conventional Pavement Systems. Federal Highway Administration, Interim Rept. FHWA-RD-76-105, April 1976.
5. B.F. McCullough, A. Abou-Ayyash, W.R. Hudson, and J.P. Randall. Design of Continuously Reinforced Concrete Pavements for Highways. Center for Highway Research, Univ. of Texas at Austin, Aug. 1975.
6. AASHTO Interim Guide for Design of Pavement Structures. American Association of State Highway and Transportation Officials, Washington, DC, 1972.

7. Operations and Procedures Manual, Vol. 4. Highway Design Division, Texas State Department of Highways and Public Transportation, Austin, 1976.
8. P.J. Strauss, B.F. McCullough, and W.R. Hudson. Continuously Reinforced Concrete Pavement: Structural Performance and Design/Construction Variables. Center for Highway Research, Univ. of Texas at Austin, Research Rept. 177-7, May 1977.
9. A. Abou-Ayyash and W.R. Hudson. Analysis of Bending Stiffness Variation at Cracks in Continuous Pavements. Center for Highway Research, Univ. of Texas at Austin, Research Rept. 56-22, April 1972.
10. J.J. Panak and H. Matlock. A Discrete Element of Analysis for Orthogonal Slab and Grid Bridge Floor Systems. Center for Highway Research, Univ. of Texas at Austin, Research Rept. 56-25, Aug. 1971.
11. W.R. Hudson and H. Matlock. Discontinuous Orthotropic Plates and Pavement Slabs. Center for Highway Research, Univ. of Texas at Austin, Research Rept. 56-6, 1966.
12. M.G. de Velasco, B.F. McCullough, and D.W. McKenzie. Summary of Comparison of 1978 and 1974 CRCP Condition Surveys for Highways. Center for Highway Research, Univ. of Texas at Austin, Research Rept. 177-21, in preparation.
13. J.S. Dhamrait, F.K. Jacobsen, and D.R. Schwartz. Condition of Longitudinal Steel in Illinois Continuously Reinforced Concrete Pavement. Illinois Department of Transportation, Springfield, Interim Rept. IHR-36, 1973.

Publication of this paper sponsored by Committee on Rigid Pavement Design.

Nomographs for the Design of Steel Reinforcement in Continuously Reinforced Concrete Pavement

C. S. NOBLE, B. F. McCULLOUGH, AND J. C. M. MA

This study sought to develop graphic procedures (nomographs) for the design of continuously reinforced concrete pavement (CRCP) by the Texas State Department of Highways and Public Transportation for a range of specified local conditions. This set of nomographs, when used as a supplementary design tool with the CRCP-2 computer program model, will facilitate CRCP design. This will substantially reduce both the time and the cost involved in the design process, while at the same time taking into account the effect of regional and local environments. First, regression equations were developed for the prediction of three design parameters (crack spacing, crack width, and steel stress), and then principles of nomography were applied to these mathematical relations to prepare three corresponding nomographs. The choice of equations was made following multiple linear and nonlinear least-squares fits to a fractional factorial of simulated observations that were output from the CRCP-2 computer program. Theoretical models, developed at the Center for Highway Research in Austin, Texas, and variations of the three design parameters with each of the relevant input variables over the range of the simulated data were considered in deciding on the form of the regression equations. Standard-error-of-residuals and R^2 (proportion of variance explained by the regression equation) statistics were considered in the final choice of coefficients for the regression equations. Confidence prediction limits were determined by using multiple linear-regression techniques for application to nomograph predictions. A recommended procedure for the use of the nomographs with appropriate limiting criteria is outlined and an example given.

Continuously reinforced concrete pavement (CRCP) is considered a relatively new pavement type by many engineers, although it has been in use since 1921, when it was first introduced by the Bureau of Public Roads on the Columbia Pike near Arlington, Virginia. The next reported use of CRCP was in 1938, when Indiana, in cooperation with the Bureau of Public Roads, constructed an experimental pavement that involved several test sections.

The state highway departments of Indiana, Illinois, Texas, California, Mississippi, New Jersey, Michigan, Maryland, and Pennsylvania have laid other pavements of this type that have provided good service for a number of years. The oldest of these is approximately 30 years of age.

After there were several successful experiences with CRCP on experimental projects, the use of CRCP increased substantially, especially during the 1960s. Several research studies in rigid pavement design led to the development of the design procedures currently used for CRCP (1-5).

In 1972, a study under the auspices of the National Cooperative Highway Research Program (NCHRP) was conducted at the University of Texas at Austin. It comprised a review of design and construction variables, theoretical studies, field surveys, and laboratory investigations. The fundamental philosophy of this review was that, through a combination of field observations and laboratory studies, reliable procedures could be achieved to develop mathematical models that simulate CRCP field performance. Based on these mathematical models, the CRCP-1 computer program was developed to calculate the stresses in concrete and steel, crack width, and crack spacing that result from concrete volume changes due to temperature and shrinkage (6).

Generally, the engineer is encouraged to design each pavement for the soil conditions, traffic, materials, and so forth at the given site and to be wary of inappropriate boundary values and practices. However, in order to cover such a wide variety of input variables, the engineer needs a large-scale experiment to anticipate the effects of the individual variations of the variables and the variations in groups. Thus, a sensitivity analysis of the behavior of CRCP that used the CRCP-1 model (7) was conducted for the Texas State Department of Highways and Public Transportation (SDHPT). From the results of this study, the relative importance of about 15 input variables was determined in order to investigate the effect of changes in values of these variables on CRCP behavior. The list of the input variables includes steel properties, concrete properties, friction-movement relations, and temperature variations. In addition to establishing the relative importance of such variables, the study revealed several inconsistencies in the initial model at extreme boundary conditions that resulted in modification of the computer program.

The next step was to include the effect of wheel-load stresses on crack-spacing history. The NCHRP study found that heavy volumes of 18-kip (80-kN) single-axle loads resulted in reduced crack spacings (6). The study of the effect of wheel-load stress on pavement behavior and its interaction with the other input variables is discussed in Ma and McCullough (8), which describes the development of the CRCP-2 model. This development process is outlined in flowchart form in the upper part of Figure 1.

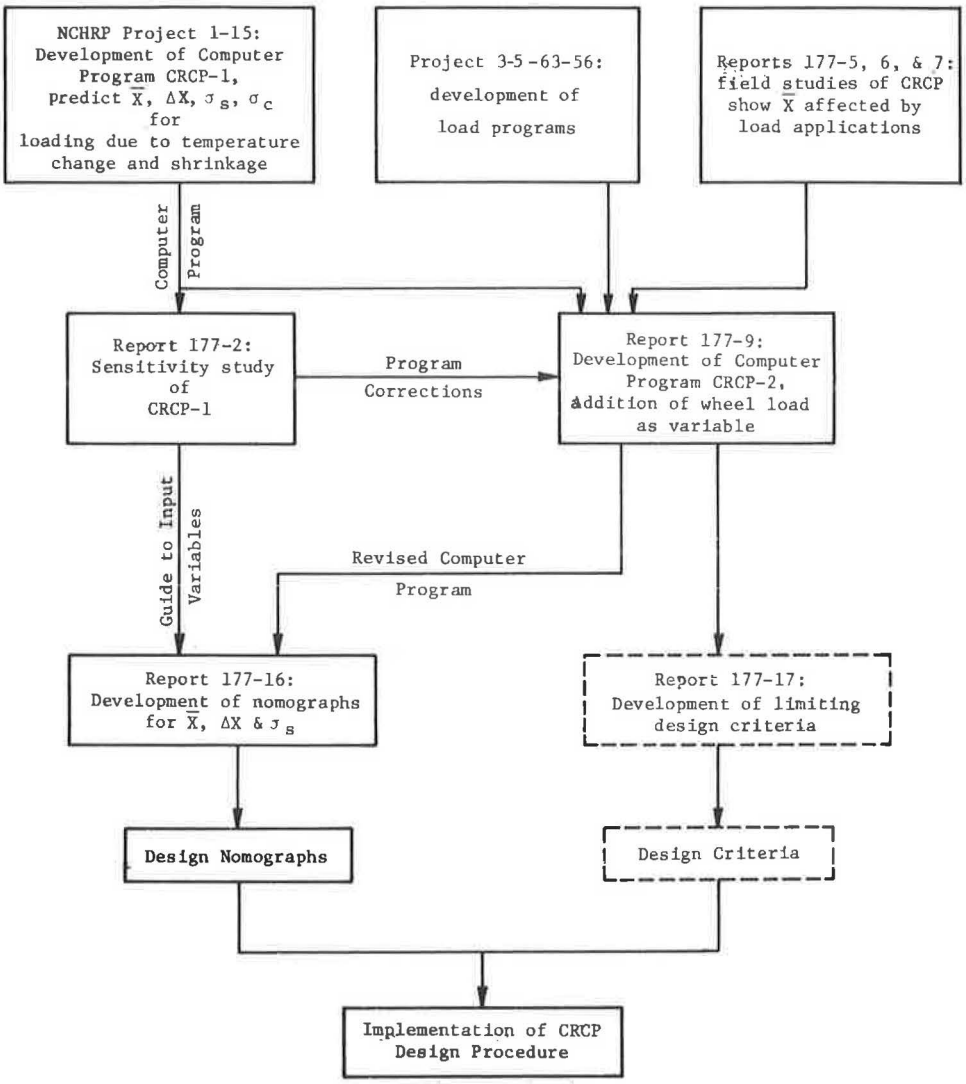

Figure 1. Flowchart related to the development of the CRCP design procedure.

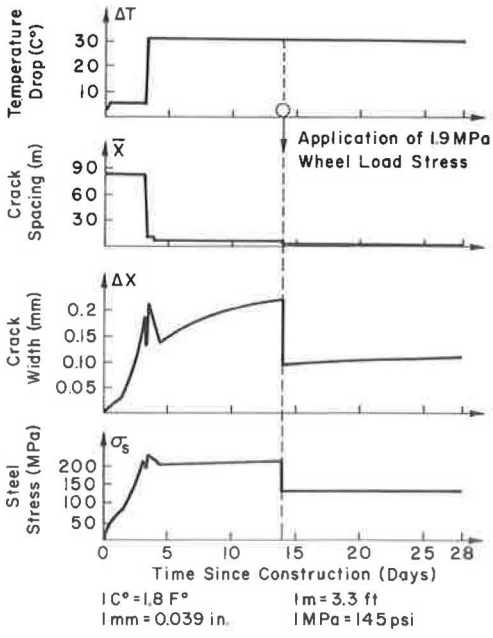

Figure 2. Time history of temperature change, crack spacing, crack width, and steel stress for a typical set of conditions.

SUMMARY CAPABILITIES OF CRCP-2

The CRCP-2 program (model) has the capability to predict the time history of crack spacing, crack width, concrete stress, and steel stress for a range of material properties, environmental conditions, and pavement-structure geometry. The concrete properties of shrinkage, strength, and stiffness and the temperature are allowed to vary with time. The remaining concrete properties, steel properties, and geometry are time invariant, with the exception that the time to the first wheel-load application may be selected.

Figure 2 shows plots of the daily temperature changes from the concrete-placement temperature, average crack spacing, steel stress, and crack-width history for a given set of conditions. The first day on which there is a 1.93-MPa (280-psi) stress that results from a wheel load placed on the pavement is also shown. These histories would vary drastically, depending on the input variables.

Thus, with established limits (i.e., design criteria) for each factor, pavement thickness and steel reinforcement may be established for the other inputs by using the computer program.

DESIGN NEEDS

In a design for estimation purposes, the need often arises for an approximate solution. Thus, the application of a detailed computer program is not necessary from the point of view of a feasibility investigation.

An alternative to this is the development of design nomographs that permit solutions for crack spacing, crack width, and steel stress after considering only the most sensitive variables and fixing the others. The designer may then obtain an approximate solution that recognizes predetermined confidence limits. At the time of final design, a more exact solution may be obtained by using the CRCP-2 computer program.

The lower portion of Figure 1 outlines the steps used in developing the design nomographs. First, a factorial computational experiment was established to obtain all relevant interactions and, hence, the basis for a statistically reliable model. Solutions of CRCP-2 were made for all the desired combinations of input variables. Regression equations were then developed that permitted solution of crack spacing, crack width, and steel stress for the most sensitive input variables. By using the regression equations, nomographs were then plotted.

STUDY OBJECTIVES

This study aimed to develop graphic (nomograph) methods for the design of CRCP that would

1. Provide sufficient steel to ensure that transverse cracks in the concrete are small enough to prevent passage of surface water downward into the underlying material and provide adequate aggregate interlock for load transfer across the crack,
2. Keep the steel stresses below the predetermined allowable values, and
3. Develop an acceptable average spacing of the transverse cracks.

Use of the nomographs will facilitate the CRCP design process by substantially reducing the time and cost involved, particularly when computer facilities are difficult to access or estimating phases of the planning process do not permit a detailed analysis.

SCOPE

This paper describes the development of a set of nomographs to be used as a supplement to the CRCP-2 computer program. The interaction, range, form, and limiting criteria for all appropriate CRCP-2 input variables are established. The significant input variables are related in mathematical and graphic models to crack spacing, crack width, and steel stress. This study quantifies these relations and presents them in graphic form (nomographs), along with boundary conditions for the appropriate inference spaces and confidence-prediction intervals.

PROBLEM AND APPROACH

In traditional CRCP design procedures, four subsystems are considered--each as an independent process. The four subsystems are (a) pavement thickness design, (b) reinforcing steel design, (c) subbase design, and (d) terminal treatment design. These subsystems are closely related, and almost the same set of variables is used for each of the procedures. Previously, these procedures were independently applied and then combined to form the resulting pavement structure (4).

The CRCP design procedures must take into account not only the stresses developed by external forces (wheel loads) but also the stresses developed by internal forces. The external forces affect pavement thickness and subbase design, and the internal forces affect the design of the reinforcing steel and the terminal treatment. These two aspects of the design problem must be treated together because it is the resulting interaction of these internal and external forces that affects overall pavement behavior.

Approach

The CRCP-2 program (8) models the interactions mentioned above and outputs predicted final values of crack spacing, crack width, and steel stress. Hence, the appropriate input variables for the graphic models (nomographs) were selected from the variables used as inputs to CRCP-2.

Further, in order to build the nomographs, it was necessary to quantify the relations between the significant input variables and the design parameters--crack spacing, crack width, and steel stress. To do this, multiple regression analysis and analysis of variance were performed by using simulated data (observations) generated as output from CRCP-2 from an appropriate set of input variable values.

The mathematical formulation of these relations was established by the regression techniques. Then, principles of nomography were applied to these equations to develop a nomograph for the prediction of each of the three design parameters.

Regression techniques were also used to determine confidence-prediction intervals for each nomograph. An analysis of the accuracy of each nomograph as a predictor of CRCP-2 output was also performed to ensure that predictions were within design tolerances.

Use of CRCP-2 Output

It is apparent (Figure 2) that the three dependent variables decrease in discrete steps with time since construction, while crack width and steel stress increase gradually between steps. Figure 2 was plotted for the first 28 days to illustrate this trend in each case and for a typical set of data (9).

However, the values of these dependent variables that were used in the regression analysis were those eventually attained when the pavement had reached equilibrium. These values appear under the heading, "At the end of the analysis period," for the typical set of data listed in Appendix B of Noble, McCullough, and Ma (9). In this manner, the values of the dependent variables used in the regression analysis were obtained from the CRCP-2 outputs for different sets of conditions. These values are summarized along with the corresponding values of the independent variables in Appendix C of Noble, McCullough, and Ma (9).

DEVELOPMENT OF REGRESSION MODELS

Regression equations were developed to model relations between relevant input variables and the design parameters--crack spacing, crack width, and steel stress. The choice of equations was made following linear and nonlinear least-squares fits to a simulated set of observations generated as output from the CRCP-2 computer program. This development occurred in several stages.

Choice of Input Variables and Design of Experiment

In order to generate the necessary observations of the three design parameters, it was decided to vary 10 of the 21 CRCP-2 input variables (factors) at three levels each while holding the other 11 constant. This decision was based on the findings from a sensitivity study (7) and subsequent studies. Values were selected to cover the appropriate inference space after consultation with the Texas SDHPT. The variables used and the values chosen are listed in Tables 1 and 2. A more detailed explanation of these variables is included in Strauss, McCullough, and Hudson (10).

In order to obtain a manageably small, yet truly representative, set of observations of variables for prediction, a $1/3^5$ replicate of a 3^{10} factorial experiment (11,12) that used a completely randomized design was carried out. This design was chosen with all two-factor interactions measurable so that all main effects and two-factor interactions could be accurately estimated from only 3^5, or 243 observations. The design factorial is incorporated in Appendix A of Noble, McCullough, and Ma (9), and a typical CRCP-2 computer printout appears as

Table 1. Values of variables used in analysis of CRCP-2.

Input Variable	Symbol	Value for Level 1	2	3
Wheel-load stress (kPa)	σ_w	414	1172	1930
Daily temperature change (°C)	ΔT_i	4	19	33
Final temperature change (°C)	ΔT_F	19	31	42
Friction-movement ratio	F/y	–10	–80	–150
Concrete slab thickness (mm)	D	178	254	305
Concrete shrinkage strain	Z	2×10^{-4}	5×10^{-4}	8×10^{-4}
Concrete tensile strength (kPa)	f_t	3447	4481	5515
Thermal coefficient ratio	α_s/α_c	0.75	1.00	1.50
Bar diameter (mm)	Φ	13	16	19
Percentage of reinforcement	p	0.40	0.65	0.90

Note: 1 kPa = 0.145 psi; 1°C = 1.8°F; 1 mm = 0.039 in.

Table 2. Variables held constant in CRCP-2 analysis.

Variable	Value
Type of reinforcement	Deformed bar
Yield stress of steel (MPa)	413.6
Elastic modulus of steel (MPa)	199 926
Thermal coefficient of steel (mm/mm/°C)	11×10^{-6}
Unit weight of concrete (kg/m^3)	2403
Flexural-tensile factor	0.86
Curing temperature (°C)	42
Number of days to full-strength concrete	28
Number of days to minimum temperature	28
Number of days to wheel-load application	14
Slab movement (mm)	–3.0

Note: 1 MPa = 145 psi; t°C = (t°F – 32)/1.8; 1 mm = 0.039 in; 1 kg/m^3 = 0.062 lb/ft^3.

Appendix B (9). A summary of the complete set of observations that resulted from the experiment, which shows values of the three design parameters for each combination of values of the 10 input variables, appears in Appendix C (9).

All important combinations of the input variable values likely to be encountered in practical CRCP design were covered in the factorial, which extended over the extremes of the ranges of each variable. Hence, this experiment can also serve as the basis for a sensitivity analysis of the CRCP-2 model.

Theoretical Background to Form of Regression Models

Theoretical relations developed at the Center for Highway Research, Austin, Texas, between the design parameters (10) and the relevant input variables (Table 1) were considered in the initial investigation of the form of the regression models. From these relations, it is apparent that crack spacing is proportional to

$$(f_t^{a1} \times \phi^{a2} \times \alpha_s^{a3})/(p^{a4} \times \sigma_w^{a5})$$

and crack width is proportional to

$$(f_t^{b1} \times \phi^{b2})/p^{b3} \times \sigma_w^{b4})$$

where a_1, a_2, a_3, a_4, a_5, b_1, b_2, b_3, and b_4 are positive constants and the other variables are as defined in Table 1.

These theoretical trends were confirmed by an inspection of each design parameter's variation with the input variables over the appropriate range by using the simulated data set generated by the factorial experiment. This was done by using a series of plots of each design parameter against each input variable, with the other input variables held constant by using all 243 observations. From these, it was clear that

1. Crack spacing increases with increasing D, f_t, α_s/α_c, and Φ but decreases with increasing σ_w, ΔT_i, ΔT_f, F/y, Z, and p;
2. Crack width increases with increasing Z, f_t, α_s/α_c, and Φ but decreases with increasing σ_w, ΔT_i, ΔT_f, D, and p; and
3. Steel stress increases with increasing ΔT_f, D, f_t, α_s/α_c, and Φ but decreases with increasing σ_w, ΔT_i, F/y, Z, and p.

Form of Independent Variables in Regression Models

In order to ensure reasonable prediction of design parameters from the nomographs for all values of the input variables (independent variables) likely to be encountered in practice, each independent variable was transformed into a format based on its extreme (boundary) values for the regression analysis. The format used for each variable is shown below:

Independent Variable	Transformation Used
σ_w	$1 + (\sigma_w/1000)$
ΔT_i	$1 + (\Delta T_F/100)$
ΔT_F	$1 + (\Delta T_F/100)$
F/y	$[1 + (1/200)](F/y)$
D	$1 + (D/20)$
Z	$1 + 1000Z$
f_t	$1 + (f_t/1000)$
α_s/α_c	$[1 + (1/2)]\ (\alpha_s/\alpha_c)$
Φ	$1 + \Phi$
p	$1 + p$

For example, for the variable for wheel-load stress (σ_w), the transformation $(1 + \sigma_w/1000)$ was used so that the value used in the regression equation would lie between 1 and 2 for all values of σ_w likely to be encountered in practice (even for the zero wheel-load case).

Regression Analysis

The final choice of regression equations was then made by following multiple linear and nonlinear least-squares fits of the transformed input variables (independent variables) to the simulated set of 243 observations of the design parameters (dependent variables) previously described. Stepwise linear-regression computer programs (13,14) were used in the linear analyses, with logarithmic transformations of both independent and dependent variables to reflect the exponential nature of the relations discussed earlier. Better fits resulted by using these transformations than any others tried (e.g., orthogonal polynomials), with more variance being explained by fewer independent variables (and less prediction error) for all three dependent variables. Also, these regression analyses confirmed the trends established by theoretical developments and plots discussed previously (9, Appendix D.1). Computer program BMDO7R-Nonlinear Least Squares (15) was used for the nonlinear analysis. This second approach was adopted because, owing to the exponential nature of the relation (and the bias introduced by the transform), some improvement in fit might be obtained by nonlinear analysis, particularly if the error was additive rather than multiplicative (9, Appendix D.2).

Residual plots, standard error of estimate, and R^2 statistics (proportion of variance explained by the regression equation) were considered in the final choice of coefficients in each regression equation. These final equations are summarized below:

$$\bar{X} = \left\{0.402\ [1 + (f_t/6890)]^{6.7}\ [1 + (\alpha_s/2\alpha_c)]^{1.15}\ [1 + (\phi/25.4)]^{2.19}\right\} \div \left\{[1 + (\sigma_w/6890)]^{5.2}\ (1 + p)^{4.6}\ (1 + 1000Z)^{1.79}\right\} \quad (1)$$

R^2 = 90.2 percent and standard error = 0.64 m

$$\Delta X = \left\{0.003\,67\,[1 + (f_t/6890)]^{6.53}\,[1 + (\phi/25.4)]^{2.20}\right\} \div \left\{[1 + (\sigma_w/6890)]^{4.91}\,(1 + p)^{4.55}\right\} \quad (2)$$

R^2 = 92.7 percent and standard error = 0.33 mm

$$\sigma_s = \left\{326\,207\,[1 + (\Delta T/556)]^{0.425}\,[1 + (f_t/6890)]^{4.09}\right\} \div \left\{[1 + (\sigma_w/6890)]^{3.14}\,(1 + 1000Z)^{0.494}\,(1 + p)^{2.74}\right\} \quad (3)$$

R^2 = 92.2 percent and standard error = 67.7 MPa

where

$\overline{X}$ = crack spacing (m),
ΔX = crack width (mm), and
σ_s = steel stress (kPa).

Analysis of variance for each equation indicated that the inclusion of further terms (independent variables) did not significantly improve either the R^2 or standard error of residuals statistics.

Nonlinear Regression Models

In general, if linear regression is performed by using logarithmic transforms of the dependent variable (Y) and the independent variables (X_1,..., X_n), the model becomes

$$\log Y = C_o + C_1 \log X_1 + \ldots + C_n \log X_n + \text{error term (E)}$$

or

$$Y = C_o X_1^{C1} \ldots X_n^{Cn} E$$

where C_o,..., C_n are constants. Hence, the error term is multiplicative in this model.

However, the nonlinear model would be

$$Y = K_o X_1^{K1} \ldots X_n^{Kn} + \text{error term (E)}$$

where K_o, ... K_1 are constants. Hence, the error term is additive in this model.

A comparison was then made of the goodness of fit of both the linear and nonlinear regression models because the form of the error term was unknown in this case. The results of this comparison are summarized in Table 3. It is apparent from these that the improvement in fit owing to the use of nonlinear coefficients was not significant at the 5 percent level for crack width and at the 25 percent level for both crack spacing and steel stress. It was thus decided to use the expressions derived from the linear regression procedures.

For all three design parameters, regression analyses that were performed with major outliers removed from the data set showed no significant improvement in prediction accuracy.

Table 3. Comparison of results of design parameter values as obtained from nomographs and regression equations.

Type of Statistic	Dependent Variable: Crack Spacing	Crack Width	Steel Stress
Statistic			
Degrees of freedom	24	12	21
Root mean square residual	1.7 m	0.4 mm	148 MPa
Coefficient of variation (%)	33	23	21
Statistic obtained when design parameters fall within	<6.1 m	<2.5 mm	<689 MPa
Degrees of freedom	14	10	11
Root mean square residual	36 cm	0.23 mm	45 MPa
Coefficient of variation (%)	20	19	11

Note: 1 m = 3.28 ft; 1 mm = 0.039 in; 1 cm = 0.39 in; 1 MPa = 145 psi.

Summary

Given the foregoing data, it was decided to use the regression equations summarized earlier in this paper as the basis for the construction of the nomographs. These equations gave satisfactory R^2 and standard error values and agreed with the format indicated by the previous theoretical development and the summary plots from the sample data. Some slight improvement in goodness of fit to the sample data was seen for the equations developed by using the nonlinear analysis. However, this was not considered sufficiently significant to offset the uncertainty that would have been introduced if these equations were used with the confidence limits described in the next section of this paper. This uncertainty would have occurred because the confidence intervals were derived by using a linear analysis (with logarithmic transforms) and, as such, are conservative on the regression equations.

CRCP DESIGN NOMOGRAPHS AND CONFIDENCE LIMITS

Design Charts--Nomographs

By using the principles of nomography (16,17) and the regression equations, separate design charts (nomographs) were prepared for the prediction of crack spacing, crack width, and steel stress in the design of CRCP. These are shown in Figures 3, 4, and 5, respectively.

Confidence-Prediction Limits

By using the CPIY linear regression program (18) and logarithmic transformations of the appropriate dependent and independent variables, the 90 percent and 97.5 percent confidence limits on each of the three design parameters--crack spacing, crack width, and steel stress--were calculated for the regression models noted earlier in this report (9, Appendix D.3). These confidence limits can then be used with the nomographs in the design procedure. To this end, graphs of the variation of these confidence limits with the value of each design parameter for the appropriate inference range appear in Figures 6, 7, and 8.

It should be noted that, because the regression equations are of an exponential form, strict confidence intervals cannot be determined by using existing computer software (e.g., from the nonlinear regression models). Hence, it is necessary to use logarithmic transformations and the linear regression techniques in the CPIY program to determine these confidence limits. Transformations of these confidence limits are then conservative for the exponential models.

In practice, use of Figures 6, 7, and 8 in conjunction with the corresponding nomographs (Figures 3, 4, and 5) enables the designer to estimate the uncertainty associated with the values of the design parameters (crack spacing, crack width, and steel stress) indicated by the nomographs. These values are for the chosen value of percentage of steel and the values of the other input variables determined by the properties of materials used and the appropriate environmental conditions. That is, a range of values in crack spacing can be determined from Figure 6 so that this parameter will be within this range, with either 80 percent or 95 percent probability. Similarly, two upper limits on each crack width and steel stress can be determined from Figures 7 and 8, respectively, so that the appropriate parameters will be below these limits, with either 90 percent or 97.5 percent probability.

Figure 3. Nomograph for prediction of crack spacing.

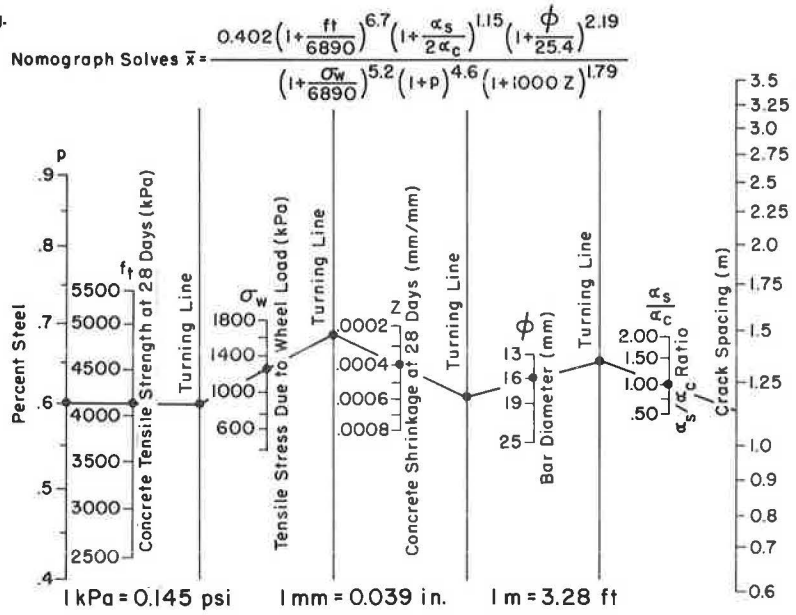

Figure 4. Nomograph for prediction of crack width.

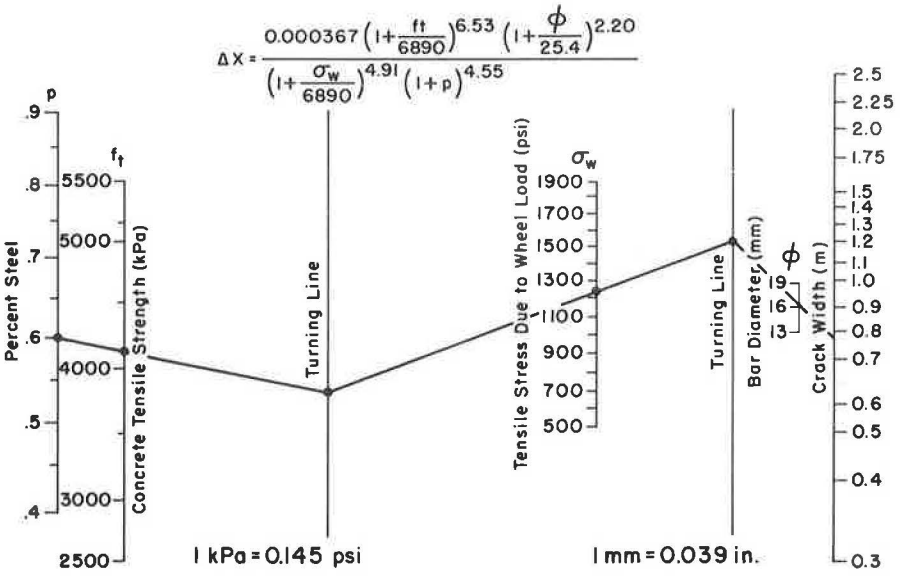

Accuracy Analysis

A set of test data comprised of 35 different combinations of the CRCP-2 input variables that had not been used in the initial regression analysis was prepared. Values for the different design parameters (crack spacing, crack width, and steel stress) corresponding to each of the 35 combinations were then computed with the CRCP-2 program.

Initially, design parameter values for some of the combinations, as obtained from the nomographs, were compared with values from the regression equations. Subsequently, the parameter values obtained from the nomographs were compared with the computed values. A further check on the amount of variation accounted for by the regression equation was accomplished by fixing values of the regression variables and varying the values of the variables not included in the regression equations.

Nomographs Compared with the Regression Equations

The nomographs compare well with the regression equations (Table 3), particularly when the values of the design parameters fall within expected maximum-boundary values. By using the root mean square residual as an estimate of variance for the samples, coefficients of variation of roughly 5 percent were obtained from the comparison within the boundary values.

Nomographs Compared with the Computed Values

When unbounded values of the design parameters are used in the comparison in Table 4, coefficients of variation defined and calculated as above are greater than those where the data set results in parameter values that fall within the proposed boundaries. In the latter case, coefficients of variation of 11-20 percent were obtained.

Variables Not Included in the Regression Equations

As confirmed by the regression analysis, the variations of the design parameter values produced purely by changing these variables are small (Table 5). The small sample of

Figure 5. Nomograph for prediction of steel stress.

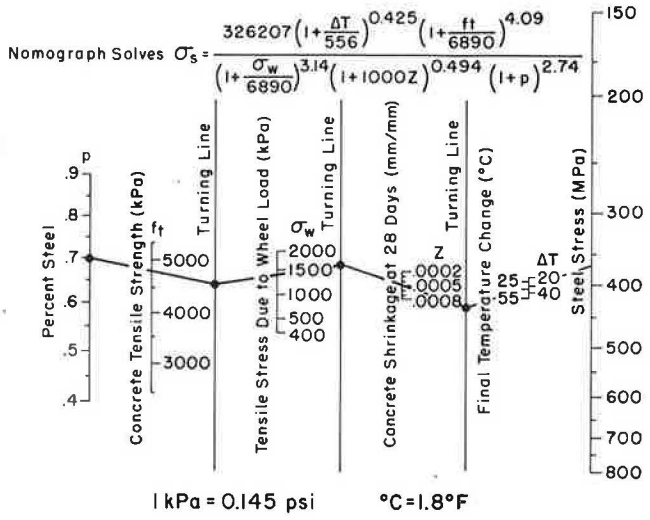

Figure 6. Confidence limits for crack spacing (to be used with Figure 3).

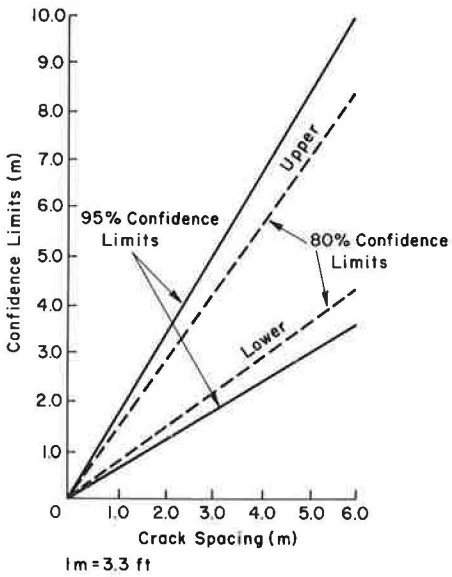

Figure 7. Confidence limits for crack width (to be used with Figure 4).

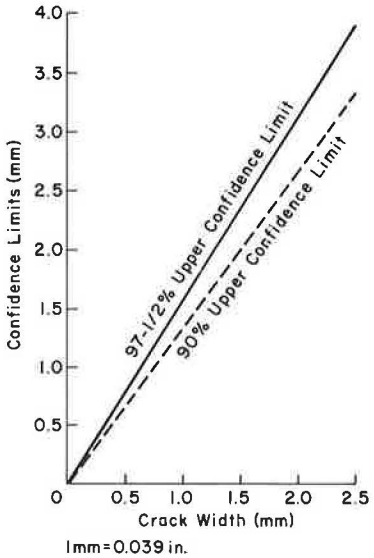

Figure 8. Confidence limits for steel stress (to be used with Figure 5).

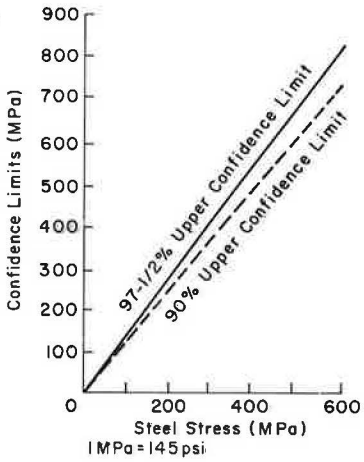

Table 4. Comparison of results of design parameter values as outlined from nomographs and computer values.

Type of Statistic	Dependent Variable: Crack Spacing	Crack Width	Steel Stress
Statistic			
Degrees of freedom	18	9	20
Root mean square residual	0.94 m	0.108 mm	97.2 MPa
Coefficient of variation (%)	17	6	14
Statistic obtained when design parameters fall within	<6.0 m	<2.5 mm	<690 MPa
Degrees of freedom	10	6	11
Root mean square residual	0.13 m	0.013 mm	12.4 MPa
Coefficient of variation (%)	5.4	1.2	3

Note: 1 m = 3.28 ft; 1 mm = 0.039 in; 1 MPa = 145 psi.

values tested shows coefficients of variations calculated as above that range from 13 to 18 percent for the different design parameters.

Summary

1. Values of the design parameters, as obtained from the nomographs, are generally within 25 percent of the computer program values, provided that the initial and resulting parameter values fall within a practical range.
2. Loss of accuracy due to the use of nomographs instead of the regression equations can be attributed primarily to the lack of accuracy of the end-result scale of the nomograph. When considering the variation and uncertainty of the input used, this small loss in accuracy is insignificant.
3. When extreme values of input parameters are used, the turning lines of the nomographs have to be very long and may have to be extended. Use of values normally encountered in the field, however, does not create such problems.

DESIGN PROCEDURE

In order to use Figures 3 through 8 to design the percentage of steel reinforcement in CRCP, the designer should first determine the values of concrete tensile strength, coefficients of thermal expansion of concrete and steel, wheel-load stress, steel bar diameter, shrinkage strain, and maximum temperature variation for the materials and environmental conditions appropriate to the design situation. A method for the selection of these values is detailed in Ma, McCullough, and Noble (19). The procedure then becomes one of estimating the percentage of steel to be used in order to satisfy the limiting criteria (19) for these

Table 5. Sensitivity of design parameter values (dependent variables) to changes in independent variables not included in regression equations.

Independent Variable	Range	Range of Values of Design Parameter (Dependent Variable)		
		Crack Spacing (m)	Crack Width (mm)	Steel Stress (MPa)
Daily temperature change, ΔT_i (°C)	4 to 33	1.3-1.0	0.99-0.79	430-380
Number of days to first wheel-load application and final temperature change, ΔT_p (°C)	8 to ∞ and 31 to 19	1.0-0.9	0.79-0.61	–
Final temperature change, ΔT_p (°C)	42 to 19	0.9-0.9	0.84-0.61	–
Friction-movement ratio, F/y	-80 to -150	0.9-0.9	0.61-0.71	316-350
Thickness of concrete, D (cm)	17.8 to 30.5	1.2-1.2	0.91-0.91	415-415

Notes: 1 C° = 1.8 F°; 1 mm = 0.039 in; 1 m = 3.28 ft; 1 cm = 0.39 in; 1 MPa = 145 psi.
The coefficient of variation for crack spacing, crack width, and steel stress is 15, 18, and 13 percent, respectively.

conditions on crack width, crack spacing, and steel stress. It should be noted here that the contemporary design slab thicknesses for CRCP range from 180 mm (7 in) to 300 mm (12 in). A selection procedure for slab thickness is also detailed in Ma, McCullough, and Noble (19).

The procedure for estimating the steel percentage to satisfy the limiting criteria, referred to above, is outlined here.

1. Mark the values of the appropriate input variables on their respective scales on each of the three nomographs.
2. Choose a likely value of the percentage of steel to be used (p) and mark this value on the scale for p on each nomograph.
3. Working from left to right, draw a line joining the marked values on scale numbers 1 and 2 for the crack-spacing nomograph; proceed until the line intersects the first turning line.
4. Draw a new line from this point, joining it to the marked values on scale number 3; proceed until it intersects the second turning line.
5. Repeat this process for the remaining two turning lines and scale numbers 4, 5, and 6 until the value of crack spacing can be read from the scale on the far right.
6. If this value is not inside the recommended range for the appropriate environmental conditions and material properties (19), repeat steps 2 through 5 for larger percentages of steel until the limiting criteria are satisfied.
7. Repeat steps 2 through 6 for the crack-width and steel-stress nomographs and relevant limiting criteria.
8. If the values obtained in steps 6 and 7 for all three nomographs are inside the respective limiting criteria, then repeat the entire process by using successively smaller values of p until one of the three nomographs indicates a final value (of crack spacing, crack width, or steel stress) that is just inside the limits. This value of p is then the design value to be recommended.
9. The designer should then enter Figures 6, 7, and 8 on the abscissa scales with values of crack spacing, crack width, and steel stress, respectively, obtained from the corresponding nomographs for the final value of p recommended in step 8. The upper and lower confidence limits for crack spacing and the upper confidence limits for crack width and steel stress should then be read from the respective ordinate scales of each figure.
10. Thus, the designer should finally recommend a steel percentage, along with both the corresponding 80 and 95 percent confidence limits on crack spacing and both the 90 percent and 97.5 percent upper confidence limits on crack width and steel stress, which use of this p will predict. That is, the designer recommends a percentage of steel, along with a range of values of crack spacing that will include the actual value 80 percent of the time (or with 80 percent certainty), as predicted by the model, as well as a slightly wider range that will include the actual value 95 percent of the time. Also, the designer recommends the corresponding upper limits on crack width and steel stress so that, for the chosen value of p, these parameters will fall below these limits 90 percent (or 97.5 percent) of the time or with 90 percent (or 97.5 percent) certainty. These ranges could be used in conjunction with limiting criteria noted in McKenzie (18), if a more conservative design is required.
11. The equations should be used as a check on the nomograph design.

CONCLUSION

Based on this study, the recommendations that follow were made.

1. A set of nomographs based on regression analysis of the results computed by the CRCP-2 computer program has been prepared. The uniaxial-force equilibrium model used in the CRCP-2 computer program is the only model available that considers the internal forces caused by the difference in thermal coefficients between the concrete and the steel materials. Therefore, it is the most suitable tool available for the CRCP analysis.
2. Spacing of transverse cracks that occur in CRCPs is the most important variable affecting the behavior of the pavement. Relatively large distances between cracks result in a higher accumulation of drag forces from the subgrade due to frictional resistance, thus producing high steel stress at the crack and large crack widths. Closer crack spacing reduces the frictional restraint and, thus, the steel stress and the crack width.
3. Nomographs produced in this study can predict steel stress at the crack (where the stress is maximum), average crack spacing, and average crack width at minimum temperature.
4. The limiting design criteria for the above dependent variables are discussed in Ma, McCullough, and Noble (19).
5. The nomographs should be used in conjunction with the limiting design criteria (19) for the design of steel percentage in CRCP given the materials chosen and local environmental conditions. Explicit guidelines for the selection of values of the input variables to be used with the nomographs and a detailed procedure for the design of slab thickness are given in Ma, McCullough, and Noble (19).
6. Charts that give confidence prediction limits should be used in conjunction with the nomographs in order that the designer can specify a range on each of the variables (crack spacing, crack width, and steel stress) corresponding to the uncertainty inherent in the procedure. These limits may also be used in place of the mean values (recommended by the nomographs) if a conservative design is warranted (19).
7. This entire CRCP-design procedure should be incorporated into the Texas SDHPT's Operations and Procedures Manual.

ACKNOWLEDGMENT

The material presented in this paper is part of a research effort on the development and implementation of the design, construction, and rehabilitation of rigid pavements conducted by the Center for Transportation Research of the University of Texas at Austin and sponsored by the Texas SDHPT and the Federal Highway Administration (FHWA). The contents of this report reflect our views. We are responsible for the facts and the accuracy of the data

presented herein. The contents do not necessarily reflect the official views or policies of the Texas SDHPT or FHWA. This report does not constitute a standard, specification, or regulation.

REFERENCES

1. B.F. McCullough and W.B. Ledbetter. LTS Design of Continuously Reinforced Concrete Pavements. Journal of the Highway Division, Vol. 86, No. HW4, Proc., American Society of Civil Engineers, Dec. 1960.
2. W. Zuk. Analysis of Special Problems in Continuously Reinforced Concrete Pavements. HRB, Bull. 214, 1959, pp. 1-21.
3. AASHTO Interim Guide for Design of Pavement Structures. American Association of State Highway and Transportation Officials, Washington, DC, 1972.
4. B.F. McCullough. Design Manual for Continuously Reinforced Concrete Pavement. U.S. Steel Corporation, Pittsburgh, Jan. 1970.
5. R.W. Carlson. Drying Shrinkage of Concrete as Affected by Many Factors. Proc., American Society for Testing Materials, Vol. 38, Part 2, 1938.
6. B.F. McCullough, A. Abou-Ayyash, W.R. Hudson, and J.P. Randall. Design of Continuously Reinforced Concrete Pavements for Highways. Center for Highway Research, Univ. of Texas at Austin, Res. Rept. NCHRP 1-15, Aug. 1974.
7. C. Chiang, B.F. McCullough, and W.R. Hudson. A Sensitivity Analysis of Continuously Reinforced Concrete Pavement Model CRCP-1 for Highways. Center for Highway Research, Univ. of Texas at Austin, Res. Rept. 177-2, Aug. 1974.
8. J.C.M. Ma and B.F. McCullough. Analysis of Load, Temperature, and Shrinkage Effect on Continuously Reinforced Concrete Pavement. TRB, Transportation Research Record 671, 1978, pp. 29-39.
9. C.S. Noble, B.F. McCullough, and J.C.M. Ma. Nomographs for the Design of CRCP Steel Reinforcement. Center for Highway Research, Univ. of Texas at Austin, Res. Rept. 177-16, May 1979.
10. P.J. Strauss, B.F. McCullough, and W.R. Hudson. Continuously Reinforced Concrete Pavement: Structural Performance and Design Construction Variables. Center for Highway Research, Univ. of Texas at Austin, Res. Rept. 177-7, Aug. 1979.
11. V.A. Anderson and R.A. McLean. Design of Experiments: A Realistic Approach. Marcel Dekker, Inc., New York, 1974.
12. W.S. Connor and M. Zelen. Fractional Factorial Experiment Design for Factors at Three Levels. U.S. Department of Commerce, National Bureau of Standards Applied Mathematics Series 54, May 1959.
13. N.H. Nie and others. Statistical Packages for the Social Sciences, 2nd ed. McGraw-Hill, New York, 1975.
14. STEP-01 Statistical Computer Program for Stepwise Multiple Regression. Center for Highway Research, Univ. of Texas at Austin, Oct. 1968.
15. W.J. Dixon, ed. Biomedical Computer Programs, 2nd ed. Univ. of California Press, Berkeley, 1976.
16. M.G. Van Voorhis. How to Make Alignment Charts. McGraw-Hill, New York, 1959.
17. A.S. Levens. Nomography, 2nd ed. John Wiley and Sons, New York, 1959.
18. D. McKenzie. CPIY Multiple Regression Program, rev. ed. Center for Highway Research, Univ. of Texas at Austin, March 1978.
19. J.C.M. Ma, B.F. McCullough, and C.S. Noble. Limiting Criteria for the Design of CRCP. Center for Highway Research, Univ. of Texas at Austin, Res. Rept. 177-17, Aug. 1979.

Publication of this paper sponsored by Committee on Rigid Pavement Design.

Implementation of New Overlay Design Procedure in Texas

STEPHEN SEEDS, B. FRANK McCULLOUGH, W. R. HUDSON, AND MANUEL GUTIERREZ DE VELASCO

A project is under way in Texas to adapt a version of the rigid pavement overlay design procedure developed for the Federal Highway Administration by Austin Research Engineers, Inc., into standard Texas State Department of Highways and Public Transportation (SDHPT) practice. This project is part of a cooperative research program between Texas SDHPT and the Center for Highway Research at the University of Texas. This paper provides some feedback on the use of this procedure and documents its successful application to an interstate rehabilitation and widening project in San Antonio. This project was unique in the sense that thickness and reinforcement designs were required for five different composite pavement structures that, by their nature, are not suitable for design by past empirical methods. In documenting the designs, the selection of design criteria, characterization of material properties, and thickness design recommendations for each section within the project are discussed. The paper provides a general description of the design procedure, discussion of the results of the design, conclusions about the applicability of the design model, and recommendations for further work. The validity and practicality of the new procedure, as well as its applicability for nationwide use, are noted.

Many of the rigid pavements that make up much of the Interstate highway system were constructed in the 1950s and early 1960s. Most were designed to last 20 years and, consequently, are approaching the end of their design life. Many now require extensive rehabilitation. The Federal Highway Administration (FHWA), recognizing the need for a practical design procedure for overlays of these pavements, sponsored a project for the development of such a design procedure (1). This project was completed in 1977.

The Texas State Department of Highways and Public Transportation (SDHPT), long interested in such a design tool, considered the new FHWA procedure workable and funded research at the Center for Highway Research (CFHR) at the University of Texas to examine the new procedure and adapt it for Texas conditions (2). The project provides for implementation of the new procedure into Texas SDHPT practice through field application on several pavement overlay projects. It also provides for incorporating other useful improvements to the design models and procedure that may aid in their implementation. This has led to further refinement of the rigid pavement overlay design model.

OBJECTIVES

The objectives of this paper are twofold: (a) to discuss the

application of the new Texas SDHPT overlay design procedure to an Interstate highway overlay project in San Antonio and (b) to show the value of the new theoretical procedure on overlay projects, especially where there is inadequate experience with design factors such as characterization of the existing pavement and the increased quantities of expected future traffic.

SCOPE

The scope of this paper includes the discussion of design criteria, materials characterization, and pavement thickness design recommendations for a single major Interstate rehabilitation project in San Antonio. A discussion of significant aspects of the project and of the design procedure is also included. Though the design models are an integral part of determining the pavement thicknesses required, detailed discussion of them is beyond the scope of this paper (1,2). Also, there are numerous economic analyses relative to the project, such as shoulder type and pavement life, which cannot be considered within the scope of this paper.

PROJECT DESCRIPTION

Coincidental with the growth of San Antonio in recent years has been the growth of traffic, particularly in the northern part of the city. Due to continued anticipated growth, the Texas SDHPT has undertaken a project to increase the traffic and load-carrying capacities of two major Interstate highways in the area: (a) I-35, which runs north-south through the city, and (b) I-410, which circles the city. A layout of the T-shaped intersection of the two is presented in Figure 1. The overlay and widening project around this interchange is of particular significance and was selected for trial application of the new design method.

The project covers existing four-lane facilities, both on I-410 and on I-35 north of the interchange, and a six-lane facility on I-35 south of the interchange. All three legs of the interchange will be widened to eight lanes to carry the estimated future traffic. Such a project presents a complex design problem because a wide range of conditions are encountered. These include the design of overlays in some areas, the design of new pavement lanes in the areas where widening will occur, and the design of reconstructed pavements where grade revisions are to be made.

The section of I-35 north of the interchange to Weidner Road is a jointed concrete pavement (JCP) structure and is to be overlaid and widened with continuously reinforced concrete pavement (CRCP). The section of I-35 south of the interchange to Walzem Road is a CRCP structure and is to be overlaid and widened with asphaltic-concrete pavement (ACP) with a continuously reinforced concrete (CRC) base slab providing support in the widened areas. The I-410 leg of the facility from I-35 to Perrin-Beitel is also a JCP structure, which, due to required grade revisions, will be reconstructed with CRCP. Further information regarding the thickness designs is discussed in the next section.

It is important to note that the basis for thickness design is the new Texas SDHPT Rigid Pavement Overlay Design Procedure as discussed in Schnitter, Hudson, and McCullough (2) along with minor improvements documented in Seeds (3) and Taute (4).

Figure 1. Layout of the existing facility showing the three legs of the project.

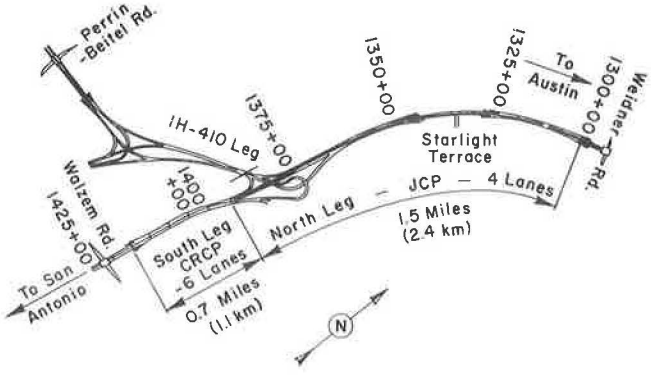

THICKNESS DESIGN

Design Procedure

The design procedure used here (2-4) has eight basic steps.

1. Select the design criteria, which include 80-kN (18-kip) equivalent single-axle load (ESAL) traffic estimates (past and projected), traffic distribution factors, overlay and shoulder types to be considered, available aggregates, bond breaker criteria, construction methods, geometric constraints, or any other criteria that constrain the overlay design.
2. Conduct a condition survey of pavements in the areas under consideration and classify the type of cracking, other distress modes observed, and soil type in the area.
3. Gather Dynaflect deflection data at approximately 30.5-m (100-ft) intervals along the length of the project.
4. Select design sections by analyzing the Dynaflect deflection profiles.
5. Characterize the material properties of the pavement and subgrade, i.e., concrete flexural strength and elastic properties for each layer. This is usually done by a combination of laboratory testing [i.e., indirect tensile tests on portland cement concrete (PCC) and other bound layers and resilient modulus tests on subgrade and base materials] and Dynaflect deflection basin fitting (e.g., for a design Dynaflect deflection basin in each section, select elastic material properties of each layer that correspond to the best-fitted basin predicted by elastic-layer theory). Results of the laboratory tests should be used to hone in on the solution. Adjustments to these layer moduli should then be made for stress sensitivity (since the design axle load is much heavier than the Dynaflect load) and predicted temperature conditions.
6. Estimate the fraction of remaining life in the existing pavement for each design section. This is obtained from estimates of the life of the existing pavement, past traffic estimates (step 1), existing pavement condition (step 2), and subgrade strength (step 5).
7. Use the rigid pavement overlay design (RPOD) computer model to generate overlay thickness design curves for each design section. Note that, due to the range in acceptable design criteria, several design curves may be generated for a particular design section.
8. Select the overlay thickness required for each design section for the estimated future traffic from the design curves generated in step 7. If alternative designs exist, the optimum should be selected based on projected cost and performance comparisons.

These are the essential steps used in determining the design thicknesses for the overlaid sections of the project. They are not quite the same for the pavements in the widened areas because there is essentially no existing pavement in these areas. Normally, the design here would be the same as for a new pavement; but, in cases where there are two load-carrying layers (in this case, a CRCP foundation layer with an overlay), there are several combinations of thicknesses of these two layers that will provide the desired life.

Consequently, another level of RPOD computer program solutions is required in which the thickness of the PCC foundation slab is varied. (Note that this PCC foundation slab would be modeled as an existing pavement with 100 percent remaining life.) Interpolation in the resulting family of design curves is then used to select the overlay and foundation slab-thickness combination best suited for any construction or cost criteria.

Design Criteria

As a result of several meetings of the CFHR project staff and Texas SDHPT personnel involved with the project, the following criteria and guidelines were established for use in the pavement designs.

1. The one-way 20-year projections of 80-kN (18-kip) single-axle loads developed by the Planning Survey Division for the three legs of the interchange are presented in Table 1. These equivalencies are based on a 20.3-cm (8-in) rigid pavement.
2. The handling of large volumes of traffic during construction emphasizes the need for an orderly construction sequence. Hence, a possible strategy of overlaying two existing pavement lanes and widening with full-depth pavement to obtain the other two lanes was eliminated in favor of widening with a concrete base for handling traffic, then overlaying the entire width with a constant thickness.
3. The availability of limestone coarse aggregates for use in PCC led to considering its properties in the design analysis. Performance studies of pavements in Texas have shown that better performance is generally obtained with limestone aggregates than with siliceous aggregates due to a smaller rate in loss of load transfer during the life of the facility. Because the probability was high that this type of aggregate was to be used on the project, it was felt that the design should reflect its use.
4. In accordance with the Highway Design Division Manual, a factor of 70 percent was used for converting the total one-directional traffic to that in the design lane. This factor corresponds to the outside lane of eight-lane divided facilities. A lower factor of 20 percent was used for the inside lane.
5. The unlimited supply of limestone fines at an economical price resulted in its exclusive use in PCC pavements near San Antonio. Unfortunately, loss of skid resistance is a problem with this type of aggregate and, consequently, future roto-milling operations for improving skid resistance must be considered in the design. For all PCC pavements subjected directly to traffic, additional thickness is provided to account for roto-milling operations during the life of the facility.
6. The geometric layout of the existing facility is such that the width of the median varies from one location to the next due to existing bridge structures. Consequently, after widening, the existing lanes will be under the inside overlay lanes in some cases and under the outside lanes in others. Therefore, the overlay design must be made on the basis that the existing pavement will be located under the outside overlay lanes.

THICKNESS DESIGN ANALYSES

The thickness designs for the pavements in this project were divided into five analyses as follows:

1. Design of the CRC overlay on the existing JCP for I-35 north of the interchange—This section deals with the design of a CRC overlay over the existing jointed pavement from just south to north of the interchange.
2. Design of the CRC base for the widened areas of I-35 north of the interchange—This section deals with the design of the CRC base (CRC foundation slab) in the widened areas of I-35 adjacent to the existing JCP.
3. Design of the asphaltic-concrete (AC) overlay on the existing CRCP for I-35 south of the interchange—This section deals with the design of the AC overlay on the existing CRCP structure south of the interchange.
4. Design of the CRCP for the widened areas of I-35 south of the interchange—This section deals with the design of the CRCP that will underlay the AC overlay in the widened areas of I-35 adjacent to the existing CRCP.
5. Design of the reconstructed CRCP on the I-410 leg of the interchange—This section deals with the design of a new CRCP to be constructed on and along the I-410 leg of the interchange.

A pavement cross section illustrating the thickness designs required for analyses 1 and 2 is shown in Figure 2. A similar cross section is illustrated by Figure 3 for analyses 3 and 4. Figure 4 shows the thickness design required for the new pavement in analysis 5.

The thickness designs for these analyses are presented in the order noted above. Due to the limitations on the length of this paper, however, detailed discussion of design analyses 3 and 4 on the project's south leg has been omitted.

Analysis 1

The existing structure shown in Figure 2 is to be widened and overlaid within the limits covering the area from north of and just to the south of the interchange, i.e., from station 1300+00 to 1380+00. It consists of a 7.6-cm (3-in) AC overlay, 25.4 cm (10 in) of plain JCP, and 35.6 cm (14 in) of crushed stone base on top of a silty-clay subgrade.

The profile of Dynaflect deflections (Figure 5) made along the project revealed two distinctly different design sections: (a) fair, those sections with a maximum deflection of less than 10.2 μm (0.4 milli-inches), i.e., from stations 1300+00 to 1330+00 and from 1342+00 to 137+00, and (b) poor, those sections with a maximum deflection of greater than 12.7 μm (0.5 milli-inches), i.e., from stations 1330+00 to 1342+00 and from 1370+00 to 1420+00. The effect of the different deflections is reflected in the characterization of the material properties for the two sections.

There was insufficient time to perform the required laboratory testing of the pavement materials. Therefore, it was necessary to characterize the properties by matching deflection basins measured in the field by the Dynaflect with those predicted by elastic-layer theory, i.e., the ELSYM5 computer program (5). These field and fitted Dynaflect basins are shown in Figure 6. The resultant elastic structures for the fair and poor sections are shown in Figure 7. The poor section (high deflection) has a lower subgrade modulus, as expected, and also a lower concrete modulus. The latter reflects increased concrete fatigue due to higher deflections during its life.

Because the Dynaflect was used to characterize the subgrade's elastic modulus, the soil's stress sensitivity must be considered and its modulus adjusted for conditions under the design 80-kN (18-kip) axle load. Accordingly, a conservative estimate of the slope of subgrade modulus versus subgrade deviator stress was selected (S_{SG} = -1.0) in the absence of laboratory data. Figure 8 shows the effect of the variation of the slope of the resilient modulus versus the deviator stress curve for the fair and poor sections. Figure 8 also shows the design subgrade modulus for each section for the selected slope of -1.0, i.e., 21 and 42 MPa

Table 1. Future traffic estimates for the project.

Location	ADT 1980	ADT 2000	Growth Rate (%)	Predicted 80-kN ESAL Applications from 1980 to 2000 (000 000s)
I-35, from I-410 north to Weidner Road	66 990	89 200	1.7	20.4
I-35, from I-410 south to Walzem Road	61 400	85 100	2.0	16.0
I-410, from I-35 west to Perrin-Beitel Road	65 700	111 300	3.7	19.7

(3000 and 6000 psi) for the poor and fair sections, respectively.

With the elastic properties of the pavement structure, it is possible to use elastic-layer theory to estimate the critical stresses after placement of the overlay and to use the improved rigid pavement overlay design procedure to determine the overlay thickness required for the design traffic values.

Inputs required by the procedure, in addition to the pavement structure thicknesses and elastic properties, include the remaining life of the existing pavement, the flexural strength of the existing concrete and the overlay, and the ratio of the field stress to the predicted elastic-layer stress.

Rough traffic estimates and engineering judgment were used to estimate a remaining life of 20 percent for the existing jointed pavement. Its minimum seven-day flexural strength required by the concrete specifications was 3965 kPa (575 psi).

An overlay flexural strength of 4482 kPa (650 psi) at 14 days was recommended and used for design due to the need for opening the facility to traffic as soon as possible.

Figure 2. Cross section of pavement structure on I-35 north of interchange after overlay construction.

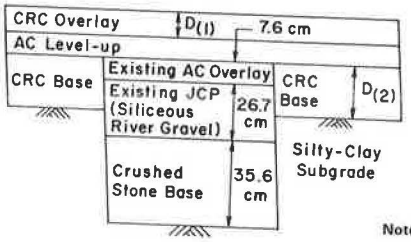

Figure 3. Cross section of pavement structure on I-35 south of interchange after overlay construction.

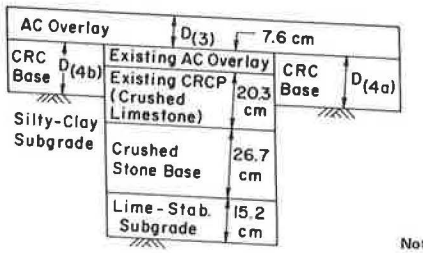

Figure 4. Cross section of CRCP structure on I-410 leg of the project after reconstruction.

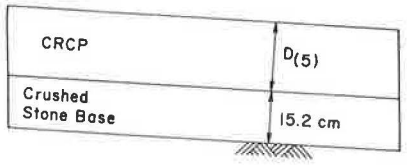

Figure 5. Dynaflect deflection profile (sensor 1) on JCP section of I-35 north of the interchange.

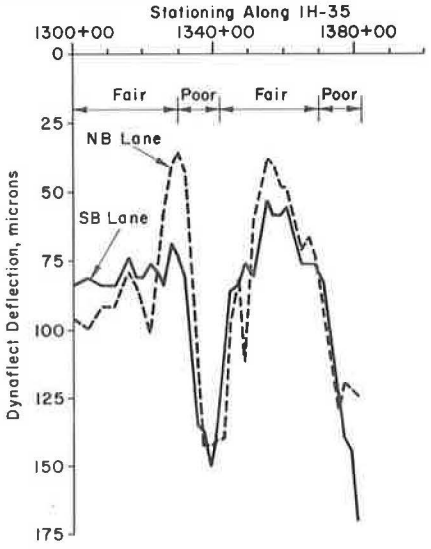

Figure 6. Field and fitted Dynaflect deflection basins for the fair and poor sections of the JCP structure on I-35 north of the interchange.

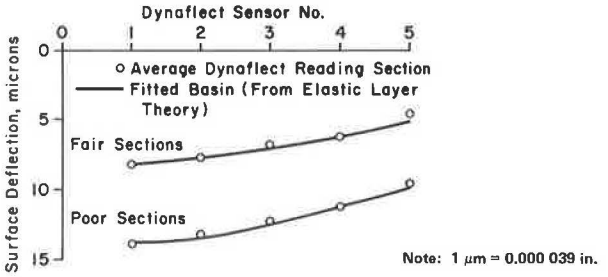

Figure 7. Elastic properties that characterize the pavement materials in the poor and fair sections of I-35 north of the interchange.

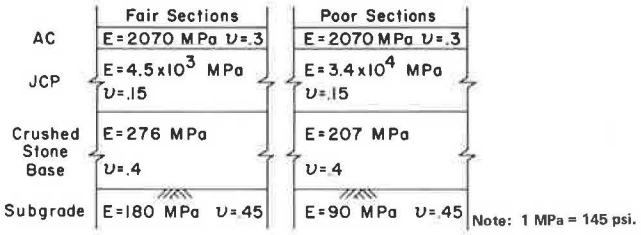

Figure 8. Subgrade resilient modulus curves for the poor and fair sections of JCP on I-35 north of the interchange.

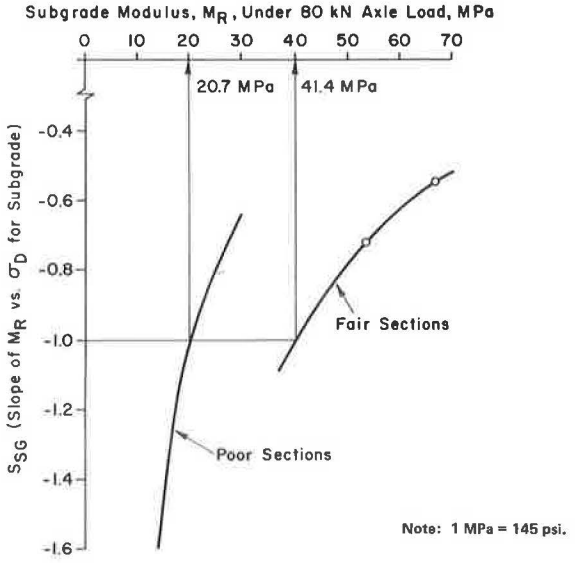

Because concrete shoulders will be incorporated into the structure, edge-loading conditions are not expected; consequently, a critical stress to elastic-layer stress ratio of 1.05 was selected for design. Though this represents an interior condition, the 5 percent increase was selected to reflect the loss of load transfer with time. Had a siliceous river gravel been used, a higher factor may have been required.

The placement of an AC level-up course was also considered in the development of the thickness design curves. These curves are shown in Figure 9. Because there was very little difference in the estimated stresses in the fair and poor sections, their design curves are almost identical. A common thickness design is recommended for both sections. The thickness differential may have been significantly different if better estimates of existing pavement remaining life were available.

Some 20 million 80-kN (18-kip) ESAL applications in one direction are expected on this structure. By using a lane distribution factor of 0.70, as recommended by the Texas SDHPT D-8 Manual, for the outside lane of an eight-lane roadway, 14 million 80-kN ESALs may be expected in the design lane. The thickness design curve in Figure 9 shows this amount of traffic requires 16 cm (6.3 in) of CRC overlay. Since two to three roto-milling operations for improving skid resistance are expected during the life of the pavement, the recommended design thickness $D_{(1)}$ of the CRC overlay is 17.8 cm (7 in).

Analysis 2

This discussion is concerned with the thickness design of the CRC base adjacent to the existing 25.4-cm (10-in) jointed pavement. The overlay thickness has been fixed by the previous design step; thus the CRC base will provide the support necessary to the 17.8-cm (7-in) CRC overlay in the widened areas to carry the estimated future traffic. A cross section of the proposed pavement structure that also gives the pertinent material properties is shown in Figure 10. The lower concrete modulus of elasticity was selected because limestone coarse aggregates are anticipated in lieu of siliceous river gravels used in the existing JCP. Because at least two roto-milling operations are expected during the life of the CRC overlay, an average thickness of 17.1 cm (6.75 in) for the surface pavement was used for design of the CRC base. Also, because the pavement structure in these widened areas is different from that of the adjacent jointed structure, the overburden stresses are different; thus, the effects of stress sensitivity of the subgrade were considered in determining its support, i.e., resilient modulus.

Other design factors apparent in Figure 10 include the level-up course, the flexural strength of the CRC base, and the absence of a subbase layer beneath the CRC base.

Because the minimum thickness of AC to be used in bringing the surface of the structure to the desired cross slope was 2.5 cm (1 in), this measure was used for design. Also, because the CRC base is well beneath the surface of the structure, its strength requirements are less than those of the overlay. Consequently, a 14-day flexural strength of 3792 kN (550 psi) is recommended and used for design. Recall that the 14-day overlay flexural strength recommended was 4482 kN (650 psi).

It was originally expected that a subbase layer would not be placed beneath the CRC base; consequently, none was used in the design. Although an AC water seal is now expected to be constructed below the base, its presence would not change the CRC base thickness design significantly.

The graph in Figure 11 provides the curves for selecting the CRC base thickness for the poor and fair sections. The CRC base thickness $D_{(2)}$ in the outside lane—by using the expected 14 million 80-kN (18-kip) ESAL applications determined earlier--should be 17.5 cm (6.9 in) for the poor sections and 16 cm (6.3 in) for the fair sections.

It is important to note that these curves also give the CRC base thickness required where widening will occur on the inside lanes. For example, if the lane distribution factor for the inside lane was 0.2, this would correspond to a design traffic of 4 million 80-kN ESAL applications and a CRC base thickness of less than 10.2 cm (4 in). Because the minimum practical construction thickness for CRCP must be considered, a CRC base thickness recommendation was not made for the inside lanes.

Analysis 3

The design analysis for this section is almost identical to that for the CRC overlay discussed in design analysis 1. Figure 5 shows where the AC overlay thickness $D_{(3)}$ is required.

After performing the materials characterization and selecting the other inputs required for the overlay design, a thickness design curve was generated. Then an overlay thickness $D_{(3)}$ of 15.5 cm (6.1 in) was recommended for the predicted future traffic of 6.4 million 80-kN (18-kip) ESALs in the design lane.

Figure 9. CRC overlay thickness-design curves for the fair and poor sections of existing JCP on I-35 north of the interchange.

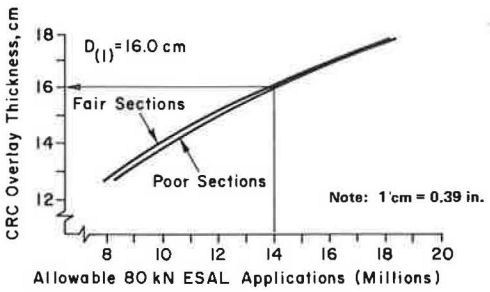

Figure 10. Pavement structure of CRC overlay and CRC base in widened areas adjacent to existing JCP along I-35 north of the interchange.

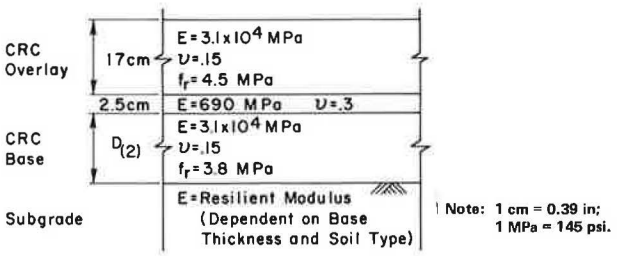

Figure 11. CRC base thickness-design curves for fair and poor sections adjacent to existing JCP along I-35 north of the interchange.

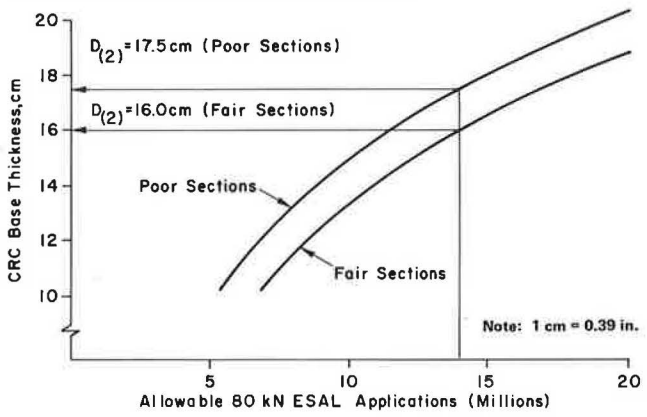

Analysis 4

The design analysis for this section is almost exactly the same as that for the CRC base discussed in design analysis 2. Figure 5 shows where the CRCP thicknesses $D_{(4a)}$ and $D_{(4b)}$ are required. Although the CRCP designed in this section will lie below an AC overlay, it is not considered a CRC base as in analysis 2 because the recommended strength is relatively high, 4482 kPa (650 psi).

A thickness design curve was generated by following the same procedure as before. The result was a thickness recommendation for $D_{(4a)}$ of 24.4 cm (9.6 in) where traffic was heavy--11.2 million 80-kN ESALs--and 17.8 cm (7 in) for $D_{(4b)}$ where traffic was light—3.2 million 80-kN ESALs.

Analysis 5

This analysis is concerned with the design of a new CRCP on the I-410 leg where an old jointed pavement is to be removed and a new grade established. The part of the overlay design model that estimates the life of an existing pavement (given its laboratory-determined material properties) was used to generate the thickness design curve for the new CRCP (Figure 12). The pertinent design parameters used to generate this curve are as follows:

1. Flexural strength of the concrete—Since heavy traffic is anticipated during the design life of the structures, a 14-day concrete flexural strength of 4482 kPa (650 psi) was selected.
2. Subbase properties--Some 15 cm (6 in) of crushed stone base was recommended and used for design. The elastic modulus of this material was assumed to be 138 MPa (20 000 psi).
3. Subgrade properties--Because this area is the same as that classified as poor in design analysis 1, the same subgrade properties were used for design. However, the effect of a different stress condition applied to the subgrade due to the different pavement structure, i.e., subgrade stress sensitivity, was again considered in the design.

Because the 80-kN (18-kip) traffic expected on this structure is also 20 million ESAL applications, the number of applications that can be expected in the design lane (by using the lane-distribution factor of 0.7 discussed earlier) is 14 million. The design thickness $D_{(5)}$ recommended, then, is 33 cm (13 in) if roto-milling operations are expected.

Figure 12. Reconstruction CRCP thickness-design curve for I-410 leg of the project.

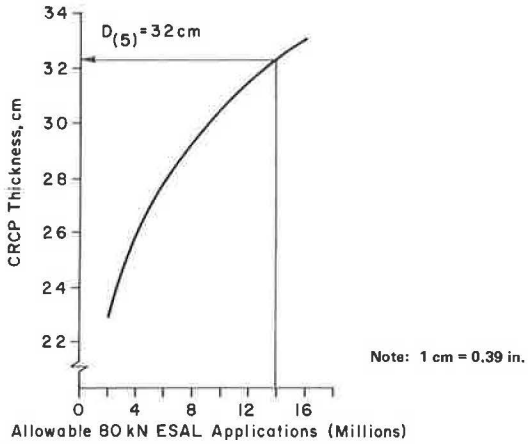

SUMMARY OF DESIGN RECOMMENDATIONS

Table 2 summarizes the thicknesses recommended as a result of the CFHR design analysis for each of the design sections. In addition, specific comments are noted that should be considered in the preparation of the project plans, specifications, cost estimates, and guidelines for construction control.

COMMENT AND RECOMMENDATIONS

The application of the design procedure in this project indicates that it is effective and provides rational results. Due to the inadequacies of past design methods, it is impossible to provide comparisons between old and new procedures. It is practical, though, to provide a summary of significant aspects and capabilities of the new procedures as they are related to the designs developed in the project. Recognition of the benefits listed below should promote acceptance and use of the new design procedure.

1. Past overlay design methods experienced difficulty in modeling the different design combinations formulated in this project; the new method with its inherent flexibility provides rational solutions. For example, no other methods are available to estimate the life of a pavement consisting of two PCC layers of different strengths separated by an AC level-up course. Also, no other methods are available that can handle the design of a composite structure, i.e., a thick AC layer on foundation CRCP. These capabilities of the new procedure make it very attractive.
2. Another significant capability is the fact that data required for making the overlay designs were gathered with a minimum of traffic interference. The Dynaflect deflection data, used to characterize the pavement materials in this project, were obtained in less than one day with only one lane closed.
3. Recent experience in urban areas shows a trend toward large future traffic volumes. This requires the use of thicker pavements than those used in the past. Consider the 14 million 80-kN (18-kip) ESALs to be carried by the 33-cm (13-in) CRCP. The crude stress model incorporated into the American Association of State Highway and Transportation Officials' Interim Guide fatigue equation makes it less reliable for thicknesses of this magnitude. The use of advanced computer models to predict the pavement response under load and environmental conditions makes the new overlay design model more reliable.
4. The new overlay design procedure can also account

Table 2. Summary of design recommendations.

Section	Recommended Thickness (cm)	Pavement Type	Comment
1	18	CRCP overlay	14-day flexural strength = 4.5 MPa, limestone coarse aggregate; 1.8 cm of pavement may be removed for improving skid resistance
2	18	CRC base	14-day flexural strength = 3.8 MPa, limestone coarse aggregate; remove surface finish requirements from specifications
3	15	AC	Design for interior
4a	25	CRCP base	14-day flexural strength = 4.5 MPa, limestone coarse aggregate; remove surface-finishing requirements
4b	18		
5	33	CRCP	14-day flexural strength = 4.5 MPa, limestone coarse aggregate

Note: 1 cm = 0.394 in; 1 MPa = 145 psi.

for effects of different aggregate types in the concrete mix on loss of load transfer and loss of skid resistance.

Few problems were encountered in the design of the pavements in this project. However, there were some areas identified where lack of sufficient data or information perhaps led to the selection of conservative estimates of necessary inputs to the procedures. Consequently, some recommendations are made here for future research that include (a) a study of heavy-traffic lane distribution in multilane facilities and (b) the development of a quicker and less expensive method for characterizing the stress sensitivity of the subgrade.

CONCLUSION

The objectives of this paper were to demonstrate the use of the theoretically based overlay design procedure now being incorporated into Texas SDHPT practice and to illustrate its value by application in a complex design situation.

Although this procedure is new and has little field verification, its design models are based on sound engineering principles so that it produces practical designs. Verification will take at least 5-10 years of observed field performance. It should be noted, too, that the procedure was effectively and easily applied to a complex pavement rehabilitation design situation that resulted in five separate design configurations.

This paper, it is hoped, will provide some basis for (a) the acceptance of the new procedure, (b) the improvements in the areas discussed previously, and (c) the incorporation of the method into nationwide practice.

ACKNOWLEDGMENT

This research was conducted at the Center for Highway Research, University of Texas at Austin. We wish to thank the Texas SDHPT whose sponsorship is gratefully acknowledged. Special thanks are also extended to Texas SDHPT staff members Raymond Stotzer, Frank Holzman, and Gerald Peck, who provided the inspiration and assistance necessary to undertake and complete the project. The contents of this report reflect our views, and we are responsible for the facts and accuracy of the data presented herein. The contents do not necessarily reflect the official views or policies of the Federal Highway Administration. This report does not constitute a standard, specification, or regulation.

REFERENCES

1. Overlay Design and Reflection Cracking Analysis for Rigid Pavements. Federal Highway Administration, Aug. 1977, Vols. 1 and 2.
2. O. Schnitter, W.R. Hudson, and B.F. McCullough. A Rigid Pavement Overlay Design Procedure for Texas SDHPT. Center for Highway Research, Univ. of Texas at Austin, Res. Rept. 177-13, May 1978.
3. S. Seeds. A Design System for Rigid Pavement Rehabilitation. Univ. of Texas at Austin, Master's thesis, May 1980.
4. A. Taute. Development of Fatigue Relationships for New and Overlaid CRC Pavements. Univ. of Texas at Austin, Master's thesis, May 1980.
5. G. Ahlborn. ELSYM5—Elastic Layered System with One to Ten Normal Identical Circular Uniform Loads. Institute for Transportation and Traffic Engineering, Univ. of California, Berkeley, March 1972.

Publication of this paper sponsored by Committee on Pavement Rehabilitation Design.

Prevention of Reflective Cracking in Arizona

GEORGE B. WAY

This report represents the culmination of more than seven years of careful planning, construction, and objective data analysis. The results should be of value to federal, state, and local agencies concerned not only with the restoration of existing roadways but also with new highway construction. The recommendations contained herein refer to overlays—in particular, thin overlays of 102 mm (4 in) or less placed over existing badly cracked, rutted, or otherwise distorted bituminous pavements. Overlaying can also improve skid resistance or rideability. However, no one treatment is a cure-all for all roadway conditions. Rather, the recommended crack-preventing treatments should be integrated into a total overlay design that is carefully tailored to the nature of the distress. Five treatments have significantly reduced reflective cracking: (a) asphalt-rubber membrane seal coat under asphalt concrete finishing course (ACFC), (b) asbestos plus 3 percent asphalt, (c) heater scarification with reclamite (surface recycling), (d) asphalt-rubber membrane flushed into asphaltic concrete overlay, and (e) 200/300 penetration asphalt. Application considerations are as follows: (a) one of the preceding treatments should be used in conjunction with a thin overlay of 102 mm (4 in) or less of asphalt concrete (AC), (b) application of an asphalt-rubber membrane seal coat under the AC or ACFC should be used with chips to provide direct transfer of vertical loads, (c) heater scarification should be to a depth of 19 mm (0.75 in) or more, and (d) the lowest possible viscosity AC asphalt with the slowest aging characteristics should be used. Findings from this project led to the use of thin overlays with special treatments. The thickness of these thin overlays varies from 19 mm (0.75 in) to 90 mm (3.5 in). If significant cracking appears on the existing highway before overlay, a special treatment is used. Treatments include either asphalt-rubber or heater scarification.

The primary objective of any pavement design is not only to provide a roadway of safe and desirable ride performance but to extend these characteristics over a maximum useful life with minimum required maintenance. However, due to the highly complex nature of flexible pavement structures, cracking, rutting, and other surface failures do occur and are primarily influenced by environmental, traffic, and original design factors. To extend the useful life of deteriorating roadways, generally accepted restoration typically involves the application of a thin asphaltic overlay formulation on the cracked and otherwise deformed pavement.

Historically, however, the application of these thin overlays—generally 102 mm (4 in) or less--results in a new and complex problem, known as reflective cracking. Reflective cracking is the migration of a subsurface cracking pattern into and subsequently through the overlay structure. Of course, once the overlay is fractured, general erosion occurs that severely affects performance and requires further and costly maintenance.

In an attempt to better understand the mechanism of reflective cracking and to pursue the development of new methods and materials to prevent its occurrence, a case study was conducted by the Arizona Department of Transportation (ADOT) in conjunction with a project of the Federal Highway Administration's National Experimental

and Evaluation Program (NEEP) on reducing reflective cracking in bituminous overlays. The NEEP project's objective was to improve and develop materials, methods, and technologies to prevent or greatly minimize the occurrence of reflective cracks in overlays placed on previously cracked bituminous pavements.

Preliminary evaluation and program study involved extensive material and treatment research, the selection and evaluation of test-site conditions, and the determination of an effective means for data accumulation and reduction. Some 18 individual roadway test sections were required to accommodate the full scope of desired test parameters. Adjacent to each test section was a control section that served as a normalizing base for comparative measurement. This approach allowed engineers to observe and accumulate qualitative results from each test section, contrast these results, and predict individual parameter influence. From these results, the determination of recommendations based on the effectiveness of crack prevention, cost, and other factors was made.

PROJECT DESIGN AND CONSTRUCTION

The test program was conducted on a 14.4-km (9-mile) section of highway (Minnetonka-East), located near Winslow, Arizona, on I-40. Winslow is considered a high desert region; it has an elevation of 1524 m (5000 ft) and less than 204 mm (8 in) of rainfall annually. Temperature variations range from -18°C (0°F) during the winter to 38°C (100°F) during the summer. Minnetonka-East had a moderate-to-heavy average daily traffic (ADT) load of 10 000, a reasonably severe climate, and a history of severe cracking problems. This section of highway had become eligible for overlay during 1967 and was selected for use in the NEEP test program in 1970--the year the program was initiated.

Preparatory to the test design, extensive preevaluation was performed to determine the nature and degree of distress. This evaluation involved many investigations, including core sampling, structural support testing, visual surveys, rut depth measurements, Benkelman beam tests, and traffic surveys.

Minnetonka-East was originally constructed as two projects: (a) I-008-4(3), originally constructed in September 1958, and (b) I-40-4(15), originally constructed in August 1962. The useful life to point-of-overlay eligibility (1967) for each highway segment was approximately nine years for I-008-4(3) and five years for I-40-4(15), with considerable intervening maintenance performed. The original materials used and their applied thicknesses are briefly described here. For I-008-4(3) (Station 208-504), completed in 1958, these materials and thicknesses were used: asphalt concrete (AC), which was plant mixed with 200/300 penetration asphalt, 89 mm (3.5 in); a bituminous-treated base of blow sand mixed with RC-2 and RC-3, 77 mm (3 in); and blow sand (select material) to a depth of 152-381 mm (6-15 in). For I-40-4(15) (Station 504-705), completed in 1962, these materials and thicknesses were used: AC (3/4-in fine mix), which was plant mixed with penetration asphalt, 101 mm (4 in); an aggregate base of Terrance sand and gravel deposit (the latter generally of a chert nature), 152 mm (6 in); blow sand (select material) to a depth of 152-304 mm (6-12 in); and a subgrade seal of blow sand, 228 mm (9 in).

Field investigations were conducted in 1969 and included Benkelman beam deflection tests, rut depth, and general condition. Data from these tests are noted in the following table (1 mm = 0.039 in):

Item	Maximum	Minimum	Average
Rutting, mm	38	0	14
Benkelman beam, mm	1.88	0.05	0.89

The condition survey found extensive cracking, including block (flexural) and shrinkage (thermal) cracks. Spalling and rutting were also noted.

Designers felt that a 127-mm (5-in) overlay was needed to properly contain the degree of distress, although federal participation was limited to an overlay thickness of 32 mm (1.25 in) for AC and 13 mm (0.5 in) for asphalt concrete finishing course (ACFC). Designers concluded that the placement of such a thin overlay would produce significant reflective cracking early in the life of the overlay—primarily due to reduced structural support. This early cracking would then warrant extensive maintenance with loss of ride and appearance. This situation, in effect, would return the roadway to an unsatisfactory condition in a relatively short period of time. However, since this was the case, Minnetonka-East was an ideal choice for a thin-overlay test program because valid conclusions would be available within a short period of time. It was on this basis that the test program was to proceed, with, in many cases, rather significant and impressive results.

After considerable consultation with materials suppliers, other states, designers, and the Federal Highway Administration, 18 test sections were developed. The 18 test sections were unique in design, treatment, and materials used. The following list gives a brief description title for each treatment by test section number:

Test Section Number	Description
1	Asphalt-rubber plus precoated chips
2	Heater scarification plus petroset
3	Asphalt-rubber membrane interlayer (placed over AC and under ACFC)
4	Asphalt-rubber membrane interlayer (placed over AC and under ACFC)
5	Asbestos-fortified AC mix
6	AC, 51 mm (2 in); no ACFC
7	Los Angeles Basin 120/150 penetration asphalt
8	Los Angeles Basin 40/50 penetration asphalt
9	Four Corners 120/150 penetration asphalt
10	Los Angeles Basin 200/300 penetration asphalt
11	Emulsion-treated base in place of AC
12	Petromat placed under overlay
13	Fiberglass placed under overlay
14	Petroset flush of overlay before ACFC placed
15	Petroset placed in cracks
16	Reclamite placed in cracks
17	Reclamite flush of old AC
18A,B,C	Heater scarification of old AC plus reclamite flush, with varying AC overlay thickness
18A	32-mm (1.25-in) AC overlay
18B	76-mm (3-in) AC overlay
18C	38-mm (1.50-in) AC overlay
Control sections	Conventional (standard) overlay

Construction

As is true with many construction projects, highway sections are not necessarily constructed in a sequential, orderly fashion. Instead, the contractor adjusts and tailors the operation to the nature of the work. Since the Minnetonka-East project involved a large number of test sections calling for different treatments, a logical construction sequence was not possible. A detailed account of the construction process appears in Way (1).

Many of the construction problems, however, were peculiar to the nature of a particular treatment and the contractor's inexperience in working with certain materials. For example, specific problems of this type included the balling up of fiberglass matting, difficulty in blade-laying the emulsion-treated base, the inability of a subcontractor to make a 10 percent latex emulsion, and construction delays in the distribution of asphalt-rubber that caused application of 4.5 L/m² (1 gal/yd²) instead of the

intended 2.5 L/m² (0.55 gal/yd²) on test section 1.

As it was, prior to and during the construction sequence, project engineers spent considerable time consulting with suppliers and other sources to determine what problems might be encountered. Although certain problems did occur, they were kept to a minimum. Whether each treatment received equitable consideration during construction can be debated, however. All suppliers and consultants were asked to comment and offer a critique during each construction phase; generally, no unfavorable comments were reported with respect to the individual treatments.

Problems

A few general construction problems did occur that were not peculiar to any particular treatment. These problems were primarily related to compaction and rutting.

The AC mix used on the eastbound highway, typically, was difficult to compact to the 92 percent minimum compaction specification. Compaction test results for the eastbound highway were 87.2 percent in September 1971 (based on an average of 50 or more tests) and 89.2 percent in March 1975 (computed from 10 cores); those for the westbound highway were 91.5 percent in September 1971 (50 or more tests).

Great effort was made to overcome this problem. More compactive force, vibratory rollers, additional asphalt, and a more viscous asphalt were all tried, but none of these techniques overcame the fundamental problem. That is, the mix, due to the harsh angular texture of the aggregate (cinders) plus the thickness of the AC mat, made compaction to 92 percent virtually impossible. A change in mix design to blend sand (blow sand)--in place of cinder sand--and vibratory rolling did increase compaction for the westbound highway.

Significant rutting on both highways made placement of 32-mm (1.25-in) AC very difficult. As a result, during April 1972, considerable additional AC was used as patching material in spalls and ruts of the eastbound highway. In some places, the actual depth of pavement placed was closer to 76 mm (3 in) in the wheel paths.

Nevertheless, when one considers the nature and magnitude of the task, the construction of the Minnetonka-East project went quite smoothly.

PROJECT MONITORING

Although various test sections were opened to traffic on an as-completed basis, final construction was completed in June 1972 and exposed to unrestricted traffic. It should be noted that, since completion of overlaying in 1972 through 1978, the highway has been subjected to loads equivalent to more than 1 million 80-kN (18-kip) cumulative single-axle equivalents.

Climatic variations were rather severe during the test period with above-average rainfall in 1972. Also, the test region had a freezing index of 260 during the 1974-1975 winter.

Table 1. Test-section ranking of treatments that significantly reduced reflective cracking, Arizona, 1975 and 1978.

Test Section Number	Treatment	Percentage of Reflective Cracking	
		1975	1978
3,4	Asphalt-rubber under ACFC	4	2.1
5	Asbestos plus 3 percent asphalt	13	5.9
18A	Heater scarification plus reclamite	6	7.4
1	Asphalt-rubber seal coat flushed into AC overlay	19	12.8
10	200/300 penetration asphalt control sections without patching	17	27

Because the Minnetonka project was designed to determine which materials and treatments would significantly reduce reflective cracking, it was necessary to accurately determine the extent and type of cracking both before and after overlay. This was accomplished by a special photographic technique and an optical grid system. The number of cracks within each grid element was programmed into a computer for analysis and subsequent time-base comparison. This technique proved very effective. All photo locations were photographed each year through 1978.

The percentage ranking figures (Table 1) represent a true perspective of the percentage of cracking after overlay. This was accomplished by dividing the percentage of area cracked after overlay by the percentage of area cracked before overlay for those sections with no patching (2,3). This test-section ranking represents one of the most important parts of this study. It clearly sets forth those five treatments that, when used in conjunction with an ACFC or other suitable open-textured surface, were capable of significantly reducing reflective cracking. These percentages are particularly significant in consideration of the very thin overlay used.

Five treatments were found to have significantly reduced reflective cracking:

1. A 2.3-L/m² (0.5-gal/yd²) asphalt-rubber membrane placed on top of a 32-mm (1.25-in) AC overlay, chips applied and then covered with a 13-mm (0.5-in) ACFC;
2. A 3 percent asbestos and 3 percent additional asphalt added to the 32-mm (1.25-in) AC overlay and covered with a 13-mm (0.5-in) ACFC;
3. Existing AC heater scarified to a depth of 19 mm (0.75 in) and a 0.5-L/m² (0.1-gal/yd²) emulsified petroleum resin applied, and then the surface (after rolling) overlayed with 32-mm (1.25-in) AC and 13-mm (0.5-in) ACFC;
4. A 32-mm (1.25-in) AC overlay flushed with 4.5-L/m² (1-gal/yd²) asphalt-rubber and coated with chips; and
5. A 200/300 penetration asphalt from the Los Angeles Basin added to the 32-mm (1.25-in) AC overlay and covered with a 13-mm (0.5-in) ACFC.

Also, it was found that basic asphalt properties influenced the reduction of reflective cracking. It was found that the viscosity of 4.0 MPa•s at 25°C (77°F) [equivalent penetration about 45, absolute unaged viscosity of 300 Pa•s at 60°C (140°F)] was critical to crack initiation. That is, the longer an asphalt can maintain a viscosity below 4.0 MPa•s, the less likely that reflective cracks will occur. Actual physical crack formation and intensity are triggered by cold temperatures. Thus, once the asphalt reaches the 4.0-MPa•s level, it becomes highly susceptible to cracking. Therefore, it is an important consideration that all system designs use the lowest-viscosity asphalt commensurate with stability requirements and to use it in such a way as to retard aging as much as possible.

CONCLUSION

It has been demonstrated that thin overlays plus special treatments can control cracking and can provide more-than-satisfactory ride and rutting performance. Such thin overlays plus treatment are economic by any measure. The mechanism by which these treatments perform can be summarized as follows:

1. Stress-absorbing membrane interlayer (SAMI)—Use of asphalt-rubber between the new AC and ACFC acts as a crack-tip retarder because it has such a low modulus of elasticity--estimated at about 34 474 Pa (5000 psi). The placement of this layer at or near the top of the overlay delays reflective cracks; however, an uncomfortable amount of shoving can occur, thus leading to a rough ride. Such a condition became apparent after the 1975 asphalt-rubber

seal coat was placed over the ACFC. This seal coat was not necessary; however, its placement helped verify the point at which flexibility can give way to instability. To be consistent with fracture mechanics theory (4), it is suggested the asphalt-rubber layer be placed on top of the old AC with the new AC on top of it. In this way, the overlay structure would comply with conclusion 1 of the Texas report (4):

> The best overlay design to reduce the appearance of cracking is, as shown in Figure 20, namely, (a) a thin layer with soft asphalt (low n) and low modulus of elasticity to serve as a stress-relieving medium overlaid by (b) a layer with soft asphalt (low n) and a high modulus of elasticity. Although this arrangement will hasten the propagation of unseen cracks through the surface of old pavement, it will slow them down considerably when they reach the surface and contact the underside of the stress-relieving layer.

2. Mechanical rearrangement of the old AC crack pattern, heater scarification--This process, which is akin to in-place recycling, remolds 19 mm to 25 mm (0.75 to 1 in) of old AC into a material similar to a new AC. In so doing, it shortens the existing crack length by 19-25 mm (0.75-1 in). This shortening of crack length can and does substantially reduce reflective cracking as demonstrated in the Texas report (4), which examines reflective cracking by using fracture mechanics.
3. Low-viscosity asphalt in the AC or over asphalted AC, 200/300 penetration, and asbestos sections—Both the 200/300 penetration and asbestos sections substantially alter the elastic modulus of the AC, thus altering certain fatigue parameters that reduce the crack-tip stress-intensity value. In some ways, this approach is akin to the asphalt-rubber interlayer, except that the layer now becomes the entire AC overlay.

The Minnetonka-East program, in conjunction with the NEEP project, was initiated in an attempt to better understand the mechanism, treatments, and methods necessary for the reduction or prevention of reflective cracking in overlays placed on severely cracked bituminous pavement.

This report represents the culmination of more than seven years of careful planning, construction, and objective data analysis. The results should be of value to federal, state, and local agencies concerned not only with the restoration of existing roadways but also with new highway construction.

Recommendations

Five treatments were found to have significantly reduced reflective cracking:

1. Asphalt-rubber membrane seal coat under ACFC,
2. Asbestos plus 3 percent asphalt,
3. Heater scarification with reclamite (surface recycling),
4. Asphalt-rubber membrane flushed into asphaltic concrete overlay, and
5. A 200/300 penetration asphalt.

Application considerations are as follows:

1. One of the above treatments should be used in conjunction with a thin overlay of less than 102 mm (4 in) of AC.
2. Application of an asphalt-rubber membrane seal coat under the AC or ACFC should be used with chips to provide direct transfer of vertical loads.
3. Heater scarification should be to a depth of 19 mm (0.75 in) or more.
4. The lowest-viscosity AC asphalt with the slowest aging characteristics should be used.
5. Existing roadways that are being considered for overlay should be carefully investigated for possible stripping tendencies. Should stripping appear likely, efforts should be made to either give less structural value to the existing AC or reconstruct the existing surface.
6. Open-texture surfaces should be placed on top of dense-graded overlays. This not only provides good skid resistance but improves the roadway's appearance by hiding narrow reflective cracks.

Implementation

During the course of this project, it became obvious that certain treatments were performing better than others. By 1975, both the heater-scarification and asphalt-rubber methods looked very promising. Both methods promised a practical means to control reflective cracking. Thus, the use of these treatments in overlays was accelerated. The number of projects and kilometers of overlays built since 1975 are as follows (1.6 km = 1 mile):

Type	Number of Projects	Number of Kilometers
Overlays > 90 mm (3.5 in); no treatment	80	864
Overlays with heater scarification	43	576
Overlays with asphalt-rubber	33	400

Generally, treatment with either heater scarification (currently referred to as surface recycling) or asphalt-rubber (also called SAMI) is used when the existing pavement has 10 percent or more cracking. Typical costs per square yard are AC, 1 in, $1.05; ACFC, 0.5 in, $0.75; heater scarification plus emulsified petroleum resin, $0.80; and asphalt-rubber plus chips, $1.30.

Projects are monitored for roughness and percentage of cracking annually. Now, both treatments are working as expected. Heater scarification has generally been used in the desert regions, whereas asphalt-rubber has been used in the high-elevation areas. ADOT is including both types of treatment in its pavement management system as beneficial overlay alternatives.

REFERENCES

1. G.B. Way. Prevention of Reflective Cracking in Arizona, Minnetonka-East (A Case Study). Arizona Department of Transportation, Phoenix, May 1976.
2. G.B. Way. Tests on Treatments for Reflective Cracking. TRB, Transportation Research Record 647, 1977, pp. 10-13.
3. G.B. Way. Prevention of Reflective Cracking, Minnetonka-East (1979 Addendum Report). Arizona Department of Transportation, Phoenix, Aug. 1979.
4. S.H. Carpenter, H. Chang, and R.L. Lytton. Prediction of Thermal Reflection Cracking in West Texas. Texas Transportation Institute, Univ. of Texas at Austin, March 1976.

Publication of this paper sponsored by Committee on Pavement Rehabilitation Design.

Dynamic Surface Deflection Measurements on Rigid Pavements Compared with the Model of an Infinite Plate on an Elastic Foundation

ALBERT J. BUSH III

The purpose of this study was to develop relations by using the Hertz theory of an infinite plate on a dense fluid subgrade between deflections measured at the point of and away from an applied load and the strength parameters of the pavement. An evaluation procedure was to be developed based on these relations, known pavement characteristics, and dynamic response data collected with the U.S. Army Engineer Waterways Experiment Station (WES) 16-kip vibrator. Deflection relations were established by using a computer program (PCADL) developed by the Portland Cement Association. The deflections were related to the radius of relative stiffness (ℓ), which is a characteristic length dependent on the rigidity of the plate. Maximum stresses were predicted by using the General Dynamics Corporation's H-51 program. From these stresses, a relation was developed between the dynamic stiffness modulus, ℓ, and the allowable single-wheel aircraft load (ASWL). Both destructive and nondestructive vibratory data were collected on 28 different pavements. Destructive data were used to characterize the pavement material properties and then, by using conventional procedures, to predict the ASWL. Deflection basin data from the WES 16-kip vibrator were used to measure ℓ by using the relations developed from the PCADL program. The study concluded that nondestructive test data can be used with more confidence than previously developed procedures to predict ℓ and ASWL as a function of ℓ.

Structural evaluation of airfield pavements has been the subject of considerable study since the early 1900s. Until recently, generally accepted methods for evaluating pavements were visual observation and destructive testing in which strength parameters are determined from field and laboratory evaluation of the individual components of the pavement system. These strength parameters were applied to some design procedures to relate to the remaining life of the pavement. The disadvantage of this evaluation procedure is that it closes the facility for a period of up to five days, depending on the length of the runway and the depth of the study. For example, the closing of two out of six runways for one day at a large hub-connection airport in early 1975 cost airlines more than $500 000 in crew and fuel costs, not to mention the inconvenience to air travelers (1). If a nondestructive test (NDT) method had been used, the testing could have taken place at night when traffic is light. Furthermore, if wind conditions or some other factor had required that the particular facility be opened, the NDT equipment could have been removed immediately and traffic resumed.

Other demonstrated advantages are that the cost of a nondestructive evaluation is less than conventional procedures and that the number of tests performed improves the statistical reliability of the procedure. If conventional procedures are used, it is not known whether the test location selected is representative of the section of pavement, whereas NDTs can be run at relatively close intervals to provide a reliable evaluation of the complete feature.

Vibratory testing of pavements was begun as early as 1933 by the German Research Society for Soil Mechanics. It was further developed by the Royal Dutch Shell Laboratory in Holland.

The U.S. Army Engineer Waterways Experiment Station (WES) commenced vibratory testing of pavements in search of nondestructive evaluation procedures in cooperation with Shell researchers in the mid-1950s. These early tests by the WES followed the procedures used by the Shell researchers. The results of this testing were reported by Heukelom and Foster (2). Different methods were presented, including wave-velocity measurements, traffic stiffness, dynamic stiffness, and laboratory stiffness.

The WES has selected the dynamic stiffness measurement for its evaluation procedure. This concept was first introduced by Van der Poel (3) in 1951. He described it as the concept of measuring the "overall rigidity of road construction" by dynamic deflections. He defined the overall rigidity (S) as the amplitude of dynamic force required to act on the pavement to produce a unit amplitude in deflection on the surface of the pavement. Today, S is more commonly referred to as the dynamic stiffness. Van der Poel noted that S was not constant but dependent on the driving frequency and that, at high frequencies, S could be expected to increase. He also pointed out the possibility of errors in interpretation due to the existence of unaccounted for resonances and significant differences between applied force and actual force acting on the pavement.

In recent work at the WES by Green and Hall (4), an evaluation procedure for both rigid and flexible pavements has been developed that uses the dynamic-stiffness concept. There is a difference in the computation of the stiffness factor from that introduced by Van der Poel; that is, stiffness is defined at a fixed frequency of 15 Hz and takes into account the nonlinear response. The dynamic load is swept from 0 to 66.7 kN (0 to 15 kips) and is plotted on an X-Y plotter versus the dynamic deflection. The inverse slope of the line generated [taken at dynamic force levels of 44.5 and 62.3 kN (10 and 14 kips)] is called the dynamic-stiffness modulus (DSM) (Figure 1). Van der Poel's stiffness was calculated as the dynamic load divided by the deflection.

In the study by Green and Hall (4), DSM was correlated directly with allowable single-wheel load (ASWL) for both flexible and rigid pavements. With this load and with other known parameters, the allowable gross load for a given aircraft was determined.

In 1975, at the Symposium on Nondestructive Test and Evaluation of Airfield Pavements (1), a method was described for evaluation of full-depth asphalt pavements by using the Hogg model of an infinite plate on an elastic foundation. For rigid pavements, the Hertz model was used. Sufficient data on full-depth asphalts have not been obtained for verification of the Hogg model; therefore, this paper will concern only rigid pavements.

STUDY PURPOSES AND SCOPE

The purposes of this study are

1. To develop relations by using the Hertz theory of an infinite plate on a dense fluid subgrade between deflections measured at the point of and away from an applied load and the strength parameters of a pavement;
2. To develop an evaluation procedure by using the relations noted here, known pavement characteristics, and dynamic response data collected with the WES 16-kip vibrator; and
3. To compare this evaluation procedure with that developed by Green and Hall (4).

This study will be limited to rigid pavements and will only cover the prediction of ASWL for a given traffic level. Procedures already established can be used to derive multiple wheel loads for varying traffic levels. Vibratory

Figure 1. Typical deflection-versus-load data with DSM calculations for the WES 16-kip vibrator.

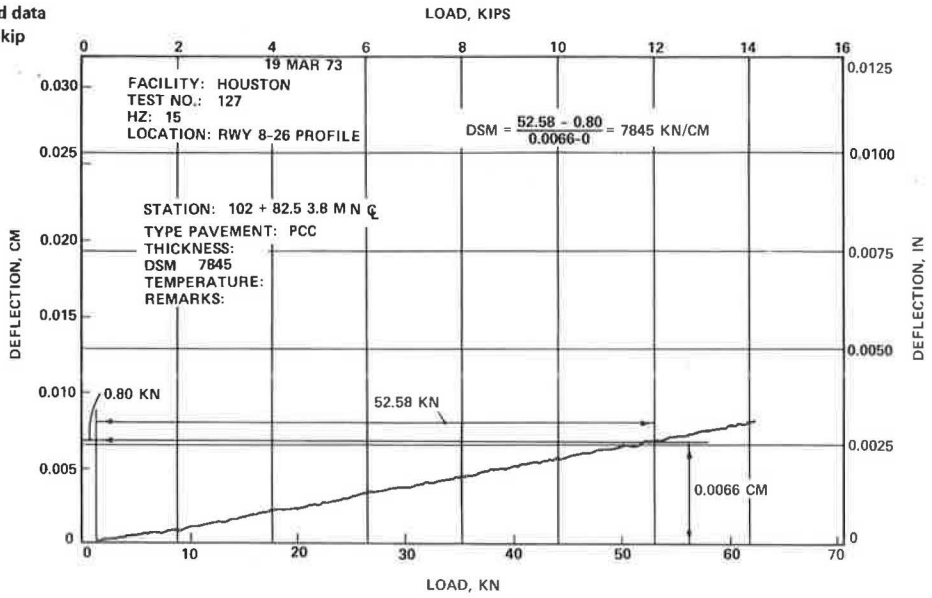

Figure 2. The WES 16-kip vibrator.

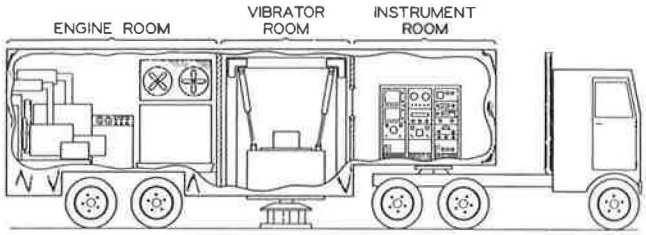

data were collected with the WES 16-kip vibrator, and the relations developed are characteristic of this vibrator. The nondestructive tests at each test site included frequency response, load deflection, and deflection basin data. Only the load deflection and deflection basin data will be considered in this report.

TEST EQUIPMENT, PROCEDURES, AND DATA COLLECTED

Test Equipment

The vibrator used in collecting the dynamic pavement response data is an electrohydraulic-actuated vibrator, designated the WES 16-kip vibrator (Figure 2). This instrument is mounted in a 10.9-m (36-ft) semitrailer that contains supporting power supplies and data-recording systems. Electric power is supplied by a 25-kW diesel-driven generator and hydraulic power is supplied by a diesel-driven pump that can deliver 144 L/min (38 gal/min) at 20.7 MPa (3000 psi).

The force generator consists of an electrohydraulic actuator surrounded by a lead-filled steel box. Its total static weight is 7.3 Mg (16 000 lb). The actuator uses up to a 5.08-cm (2-in) double-amplitude stroke to produce a vibratory load ranging from 0 to 66.7 kN (0 to 15 kips) with a frequency range of 5-100 Hz for each load setting. When the force generator is lowered to the pavement, its entire weight rests on the pavement. The static and dynamic force is transmitted to the pavement through three load cells that are connected to a steel loading plate 45.7 cm (18 in) in diameter. The signal from each load cell is summed to produce the force output of the system.

A velocity sensor is mounted directly on the loading plate, and the integrated output of the sensor is used for deflection measurements. The actual measurement system consists of an 870-ohm, 3-Hz velocity sensor that is shunted to a damping factor of 0.7 and an 0.8-Hz integrator. The deflection basin is measured by placing four velocity sensors at specified distances away from the plate. A digital printer is used to record the output of the frequency counter, the summation of the three load cells, and each of the velocity sensors. In addition, data are plotted on an X-Y recorder to produce a load-versus-deflection plot.

For destructive-type tests to determine the properties of the pavement layers, a small-aperture procedure (5) was selected. A small, trailer-mounted drill rig (Figure 3) was used for cutting a core hole 15.2 cm (6 in) in diameter through the pavement. Through this core hole, California bearing ratios (CBRs) and layer thicknesses were measured and samples collected for laboratory classification tests.

Test Procedures

Small-aperture testing was conducted at each test site prior to vibratory testing. This procedure consists of extracting a 15.2-cm (6-in) diameter core from the pavement, then measuring CBRs on the base course or courses and on the subgrade. Samples of each pavement layer were collected, and gradation tests and Atterberg limits tests were performed on each to classify the pavements. The portland cement concrete (PCC) core was tested by using the tensile-splitting method (6). These results were then converted to flexural strength (7).

Nondestructive tests included a load-versus-deflection test at each site. During this test, the peak load is varied from 0 to 66.7 kN (0 to 15 kips) with the frequency held constant at 15 Hz (Figure 1). Also included at each site are deflection basin measurements. The load is held constant at a constant frequency (15 Hz) for this test. Data were generally collected at a constant load of 40 kN (9 kips). During both tests, the measurements were made at the slab center. Velocity pickups were placed in the direction of the largest dimension of the slab so as not to traverse a joint.

Normally a crew of three people is used, one of whom also serves as the driver of the semitrailer truck. To make the measurements, the vehicle is stopped at a measurement location and the force generator is lowered with the hydraulic lift mechanism directly through the floor of the semitrailer to the pavement.

Data Collected

Data for this study were collected during two test programs,

Figure 3. Small-aperture drill rig.

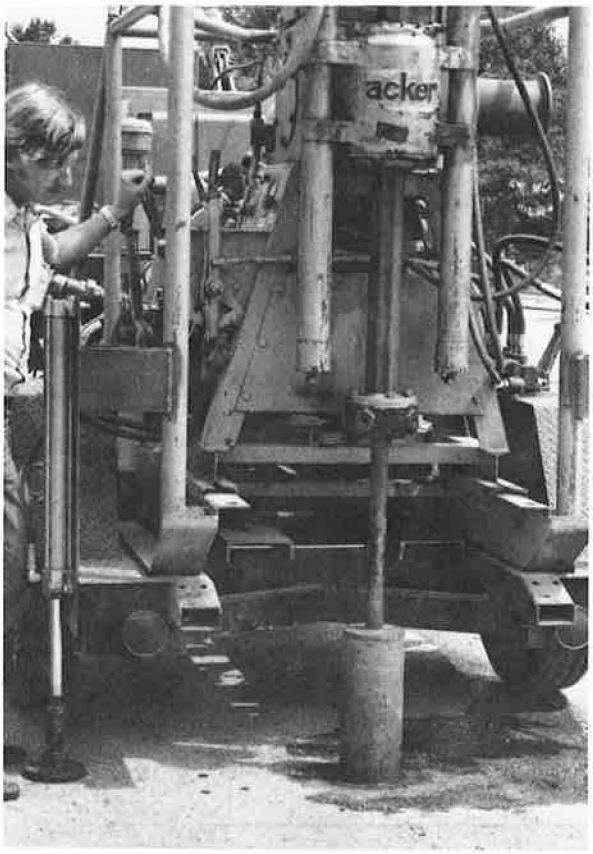

both of which were sponsored by the Federal Aviation Administration (FAA). The first study was the development of the evaluation methodology reported by Green and Hall (4). These data were collected during the period November 1972-December 1973. The second study was to determine if significant differences occurred in dynamic test data when pavement strength, condition, and temperature were varied. This study was cancelled prior to completion and, therefore, is not reported. Data for the significant-difference study were collected during the period June-October 1975. The following list notes the facilities where these data were collected and gives the letter designation used in this paper's tables and figures: National Aviation Facilities Experimental Center (NAFEC), Atlantic City, New Jersey (N); Houston Intercontinental Airport (H); Jackson Municipal Airport (J), Mississippi; Dallas-Fort Worth Regional Airport (DFW); Stapleton International Airport (DZ), Denver; Tucson International Airport (TZ); and Tulsa International Airport (TA), Oklahoma.

Results of small-aperture testing are shown in Table 1. Classification of the base course and subgrade materials are presented in two forms. The first is according to the FAA procedure (8). The second is according to the Unified Soil Classification System (9); these are noted in parentheses.

NDT results are listed in Table 2. Also listed are the ASWL and ℓ for each test pavement. The ASWL is computed from destructive test data and based on 1200 annual departures and a 20-year life for an aircraft with a 1639-cm² (254-in²) contact area on a single main gear. The contact area is also the area of the load plate on the vibrator and is in the range of most of the critical aircraft that use today's civilian airports.

The ℓ, a measure of the stiffness of a PCC slab relative to that of the subgrade, is computed from the formula:

$$\ell = [Eh^3/12(1 - \mu^2)k]^{1/4} \quad (1)$$

Table 1. Physical properties of pavements that underwent small-aperture testing.

Test Site Number	Facility	PCC Thickness (cm)	Flexural Strength (MPa)	Material[a]	Thickness (cm)	k (kPa/cm)	Subgrade Material[a]
N7	N-S runway	17.8	5.6	E-1 (GW)	20.3	950	E-4 (SP-SM)
N8	N-S runway	17.8	6.1	E-1 (GW)	20.3	977	E-4 (SP-SM)
N9	E-W runway	25.4	5.0	E-1 (GW)	20.3	882	E-4 (SP-SM)
N10	E-W runway	17.8	5.7	E-2 (GP)	20.3	774	E-4 (SP-SM)
N11	E-W runway	17.8	6.2	E-7 (ML-CL)	20.3	543	E-4 (SP-SM)
N13	Firehouse ramp	17.8	6.3	E-2 (GP)	20.3	1222	E-4 (SP-SM)
N15	E-W runway	25.4	6.0	E-7 (ML-CL)	22.9	271	E-4 (SP-SM)
N16	NAFEC ramp	38.1	5.2			1004	E-4 (GP)
N17	ANG ramp	19.1	5.7			423	E-6 (ML)
H1	Taxiway K	35.6	6.0	Soil-cement	22.9	556	E-6 (ML)
H3	Taxiway K	30.5	6.4	Soil-cement	20.3	1018	E-6 (ML)
H7	Taxiway B	30.5	6.4	E-5 (SP-SM)	14.0	1018	E-6 (ML)
H9	Taxiway B	31.8	6.1	E-5 (SP-SM)	29.2	1154	E-6 (ML)
H11	Taxiway B	31.8	6.2	E-5 (SP-SM)	27.9	1222	E-6 (ML)
J1	W runway	24.1	5.2	Soil-cement	15.9	516	E-7 (CL)
J2	W runway	27.9	5.0	Soil-cement	10.1	475	E-7 (CL)
J3	Light-plane ramp	19.1	5.1	Soil-cement	12.0	624	E-7 (CL)
J4	W runway	29.2	4.9	Soil-cement	15.2	529	E-7 (CL)
J5	W runway	22.2	6.7	Soil-cement	20.3	570	E-7 (CL)
DFWAG	AA-ramp	43.8	5.1	CSB[b]	23.5	543	E-11 (MH)
DFWAC	AA-ramp	43.8	5.1	CSB[b]	23.5	543	E-11 (MH)
DZ3	Taxiway Z3	38.7	6.0	CSB[c]	15.2	1357	E-2 (SM)
TZ2969G	Old terminal apron	18.4	5.2			909	E-5 (SC)
TZ2969C	Old terminal apron	18.4	5.2			909	E-5 (SC)
TZ15	Warm-up apron	38.7	4.9	SSG[d]	12.7	1235	E-4 (SC)
TZ74	ANG apron	27.9	5.4			1140	E-7 (CL)
TA4G	Warm-up apron	27.9	4.6	E-1 (SW-SM)	20.3	543	E-8 (CH)
TA5	Warm-up apron	40.6	5.3	E-1 (SW-SM)	20.3	543	E-7 (CL)

[a] FAA classification is given first; Unified Soil Classification appears in parentheses.
[b] CSB = cement-stabilized base (clay gravel) over 44.5 cm (17.5 in) of lime-stabilized clay.
[c] CSB = cement-stabilized base over 30.5 cm (12 in) of cement-treated sand.
[d] SSG = stabilized-sand gravel.

Table 2. ASWL, DSM, and ℓ for pavements.

Test Site Number	ASWL (t)	DSM (kN/cm)	ℓ (cm)				
				Predicted			
			Computed	Δ_{102}/Δ_0	Δ_{132}/Δ_0	Δ_{102}/Δ_{46}	Δ_{132}/Δ_{46}
N7	11.9	3187	61.2	58	66	56	66
N8	13.0	2592	60.7	53	58	53	61
N9	17.8	3187	81.5	56	61	61	66
N10	11.7	4273	64.3	69	81	69	81
N11	11.9	1767	70.4	71	76	69	76
N13	14.1	4098	57.4	84	91	74	86
N15	17.8	4623	109.2	66	74	66	79
N16	35.8	6515	106.9	81	99	74	99
N17	11.6	2294	78.7	69	79	66	81
H1	39.0	6164	90.2	84	107	117	130
H3	35.8	8406	89.9	99	122	135	157
H7	30.9	6270	88.6	99	127	122	157
H9	32.1	4623	125.7	97	122	124	155
H11	32.5	6480	96.8	89	114	117	150
J1	18.1	5149	95.8	119	122	130	127
J2	19.6	3100	104.1	157	155	183	168
J3	12.8	3608	76.5	81	84	86	89
J4	21.7	5114	106.7	117	132	119	145
J5	23.2	3082	93.0	89	99	107	117
DFWAG	45.4	8336	145.8	84	99	175	185
DFWAC	45.4	5709	145.8	66	81	226	175
DZ3	48.0	7565	104.4	74	89	356	246
TZ2969G	11.5	1909	63.5	86	86	94	91
TZ2969C	11.5	1716	63.5	81	84	89	89
TZ15	38.2	3485	106.4	71	86	150	152
TZ74	23.3	2907	81.3	89	102	140	130
TA4G	17.7	3187	99.0	104	114	124	132
TA5	36.8	5359	132.1	152	173	183	208

Figure 4. Deflection versus distance from centerline of load plate for pavements tested during the Green and Hall study.

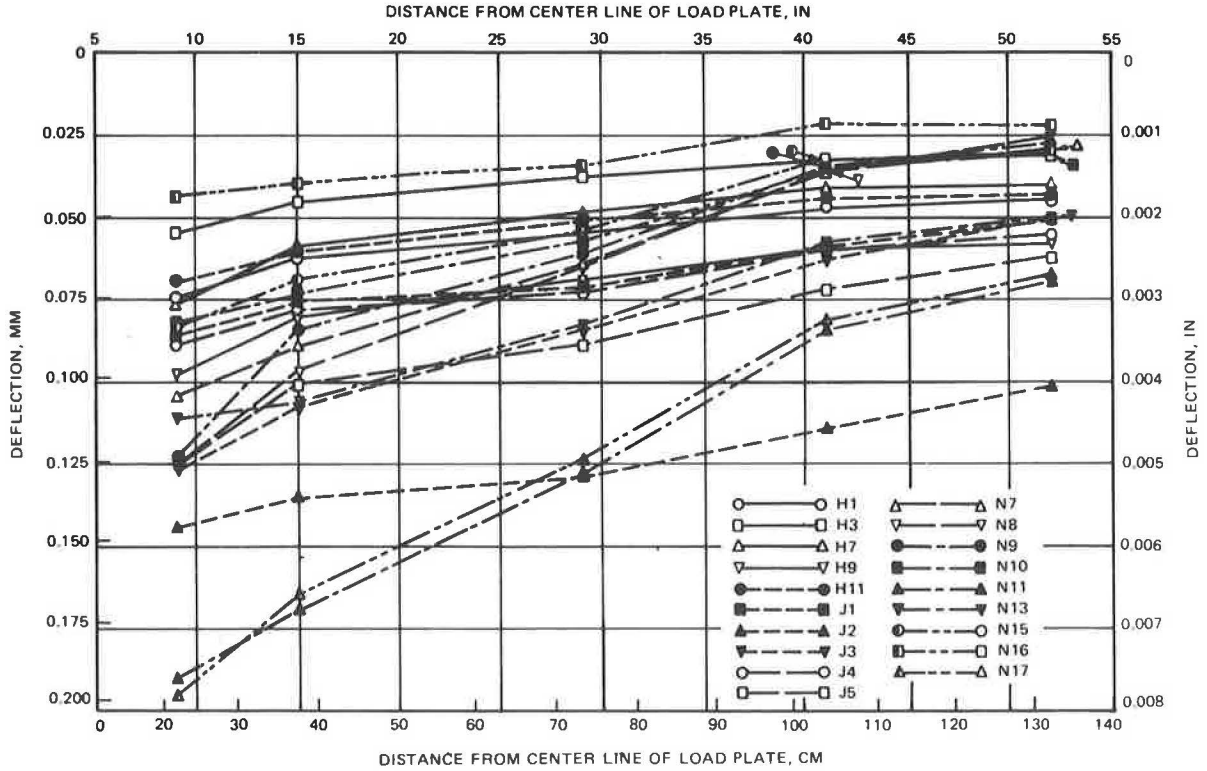

where

ℓ = radius of relative stiffness (cm),
E = modulus of elasticity of concrete (Pa),
h = thickness of PCC slab (cm),
μ = Poisson's ratio of concrete, and
k = modulus of soil reaction (Pa/cm).

In this study, these assumptions were made for concrete: E = 27.6 GPa (4 000 000 psi) and μ = 0.15.

Deflection basin data are presented in Figures 4 and 5. Data were collected at a constant frequency of 15 Hz and a peak dynamic load of 40 kN (9 kips). Data presented in Figure 4 were collected during the Green and Hall study (4). Velocity sensors were located at 38, 74, 104, and 132 cm (15, 29, 41, and 52 in) from the center of the plate. Data in

Figure 5. Deflection versus distance from centerline of load plate for pavements tested during the significant-difference study.

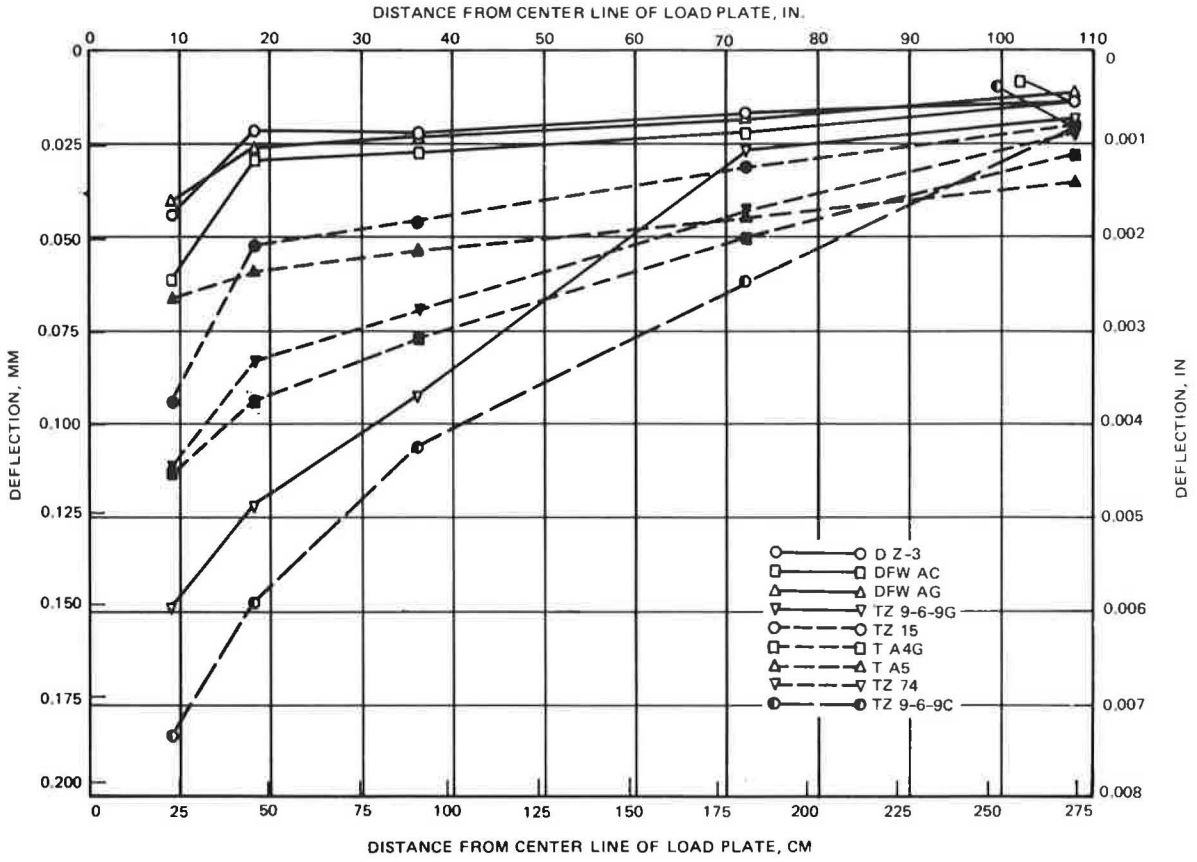

Figure 5 were collected during the significant-difference study. During this study, velocity sensors were located at 46, 91, 183, and 274 cm (18, 36, 72, and 108 in) from the center of the plate.

DATA ANALYSIS

Development

The method that will be further developed here is based on the two-component Hertz model of an infinite elastic plate on a dense fluid subgrade.

Heinrich Hertz, the physicist, solved the problem of the deflection of an elastic plate floating on a heavy fluid acted on by a point load (10). In developing the mathematical formulation, the vertical strain in the plate is ignored, the horizontal shear stresses at the base of the plate are assumed to be equal to zero, and the vertical contact stress is assumed to be proportional to the vertical displacement. This model is essentially the well-known spring model frequently used in soil mechanics and associated with E. Winkler (11).

The two physical parameters characterizing the system as described by Hertz are ℓ and k, where ℓ is a characteristic length depending on the rigidity of the plate and the density (k) of the fluid. Hertz developed his theory because he became interested in the problem of the equilibrium of a floating sheet of ice on which a man stands. Though Hertz was primarily concerned with the deflection of the ice, he also calculated the resulting stresses and, hence, the failure load for various thicknesses of ice assuming values of the failure stress, Young's modulus, and Poisson's ratio.

Hertz's model has been used by Westergaard as a basis for calculating the stresses induced in concrete slabs on soil subgrades (12). The soil subgrade is assumed to behave in a manner analogous to that of the heavy fluid, providing a vertical reaction proportional to the vertical displacement of the slab. The constant of proportionality is known as the coefficient of subgrade reaction (k), has the same dimensions as density, and is assumed to be independent of the geometry of the loaded area.

Determination of k has been a weakness of the NDT and evaluation procedure currently in use at the WES. In order to predict the allowable loads of multiple-geared aircraft, k must be measured destructively or assumed by using known material properties. This assumption may not be valid in cases of varying moisture conditions, differences in compaction effort in construction and due to traffic, and variations in subgrade properties over the length of feature evaluated.

The method that will be developed will use the deflection basin measurements to predict ℓ. By using this ℓ and DSM, the ASWL will be predicted.

Prediction of ℓ

By using influence charts for the area loadings, relations between a deflection basin and ℓ can be developed. To generate the needed deflection data, a computer program (PCADL) obtained from the Portland Cement Association was used. This program computes deflections of a pavement on a liquid subgrade (Hertz model) by using influence areas. The relations shown in Figure 6 were developed. Plotted are the deflection ratio (i.e., the deflection Δ_r at an offset distance r divided by the center deflection Δ_0) as a function of the offset distance. The following properties were held constant while thickness (h) and the coefficient of subgrade reaction (k) were varied: load = 40 kN (9 kips); contact area = 1639 cm² (254 in²) on a single wheel; E = 27.6 GPa (4 000 000 psi); and $\mu = 0.15$.

Because the load plate on the vibrator is nearly rigid and

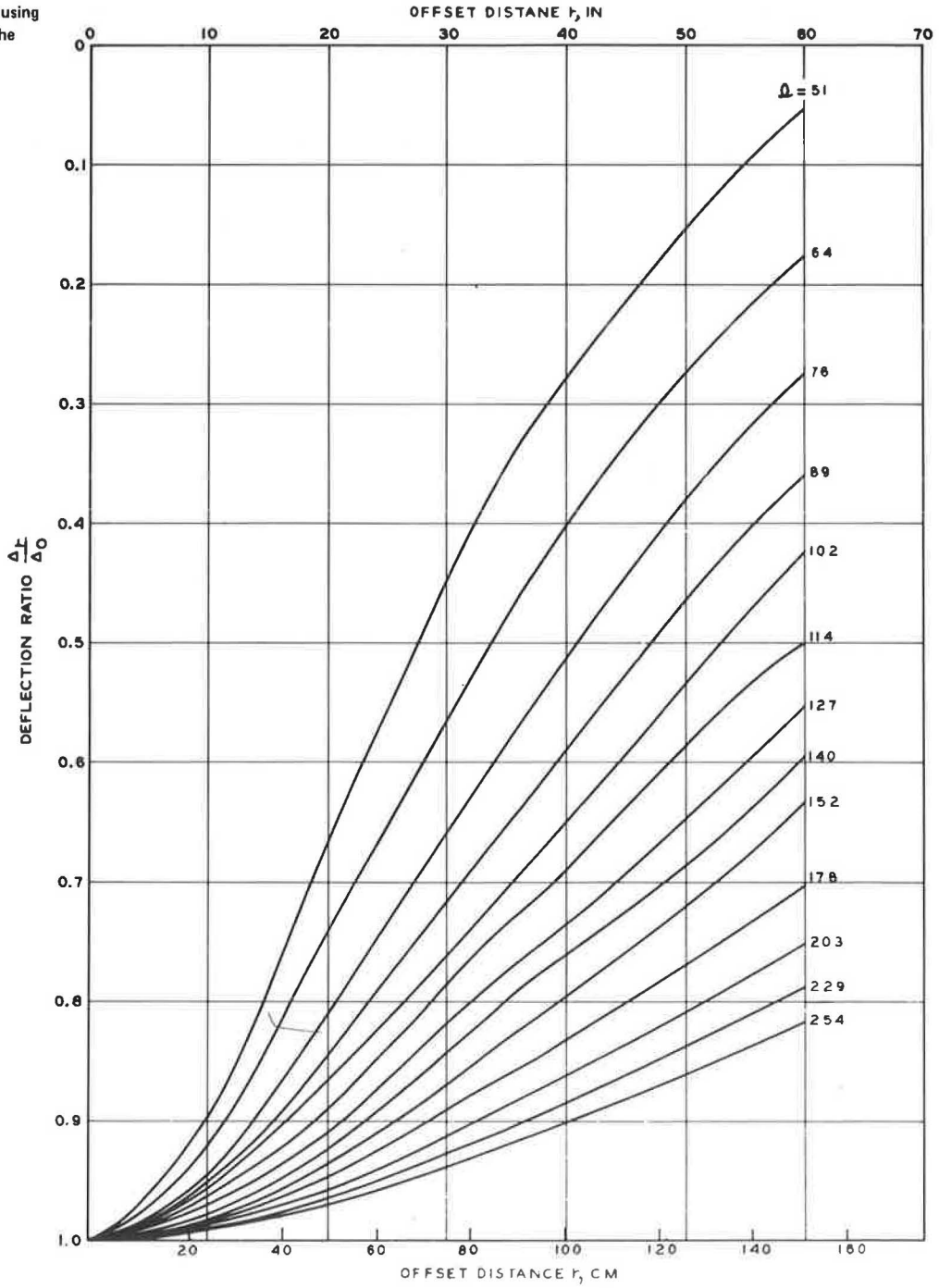

Figure 6. Relations for ℓ by using a deflection at the point of the applied load.

to eliminate any edge effects, the relation shown in Figure 7 was developed. In this case, the deflection ratio consisted of dividing the deflection at an offset distance r by the deflection 46 cm (18 in) away from the center of the 1639-cm² (254-in²) loading area—i.e., 23 cm (9 in) from the edge of the plate. This offset distance was selected because it was the location of a pronounced break in the slope of the deflection basin (Figure 5).

By using the deflection basin data (Figures 4 and 5) and the curves developed from the computer program (Figures 6 and 7), ℓ was obtained for offset distances (r's) of 102 and 132 cm (40 and 52 in), respectively. These values are shown in Table 2 and will be noted as measured values because they were derived from measured deflection basin data.

To assess the accuracy of the prediction, a linear regression analysis was performed by comparing each group measured (ℓ_m) with those computed (ℓ_c) from destructive data. The results of this analysis are shown in Table 3.

Although the best-fit line for the data that use Δ_0 showed that the variables were nearly equal, the correlation coefficient was very poor. A good correlation coefficient was obtained when the deflection at 132 (Δ_{132}) cm (52 in) was divided by the deflection at 46 (Δ_{46}) cm (18 in). These data are presented in Figure 8.

Prediction of ASWL

In the procedure developed by Green and Hall (4), DSM was correlated directly to ASWL. It has been proposed that another variable (ℓ) be interjected into this concept (1).

To develop this relation, two computer programs were

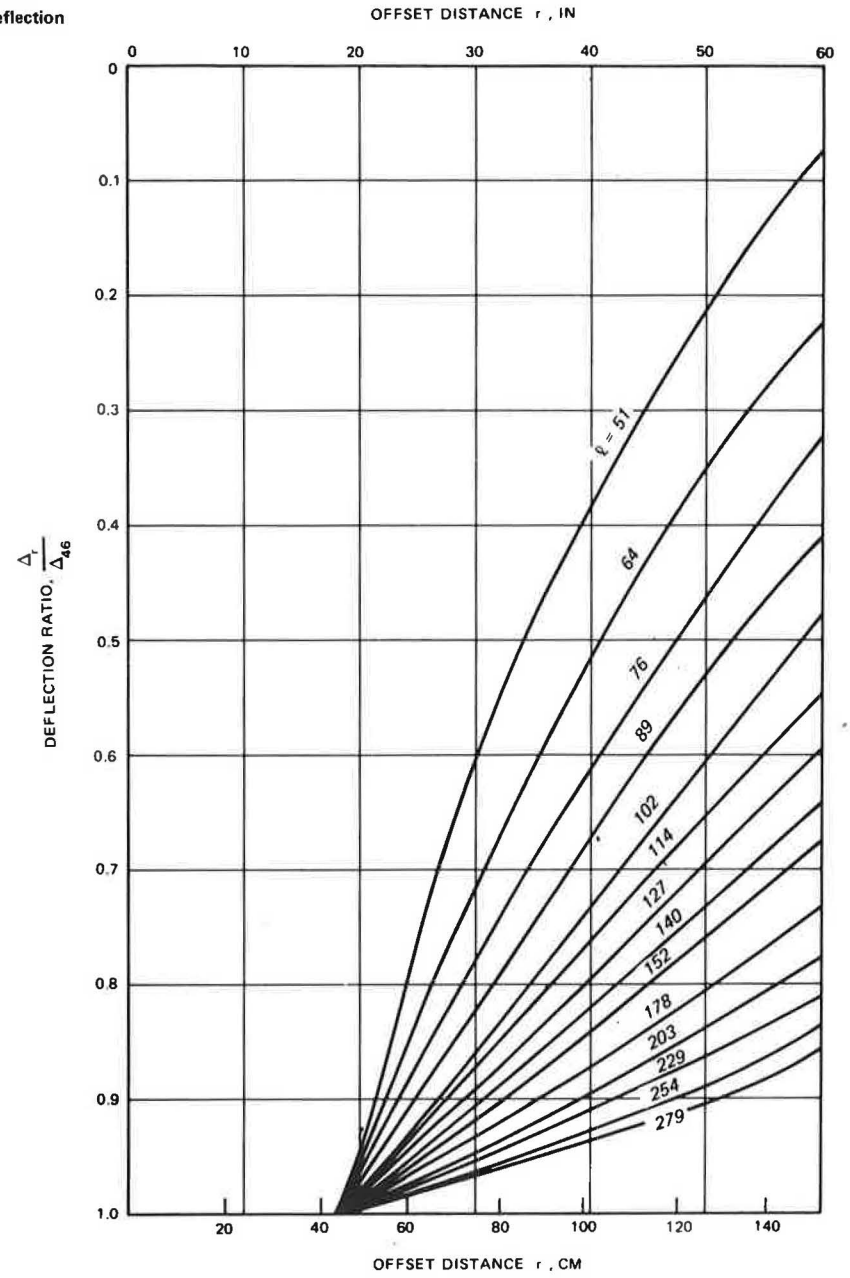

Figure 7. Relations for ℓ by using a deflection 46 cm from the applied load.

Table 3. Results of linear regression analysis of ℓ_m and ℓ_c based on destructive data.

Deflection Ratio Location	Equation for Best-Fit Line Through 0.0	Correlation Coefficient	Standard Error of Estimate (cm)
Δ_{102}/Δ_0	$\ell_c = 1.009\ 7\ \ell_m$	0.3567	23.5
Δ_{132}/Δ_0	$\ell_c = 0.899\ 88\ \ell_m$	0.4696	22.2
Δ_{102}/Δ_{46}	$\ell_c = 0.657\ 07\ \ell_m$	0.5950	20.2
Δ_{132}/Δ_{46}	$\ell_c = 0.699\ 35\ \ell_m$	0.7296	17.2

used. The PCADL program described previously was used to determine the deflection under an applied load. The deflection was converted to DSM by dividing the load in kips by the deflection for a given set of pavement properties. These properties were used as input to the H-51 program, developed by General Dynamics Corporation, that calculates the maximum stress in a slab when an edge load is applied. It should be noted that NDT data were collected at the slab center. More consistent results can be obtained because the DSM at this location is least affected by edge condition and joint type.

The H-51 program is based on the Westergaard equations for a slab over a liquid subgrade. In a paper by Pickett and Ray (13), solutions for the Westergaard equations were presented in the form of influence charts that greatly simplified the determination of the theoretical deflections and moments caused by wheel loads on pavement slabs. These charts were digitized in the H-51 program. The program actually counts the number of influence areas as a function of ℓ, contact area, and gear configuration. The moment (M) produced by a single wheel is then computed according to the following formula:

$$M = q\ell^2 N/10\ 000 \quad (2)$$

where

M = moment at point 0 on the chart (N•m);

q = load intensity on the contact area obtained by dividing the wheel load by the contact area (Pa);

Figure 8. Correlation between ℓ from deflection measurements (Δ_{132}/Δ_{46}) and ℓ computed from pavement properties.

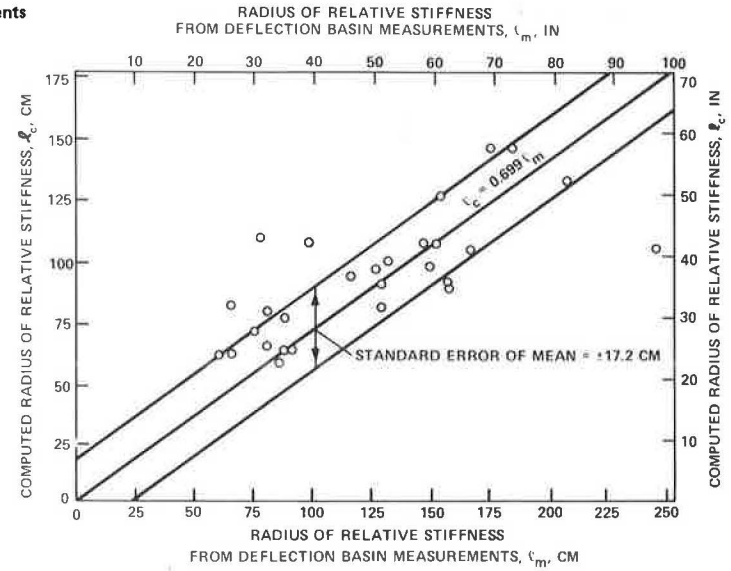

Figure 9. ASWL versus DSM for varying ℓ values.

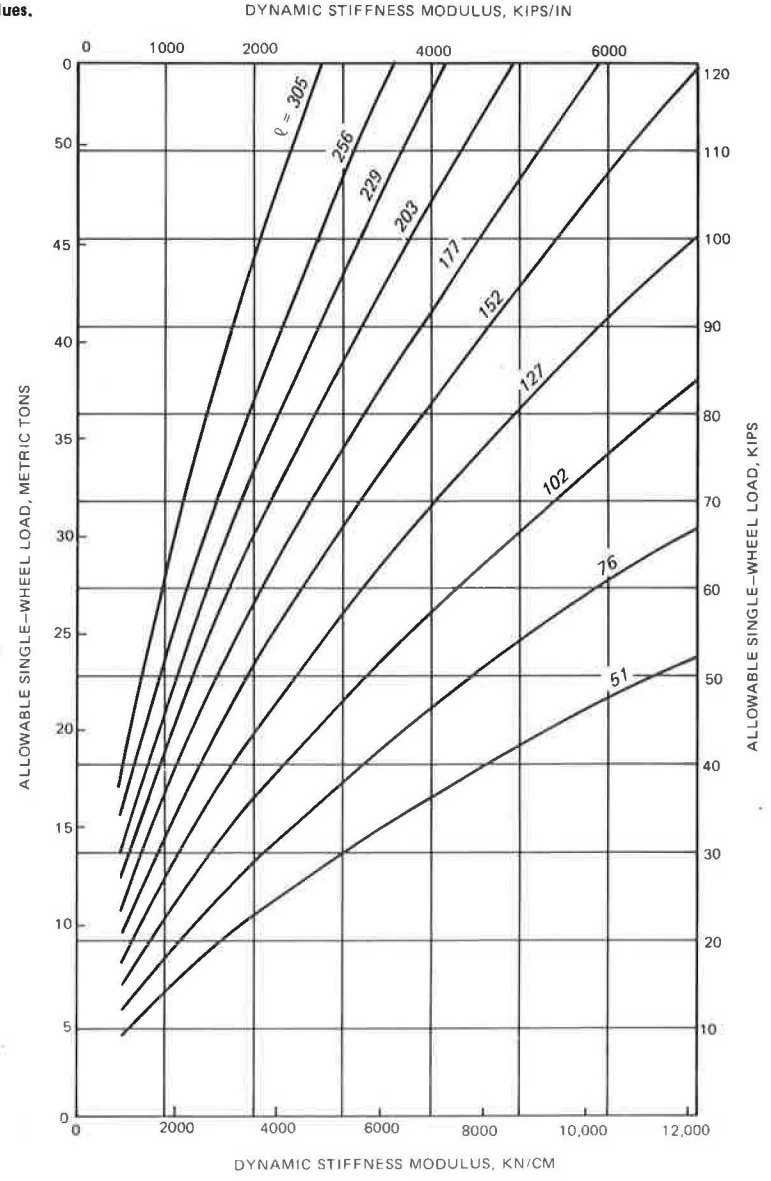

Table 4. Predicted ASWL values based on destructive data and linear regression analysis.

Deflection Ratio Location	Equation	Correlation Coefficient	Standard Error of Estimate (t)
Δ_{102}/Δ_0	ASWL = 1.427 predicted ASWL	0.666	9.2
Δ_{132}/Δ_0	ASWL = 1.245 predicted ASWL	0.745	8.3
Δ_{102}/Δ_{46}	ASWL = 1.005 predicted ASWL	0.865	6.2
Δ_{132}/Δ_{46}	ASWL = 0.974 predicted ASWL	0.904	5.3

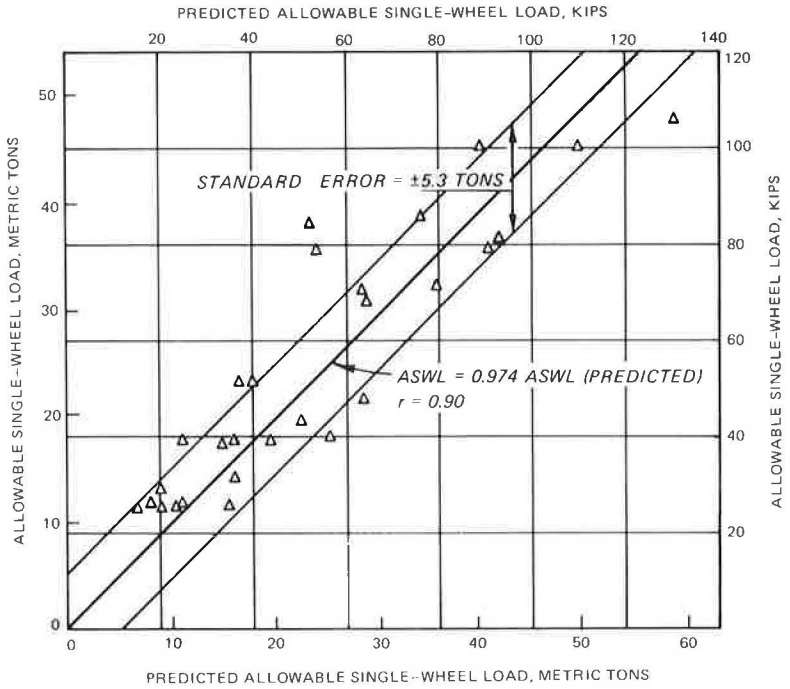

Figure 10. Correlation between ASWL from deflection measurements (DSM, uncorrected ℓ, Δ_{132}/Δ_{46}) to ASWL computed from pavement properties.

ℓ = radius of relative stiffness of the pavement (m); and
N = number of influence areas, including fractional parts, falling within the scaled footprint.

The edge stress (σ_e) produced by the wheel is computed as follows:

$$\sigma_e = 6M/h^2 \quad (3)$$

where

σ_e = edge stress (Pa),
M = moment due to wheel load (N•m), and
h = thickness of PCC slab (m).

This stress must then be equated to the allowable stress in the slab. The procedure used in this case was reported by Hutchinson (14) and is as follows:

$$R = \sigma_e(DF)(LT) \quad (4)$$

where

R = design flexural strength of concrete (Pa),
σ_e = edge stress (Pa),
DF = design factor based on repetitive loading and stresses (1.3 is used in this study), and
LT = load-transfer factor (it is assumed that 25 percent of the load is transferred by the joint in this study; therefore, this value is 0.75).

By rearranging factors, the following will result: $\sigma_e = R/0.975$. If R is assumed, curves as shown in Figure 9 can be developed. In this case, a 4826-kPa (700-psi) R was assumed.

Two methods of predicting ASWL were tested. First, the values for ℓ measured from the basin data (Table 2) along with the measured DSMs were used for input to Figure 9. These values of ASWL were compared with the values determined from destructive test data, and k was determined by using the small-aperture procedure of measuring CBR and converting CBR to k (5). R was determined from the tensile-splitting tests. The results of the linear regression analysis are shown in Table 4. Again, as with ℓ, the Δ_{132}/Δ_{46} produces the best correlation (Figure 10). This is an improvement over the correlation presented by Green and Hall (4). In that study, a modulus of PCC of 41.4 GPa (6 million psi) and a Poisson's ratio of 0.2 were used. Later, these data were presented by Hall (15) with a modulus value of 27.6 GPa (4 million psi) and a Poisson's ratio of 0.15. The regression analysis data for both studies are given in Table 5. The use of ℓ computed from the basin data along with DSM produced a much better correlation coefficient with about the same standard error.

The next comparison would be to use the corrected ℓ, along with DSM, to predict ASWL. In the previous correlation, the value for ℓ was taken directly from either Figure 6 or Figure 7. In this comparison only, the Δ_{132}/Δ_{46} data will be used, and the value of ℓ will be corrected for the correlation shown in Figure 8, i.e., the value of ℓ from Figure 7 will be multiplied by 0.699. A correlation with these values produced a standard error of 5.6 t (12.3 kips) and a correlation coefficient of 0.90, as shown in Figure 11. In this case, the ℓ would be of the correct magnitude. The correlation coefficient is the same, but the standard error is larger when the uncorrected ℓ is used.

By using the corrected ℓ, a value for k can be derived if a value for E and μ for PCC is assumed. It is recommended that engineering judgment be used in interpreting k from these types of data because variations

Table 5. Summary of regression analysis studies to predict ASWL.

Parameter				
E (GPa)	μ	Equation	Correlation Coefficient	Standard Error of Estimate (t)
41.4	0.2	ASWL = 0.178 DSM	0.77	±5.3
27.6	0.15	ASWL = 0.1896 DSM	0.77	±5.6

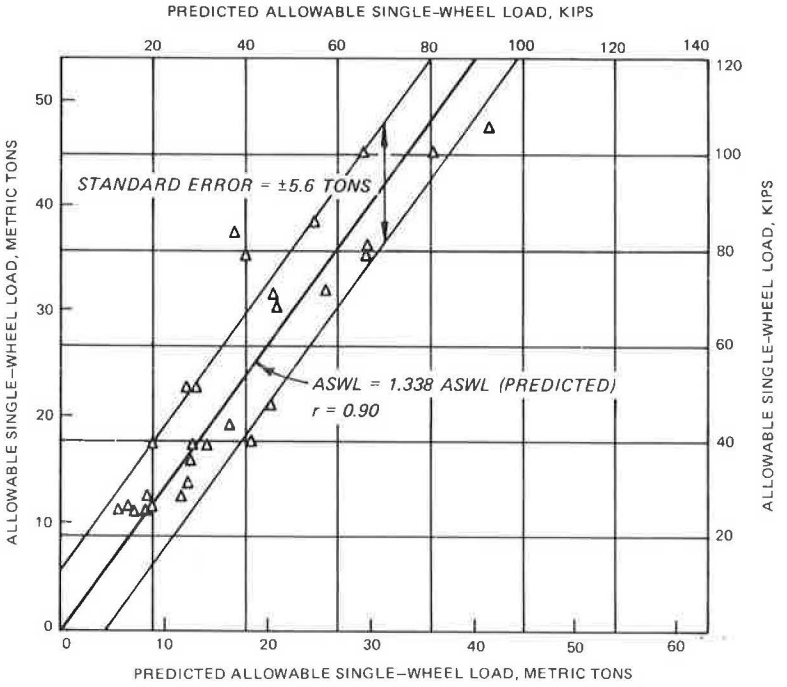

Figure 11. Correlation between ASWL from deflection measurements (DSM, corrected ℓ, Δ_{132}/Δ_{46}) to ASWL from pavement properties.

from commonly used values will occur. It should be remembered that ℓ is also a function of h, E, and μ, which can vary and influence its value.

SUMMARY

The purpose of this study was to develop relations by using the Hertz theory of an infinite plate on a dense fluid subgrade between deflections measured at the point of and away from an applied load and the strength parameters of the pavement. An evaluation procedure was to be developed that would be based on these relations, known pavement characteristics, and dynamic response data collected with the WES 16-kip vibrator.

The PCADL program was used to predict deflections at the point of and away from an applied load. The deflections were related to the radius of relative stiffness (ℓ).

The H-51 program was used to predict maximum stresses in the PCC pavements. From these stresses, a relation was developed between DSM, ℓ, and ASWL.

Both destructive and nondestructive vibratory data were collected on 28 different pavements. Destructive data were used to characterize each pavement's material properties and then, with conventional procedures, to predict ASWL. Deflection basin data from the WES 16-kip vibrator determined ℓ by using the relations developed with the PCADL program. Also, ℓ and DSM were used to predict ASWL.

Based on the results of this study, it is concluded that (a) NDT data from the WES 16-kip vibrator can be used to predict ℓ, therefore eliminating the need to assume values of Young's modulus, Poisson's ratio, and modulus of soil reaction, and (b) the ASWL can be predicted by using either the measured ℓ or a corrected ℓ with a higher degree of accuracy than relations developed in earlier studies.

It is recommended that these relations for ℓ and ASWL, based on deflection basin data, be adopted and integrated into the evaluation procedures currently in use for rigid pavements.

ACKNOWLEDGMENT

The work reported in this study was done at the Soils and Pavements Laboratory of the U.S. Army Engineer Waterways Experiment Station, Vicksburg, Mississippi. Experimental results were obtained under a research contract with the Federal Aviation Administration. I wish to express appreciation to my supervisor, Jim W. Hall, Jr., for his continued support and advice on this project, along with other members of the Pavement Evaluation Branch.

REFERENCES

1. R.L. Hutchinson and others. Symposium on Nondestructive Test and Evaluation of Airport Pavement. U.S. Army Engineer Waterways Experiment Station, Vicksburg, MS, May 1976.
2. W. Heukelom and C. R. Foster. Dynamic Testing of Pavements. Soil Mechanics and Foundations Journal, ASCE, Vol. 86, No. SM1, Part 1, Feb. 1960.
3. C. Van der Poel. Dynamic Testing of Road Construction. Journal of Applied Chemistry, Vol. 1, Part 7, July 1951.
4. J.L. Green and J.W. Hall. Nondestructive Vibratory Testing of Airport Pavements: Volume 1, Experimental Methodology and Procedure. U.S. Army Engineer Waterways Experiment Station, Vicksburg, MS, Tech. Rept. S-75-14, Sept. 1975.
5. J.W. Hall and D.R. Elsea. Small-Aperture Testing for Airfield Pavement Evaluation. U.S. Army Engineer Waterways Experiment Station, Vicksburg, MS, Misc. Paper S-74-3, Feb. 1974.
6. Method of Test for Splitting Tensile Strength of

Molded Concrete Cylinders (Tentative). In 1964 Book of ASTM Standards, American Society for Testing and Materials, Philadelphia, C 496-647, 1964.
7. G.M. Hammitt II. Concrete Strength Relationships. Texas A&M Univ., College Station, Dec. 1971.
8. Airport Pavement Design and Evaluation. Federal Aviation Administration, Advisory Circular AC 150/5320-6B, May 1974.
9. The Unified Soil Classification System. U.S. Army Engineer Waterways Experiment Station, Vicksburg, MS, Tech. Memorandum 3-357, 1953.
10. H. Hertz. On the Equilibrium of Floating Elastic Plates. In Miscellaneous Papers by Heinrich Hertz (D.E. Jones and G.A. Schott, trans.) MacMillan and Co., Ltd., London, 1896.
11. S.P. Timoshenko. History of Strength of Materials. McGraw-Hill, New York, 1953.
12. H.M. Westergaard. New Formulas for Stresses in Concrete Pavements of Airfields. Transactions, American Society of Civil Engineers, Vol. 113, No. 2340, 1948.
13. G. Pickett and G. Ray. Influence Charts for Concrete Pavements. Trans., American Society of Civil Engineers, Vol. 116, No. 2425, 1951.
14. R.L. Hutchinson. Basis of Rigid Pavement Design for Military Airfields. U.S. Army Engineer Ohio River Division Laboratories, Cincinnati, Misc. Paper 5-7, May 1966.
15. J.W. Hall, Jr. Nondestructive Evaluation Procedure for Military Airfields. U.S. Army Engineer Waterways Experiment Station, Vicksburg, MS, Misc. Paper S-78-7, July 1978.

Publication of this paper sponsored by Committee on Rigid Pavement Design.

Fatigue Cracking of Asphalt Pavements

D. V. RAMSAMOOJ

This paper validates a theoretical expression for the rate of fatigue crack propagation experimentally for asphalt concrete and sand asphalt beams supported on an elastic solid. The properties of the materials were determined experimentally from fracture tests on simply supported beams, and the rates of crack propagation under fatigue loading were determined from fatigue tests on the beams that were supported on an elastic solid. The results for the rates of crack propagation predicted from the fracture tests were then compared with those obtained experimentally; they were found to be in reasonable agreement. The theory is then used to predict the fatigue life of a full-depth asphalt pavement. The result appears in reasonable agreement with the expected life for such a pavement.

Previous research (1-3) has shown that fatigue cracking of asphalt pavements obeys the principles of fracture mechanics. The law of crack propagation was found to be $dc/dN = A[(\Delta K)^4 - K_0^4]$, where dc/dN = the crack growth per cycle, K = the stress-intensity factor, K_0 = the value of K at the endurance limit, and A = a material constant to be found experimentally from fatigue tests.

Recently, Wnuk (4) derived the nonlinear differential equation that governs subcritical growth of a crack embedded in an elastic-plastic matrix up to the point of gross instability:

$$[(\pi E/12\sigma_y^2\eta)\, G(dG/d\sigma)/(d\sigma/dc)] + G = G_c \quad (1)$$

where

E = Young's modulus;
σ_y = yield stress in tension;
$\eta = 1 - \nu^2$, or 1 for plane strain or plane stress, respectively;
ν = Poisson's ratio;
σ = applied stress;
c = crack length;
$G = K^2\eta/E$;
$G_c = K_c^2\eta/E$; and
K_c = critical stress-intensity factor.

By using this nonlinear differential equation, it will be shown that the law of crack propagation for high cycle fatigue (small K/K_c) for a beam on elastic foundation loaded as shown in Figure 1 is given by

$$dc/dN = (\pi/24 K_{1c}^2 \sigma_y^2)[(\Delta K_1)^4 - K_0^4] \quad (2)$$

in which K_{1c} = plane strain critical stress-intensity factor. This means that the rate of fatigue cracking is given explicity in terms of material properties and stresses. Moreover, the material properties K_{1c} and σ_y can be determined very simply from fatigue tests.

THEORETICAL ANALYSIS OF CRACK PROPAGATION RATE

Consider a beam supported on an elastic solid as shown in Figure 1. The beam contains a centrally located crack of length c and supports a load P distributed over a width 2a. From Equation 1, the following is obtained:

$$d\sigma/dc = (G_c - G)(12\sigma_y^2\eta/\pi E)(1/G)(d\sigma/dG) \quad (3)$$

where

$G = K^2\eta/E$,
K = stress-intensity factor $= \sqrt{\pi\sigma c}\, f(c/d)$,
σ = nominal bending stress calculated on the uncracked section,
$f(c/d)$ = a function of the crack-depth ratio,
$G = (\pi\eta/E)\,\sigma^2 f^2(c/d)$,
$dG/d\sigma = (2\pi\eta/E)\,\sigma f^2(c/d)$,
$(1/G)(d\sigma/dG) = E^2/[2\pi^2\eta^2\sigma^3 f^4(c/d)]$,
$d\sigma/dc = \{G_c[1-(G/G_c)]\,(12\sigma_y^2\eta/\pi E)\} \times \{E^2/[2\pi^2\eta^2\sigma^3 f^4(c/d)]\}$
$= G_c(12\sigma_y^2 E)/[2\pi^3\eta\sigma^3 f^4(c/d)]$ for $G/G_c = (K/K_c)^2 << 1$, and
$dc/d\sigma = [\pi^3\eta\sigma^3 f^4(c/d)]/6G_c E\sigma_y^2$.

Now consider a single cycle of fatigue growth for high cycle fatigue. When K_1/K_{1c} is small, the above equations may be integrated as follows [see Wnuk (4) for a full discussion of the approximation involved]:

$$(dc)_{\text{per cycle}} = \int_{\sigma_\sigma}^{\Delta\sigma} [\pi^3\eta\sigma^3 f^4(c/d)\, d\sigma]/6G_c E\sigma_y^2$$

In this approximation, σ_σ = the lower threshold stress for crack growth and $\Delta\sigma$ = applied increment in stress and is equal to the difference between the maximum and minimum stresses during one excursion of the load. These stresses are related to the endurance limit K_0 and the

Figure 1. Asphaltic beam on elastic solid.

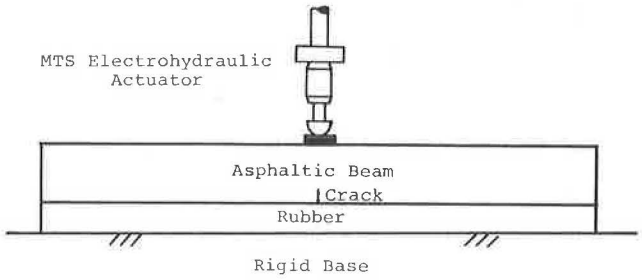

increment in the stress-intensity factor ΔK_1 as follows:

$$K_0 = \sqrt{\pi}\,\sigma_0 f(c/d) \text{ and } \Delta K_1 = \sqrt{\pi}\,\Delta\sigma f(c/d).$$

The endurance limit K_0 is defined as the lower threshold stress-intensity factor below which a crack will not propagate.

Performing the integration produces the following:

$$(dc)_{\text{per cycle}} = \{\pi^3 \eta f^4 (c/d)\,[(\Delta\sigma)^4 - \sigma_0^4]\}/24 G_c E \sigma_y^2$$

$$= \{\pi^3 \eta f^4 (c/d)\,[(\Delta\sigma)^4 - \sigma_0^4]\}/[24(K_c^2 \eta/E) E \sigma_y^2]$$

$$= (\pi/24 K_{1c}^2 \sigma_y^2)\,\pi^2 f^4 (c/d)[(\Delta\sigma)^4 - \sigma_0^4] \text{ for plane strain}$$

$$= (\pi/24 K_{1c}^2 \sigma_y^2)[(\Delta K_1)^4 - K_0^4]$$

That is,

$$dc/dN = (\pi/24 K_{1c}^2 \sigma_y^2)[(\Delta K_1)^4 - K_0^4]$$

is the rate of crack growth per cycle in the opening mode. This result is identical in form to that obtained by Wnuk (4) for crack propagation in the direct tensile mode. Evidently, the stress-intensity factor appears to fully account for changes in the geometry and configuration of loading.

EXPERIMENTATION

In order to verify the crack propagation law, experiments were conducted on two paving mixtures--sand asphalt, the same mix referred to in Ramsamooj (5), and an asphalt concrete. The sand asphalt specimens were fabricated in the laboratory and the mixture characteristics are described here. The asphalt concrete specimens were cut out of an existing pavement from an untrafficked area in a parking lot near the Civil Engineering Laboratory at California State University, Fullerton. No attempt was made to determine all of its mixture characteristics.

The test characteristics of sand-asphalt mixtures include the following:

1. Asphalt cement (60/70): specific gravity = 1.010; softening point (ring and ball) = 123°F; ductility (77°F) = 150+ cm; penetration, 100 g every 5 s at 77°F = 63; penetration, 200 g every 60 s at 39.4°F = 23.5; and flash point (Cleveland open cup) = 455°F.
2. Mixture: 6 percent asphalt cement by weight, average density = 2.052 ± 0.011 g/cm^3, and average air voids = 17.0 ± 0.5 percent.
3. Aggregate: percentages passing selected sieve numbers and percentages required for ASTM Specification D1663-59T:

Sieve Number	Percentage Passing	ASTM Requirement (%)
16	100.0	85-100
30	88.0	70-95
50	64.2	45-75
100	30.1	20-40
200	15.7	9-20

MATERIAL PROPERTIES

The critical stress-intensity factor (K_{1c}), the flexural tensile strength (σ_y), and the modulus of elasticity (E) were determined experimentally by using the three-point bend-testing configuration [span = 25.4 cm (10 in), depth = 6.36 cm (2.5 in), and width = 5.08 cm (2 in)]. Because of the rate dependency of the stress and strain curves for asphaltic mixtures, the above properties were determined by using a constant rate of loading based on the flexural stresses in the uncracked beam. This rate of loading was 13 780 kPa/s (2000 psi/s) to ensure essentially elastic action.

For a full discussion of the concepts of fracture mechanics relevant to pavement design, the reader is referred to Majidzadeh and Ramsamooj (6). This paper discusses the physical meaning of the stress-intensity factor (K_1), its critical value (K_{1c}), and how it may be used in describing fatigue crack growth. The testing procedure for determination of the material properties for use in fracture mechanics and the necessary precautions to be observed are discussed in Majidzadeh and others (7).

In the experimental determination of the values of K_{1c} and σ_y, a ramp-loading function was applied by the MTS electrohydraulic system in stroke control to simulate a hard testing machine. The rate of loading was maintained at 13 780 kPa/s (2000 psi/s) in all cases; the only difference in the two tests was that the beams for determining K_{1c} had notches equal to half the depth of the beam, while those for σ_y were unnotched. It should be pointed out that σ_y is the ultimate flexural tensile strength; this value is considerably greater than the direct tensile strength. In my opinion, this is the appropriate value to use for bending fatigue. The value of the modulus of elasticity, E, was taken to be equal to the dynamic modulus. This modulus was determined by using the same loading function as that for the fatigue tests (Figure 2). The rate of loading was maintained at 13 780 kPa/s (2000 psi/s), and the stress level was made equal to the stress generated at the bottom of the asphalt layer due to the passage of a vehicular wheel load. The results are presented in Table 1, together with the calculated values of the fatigue constant $A = \pi/24 K_{1c}^2 \sigma_y^2$.

FATIGUE TESTS

Fatigue tests were conducted on beams supported on an elastic solid consisting of a silicone rubber pad whose modulus of elasticity was 9714 kPa/s (1400 psi/s) for the stress range used in the tests. The test configuration is shown in Figure 1. The load was applied by an MTS electrohydraulic system, using a haversine function. The loading and the deflection response of the beam on elastic solid is shown in Figure 2. The rate of loading was maintained at 13 780 kPa/s (2000 psi/s). Both notched and unnotched beams were tested. The crack growth was monitored visually by using a magnifying glass and placing a drop of ink in the vicinity of the crack tip. The crack tip is thus made visible by the ink bubbling in the tip of the crack.

The crack growth was then plotted as a function of time. For each test the rates of the crack propagation at c/d = 0.25, 0.30, and 0.35, respectively, were plotted versus the corresponding values of $(\Delta K_1)^4$. The results are shown in Figure 3 for sand asphalt and in Figure 4 for asphalt concrete. From these graphs, the following results were obtained:

For sand asphalt:

$A = 8.71 \times 10^{-14}$ m^7/kN^4 per cycle (5×10^{-12} in^7/lb^4 per cycle) and $K_0 \approx 0$.

For asphalt concrete:

$A = 3.48 \times 10^{-15}$ m^7/kN^4 per cycle (2×10^{-13} in^7/lb^4 per cycle) and

$K_0 \approx 105.4$ kN·m$^{-3/2}$ (96 lb·in$^{-3/2}$).

Figure 2. Deflection and load versus time curves used in fatigue tests.

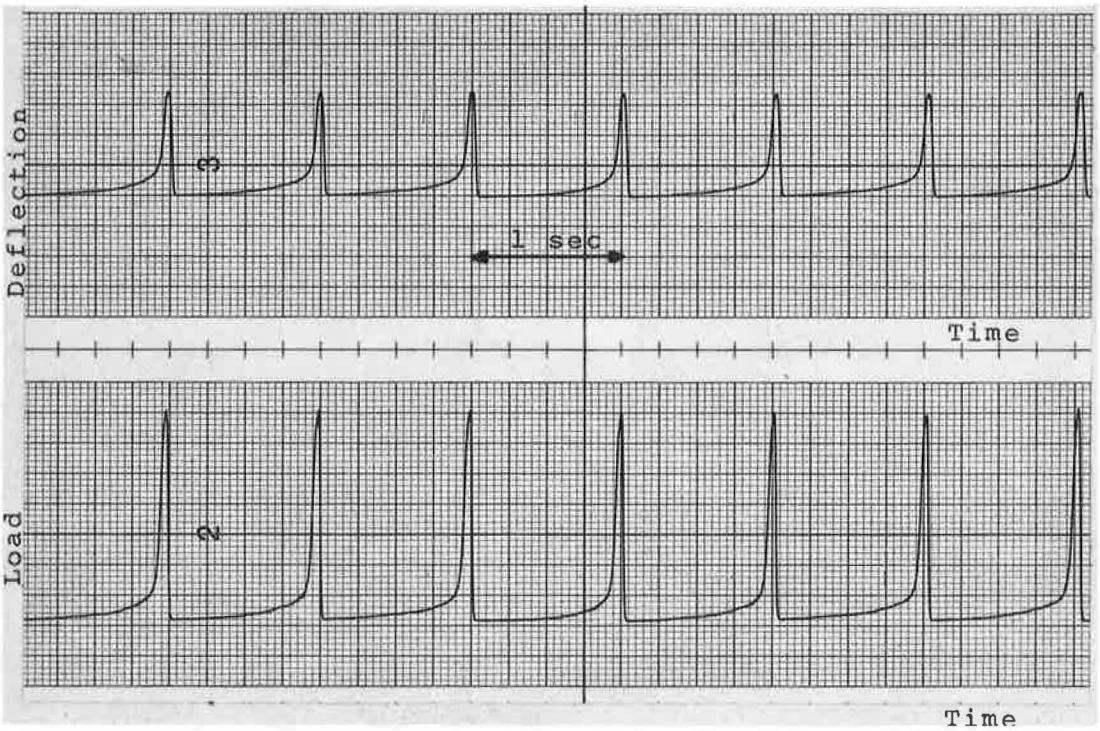

Table 1. Material properties for sand asphalt and asphalt concrete.

Type of Mix	K_{1c} (kN·m$^{-3/2}$)	σ_y (kPa)	E (kPa)	A (m^7/kN^4 per cycle)
Sand asphalt	428	2792	330 720	9.17×10^{-14}
Asphalt concrete	604	5305	4 168 450	1.27×10^{-14}

Note: 1 kPa = 0.145 psi; 1 kN·m$^{-3/2}$ = 0.911 lb·in$^{-3/2}$; 1 m^7/kN^4 = 57.4 in^7/lb^4.

RESULTS

The predicted values of the fatigue constant $A = \pi/(24 k_{1c}^2 \sigma_y^2)$ are as follows:

For sand asphalt:

$A = 9.17 \times 10^{-14}$ m^7/kN^4 per cycle (5.26×10^{-12} in^7/lb^4 per cycle).

For asphalt concrete:

$A = 1.27 \times 10^{-14}$ m^7/kN^4 per cycle (7.29×10^{-13} in^7/lb^4 per cycle).

While the prediction for sand asphalt is excellent, the theoretical prediction for asphalt concrete appears conservative. Nevertheless, agreement is considered satisfactory in view of the statistical nature of fatigue and the inherent large scatter of experimental results.

For sand asphalt no endurance limit was found, but for asphalt concrete there appears to be an endurance limit $K_0 \approx 0.17\ K_{1c}$. No attempt was made to determine this limit by direct testing because this would mean about 1157 days of continuous testing for only one test, consisting of 100 000 000 cycles of load.

APPLICATION

The law of crack propagation as applied here to predict the fatigue life of a typical pavement is based on several assumptions. These are briefly described below.

First, to predict fatigue life, it is necessary to know the average size and spacing of the starter cracks in the underside of the pavement and the extent of cracking that corresponds to the terminal serviceability of the pavement. The former can be determined experimentally, but the latter is much more difficult. It requires the use of numerical techniques, such as the finite element method, to calculate the changes in the stresses in the underlying paving layers that result from the pattern of cracking in the surface layer. Such techniques are available but are expensive to use. To simplify the problem considerably it will be assumed, arbitrarily, that the terminal serviceability is reached when the average starter crack within a radius of influence R of the loaded tire grows to a length 2c equal to 60.96 cm (2 ft).

Second, the stress-intensity factor K_1 is the dominant parameter in the fatigue analysis, and its evaluation for a typical pavement again requires the use of the finite element method. However, a reasonable approximation of the stress-intensity factor K_1 can be determined from Figure 5 (8) for a slab supported on an elastic foundation,

where

σ^* = maximum tensile stress in the underside of the slab (the reference bending stress);
E, ν, h = Young's modulus, Poisson's ratio, and thickness of the asphaltic layer;
E_s, ν_s = Young's modulus and Poisson's ratio of the subgrade;
$D = Eh^3/12(1-\nu^2)$;
k = coefficient of subgrade reaction = $\sqrt[3]{E_s/E}[E_s/(1-\nu^2)h]$;
$\lambda = \sqrt[4]{k/D}$;
$2c$ = crack length; and
$\lambda' = \lambda c$.

The slab has a crack of length 2c and is loaded so that the bending stress along the crack, calculated for an uncracked pavement, is constant. This is a reasonable approximation for a load moving across a relatively short crack ($c < 30.48$ cm). The following approximation is useful

Figure 3. Results of dc/dN versus $(\Delta k_1)^4$ for sand asphalt.

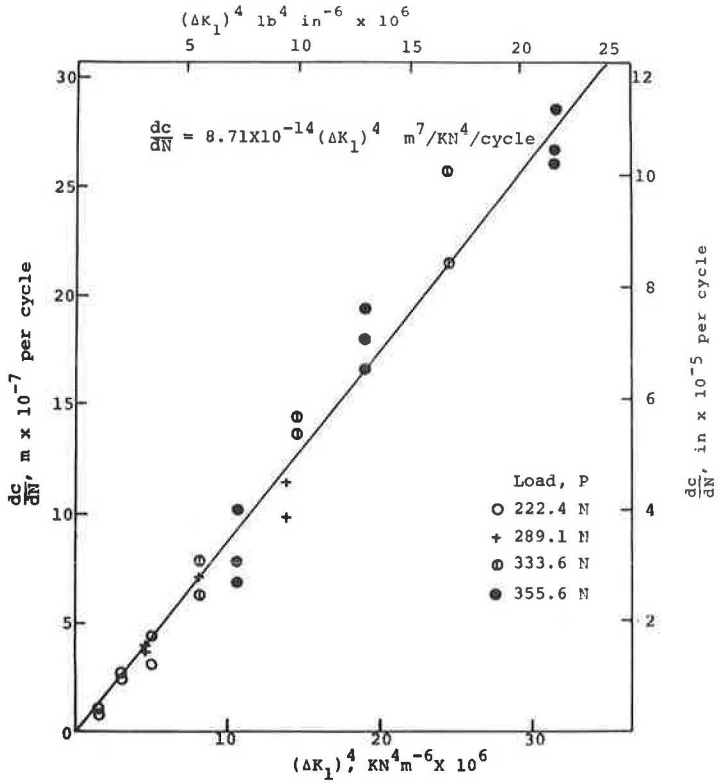

Figure 4. Results of dc/dN versus $(\Delta k_1)^4$ for asphalt concrete.

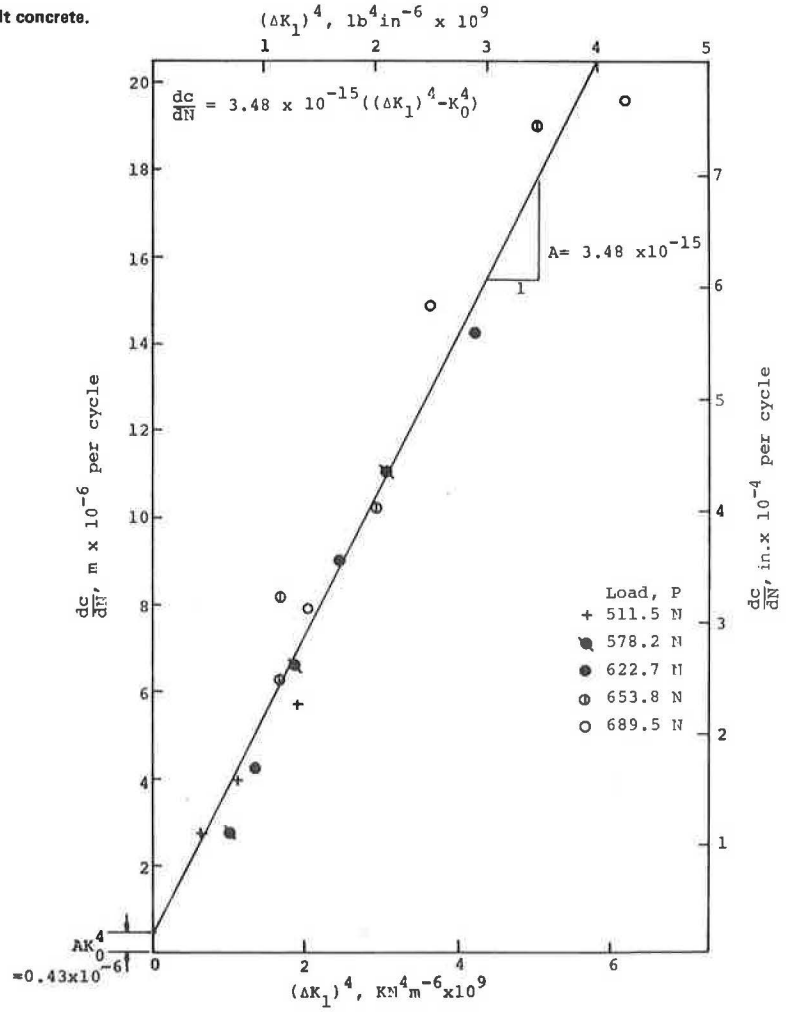

Figure 5. Stress-intensity factor versus λ'.

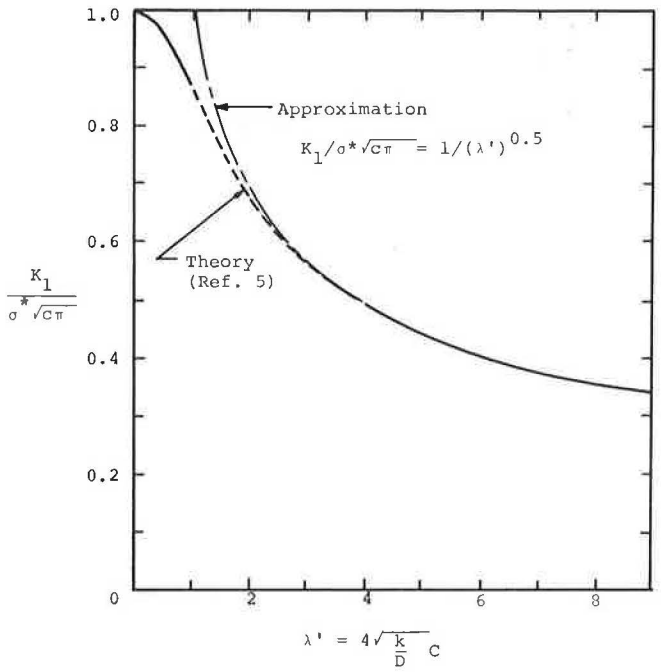

Figure 6. Pavement cross section.

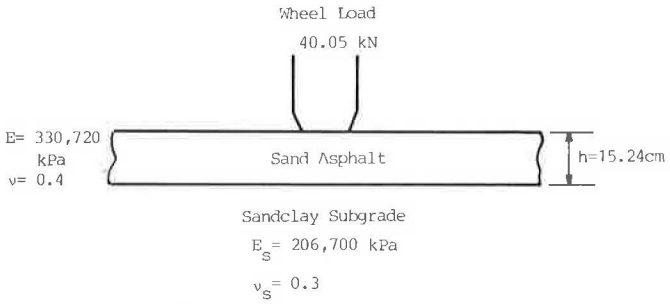

for analytical purposes: In Figure 5, when $\lambda' < 1$, $K_1 \approx \sigma^*\sqrt{c\pi}$ and when $\lambda' > 1$, $K_1 \approx \sigma^*\sqrt{\pi/\lambda}$.

Finally, only crack growth in the opening mode has been discussed. For a pavement, the stresses are such that crack growth in the in-plane sliding and tearing modes are also possible. However, my research indicates that the rates of crack propagation in these modes are several orders of magnitude smaller than those in the opening mode. Hence, only the opening mode of crack growth will be considered.

Based on these assumptions, it becomes a relatively simple matter to predict the life of a pavement, as the following example will show.

Consider the pavement cross section shown in Figure 6. Assume the design temperature is constant at 18.3°C (75°F). The surface layer consists of a sand asphalt whose properties were noted earlier in this paper. The properties of the pavement are then as follows:

(a) sand asphalt surface—K_{1c} = 428 kN·m$^{-3/2}$ (390 lb·in$^{-3/2}$), σ_y = 2792 kPa (405 psi), E = 330 720 kPa (48 000 psi), ν = 0.4 (assumed), and h = 15.24 cm (6 in); (b) subgrade (material properties assumed)—E = 206 700 kPa (30 000 psi) and ν_s = 0.3; and (c) pavement system—$k = \sqrt[3]{E_s/E}\cdot[E_s/(1-\nu^2)h]$ = 4.4 x 10^6 kN·m^{-3} (16 480 pci), $D = Eh^3/12(1-\nu^2)$ = 1.16 x 10^5 N·m (1.029 x 10^6 lb·in), c_0 = 0.254 cm (0.10 in), c_f = 30.48 cm (12 in), $\sigma^* = 0.275(1+\nu)(P/h^2)\,(\log_{10})\,(Eh^3/kb^4)$ = $\Delta\sigma$ = increment in the bending stress during one excursion of the load, $b = \sqrt{(1.6r^2 + h^2)} - 0.675h$ ($r < 1.724h$), r = radius of the loaded area = 16.26 cm (6.4 in), b = 15.24 cm (6 in), P = 40.05 kN (9000 lb), and σ^* = 171.56 kPa (24.9 psi).

The rate of crack growth is given by

$$dc/dN = (\pi/24\,K_{1c}^2\,\sigma_y^2)(\Delta K_1)^4 \quad (K_0 \approx 0)$$

$$= 9.17 \times 10^{-14}\,(\Delta K_1)^4 \text{ m/cycle. Then,}$$

$$N = (10^{14}/9.17)\int_{c_0}^{c_f}[1/(\Delta K_1)^4]\,dc \text{ cycles.}$$

When $\lambda' = 1$, $c = 1/14.02 = 0.0713$ m,

$$N = 10^{14}/9.17\int_{0.002\,54}^{0.0713}[dc/(\sigma^*\sqrt{c\pi})^4]\int_{0.0713}^{0.3048}[dc/(\sigma^*\sqrt{\pi/\lambda})^4] \text{ cycles}$$

= 557 000 cycles.

According to the AASHO Interim Guide, the design life of such a pavement is about 100 000 cycles of equivalent 18-kip single-axle loads.

The above result, therefore, seems reasonable because the AASHO method considers the performance of pavement for all forms of distress, not just fatigue cracking.

CONCLUSIONS

The experimental results show reasonably good agreement with the theory. However, the scope of the experimental investigation was limited, and more research is needed to be conclusive. Nevertheless, the agreement between theory and experiment is encouraging and enhances the applicability of fracture mechanics to the design of pavements against fatigue distress.

An order-of-magnitude agreement was also obtained between the predicted fatigue life of a sand asphalt pavement and that of the design life of the same pavement according to the AASHO method of design. Because the fatigue life is given explicitly in terms of the stress-intensity factor and the invariant material properties of the pavement, the validity of this theory would mean that the task of designing fatigue-resistant pavements would be considerably simplified and the need for expensive trial-and-error solutions in practice minimized.

ACKNOWLEDGMENT

I am grateful to California State University, Fullerton, for providing the facilities for this research and to graduate students J. Allen and J. Langston for their assistance with some of the experimental work.

REFERENCES

1. D. V. Ramsamooj, K. Majidzadeh, and E. M. Kauffmann. The Analysis and Design of the Flexibility of Pavements. Proc., Third International Conference on the Structural Design of Asphalt Pavements, Univ. of Michigan, 1972.
2. K. Majidzadeh, E. M. Kauffmann, and D. V. Ramsamooj. Application of Fracture Mechanics in the Analysis of Pavement Fatigue. AAPT, Vol. 40, 1971.
3. K. Majidzadeh and D. V. Ramsamooj. Development of Testing Procedures and a Method to Predict Fatigue Failures of Asphaltic Concrete Pavement Systems. Ohio State Univ. Research Foundation, Final Rept., Proj. RF2873, March 1971.
4. M. P. Wnuk. Subcritical Growth of Fracture in Elastic Fatigue. International Journal of Fracture Mechanics, Vol. 7, 1971.
5. D. V. Ramsamooj. The Design and Analysis of the Flexibility of Pavements. Ohio State Univ., Ph.D. dissertation, 1970.
6. K. Majidzadeh and D. V. Ramsamooj. Mechanistic Approach to the Solution of Cracking in Pavements. In Structural Design of Asphalt Concrete Pavements to

Prevent Fatigue Cracking, HRB, Special Rept. 140, 1973, pp. 143-157.
7. K. Majidzadeh and others. Application of Fracture Mechanics for Improved Design of Bituminous Concrete. Federal Highway Administration, Rept. FHWA-RD-76-92, June 1976.
8. E. S. Folias. On a Plate Supported by an Elastic Foundation and Containing a Finite Crack. International Journal of Fracture Mechanics, Vol. 6, 1970.
9. S. P. Timoshenko and S. Woinowsky-Krieger. Theory of Plates and Shells, 2nd ed. McGraw-Hill, New York, 1959.

Publication of this paper sponsored by Committee on Flexible Pavement Design.